A QUEST TO REVEAL NOVEL PLAYERS IN NUCLEOTIDE EXCISION REPAIR

From proteomics to mechanistic insights

Yasemin Türkyilmaz

ISBN: 978-94-6332-632-2
Available online: hdl.handle.net/1765/126493

Cover Image: Sea of Clouds in Camlihemsin, Turkey by Yasemin Türkyilmaz
Cover Design: Yasemin Türkyilmaz
Thesis Layout: Yasemin Türkyilmaz & Maarten van der Velden
Printed by: GVO drukkers & vormgevers B.V

The research presented in this thesis was performed at the Department of Molecular Genetics at Erasmus University Medical Center in Rotterdam, the Netherlands.

A QUEST TO REVEAL NOVEL PLAYERS IN NUCLEOTIDE EXCISION REPAIR

From proteomics to mechanistic insights

EEN ZOEKTOCHT NAAR NIEUWE FACTOREN IN
NUCLEOTIDE EXCISIE REPARATIE
Van proteomics tot mechanistische inzichten

Thesis

to obtain the degree of Doctor from the
Erasmus University Rotterdam
by command of the
rector magnificus

Prof. dr. R.C.M.E. Engels

and in accordance with the decision of the Doctorate Board.
The public defense shall be held on
Friday, July 3, 2020 at 13:30

by

Yasemin Türkyilmaz

Born in Ankara, Turkey

Erasmus University Rotterdam

Promoter:
Prof. dr. W. Vermeulen

Other members:
Prof. dr. G.T.J. van der Horst
Prof. dr. A.B. Houtsmuller
Prof. dr. A.C.O. Vertegaal

Copromoter:
Dr. J.A.F. Marteijn

Table of Contents

Chapter 1

General introduction and the scope of this thesis

DNA DAMAGE

Cells are the building blocks of every organism and all living cells have a DNA molecule in a double helix structure to preserve their hereditary information, the genome. In the genome, all the necessary information to build and maintain an organism is stored in the form of genes. Yet such an invaluable resource is not immune to damage. The integrity of our genome is constantly threatened by endogenous and exogenous agents which can induce a variety of DNA lesions. It has been estimated that each human cell is confronted with approximately 100,000 lesions a day (1). These lesions can interfere with vital cellular processes such as DNA replication and RNA transcription, causing mutations, cell-cycle arrest or cell death in the short term and cancer development or accelerated aging in the long term (2,3).

DNA damage can be caused by three main processes, environmental agents, byproducts of cellular metabolism, and spontaneous DNA alterations (Figure 1) (2). Ultraviolet (UV) light present in sunlight is one of the most common environmental DNA damaging agents. Merely several hours of exposure to sunlight could induce up more than 100,000 lesions of cyclobutane pyrimidine dimers and 6-4 photoproducts, the two types of UV-induced DNA lesions, in skin cells (3,4). In addition, ionizing radiation produced by X-ray scans cause oxidative base damage and can generate single-strand and double-strand DNA breaks (5). Moreover, anti-tumor agents used for chemotherapy, such as cisplatin and mitomycin C can covalently crosslink bases on complementary DNA strands causing interstrand cross-links (6). Among the environmental agents that most frequently induce cancer, those found in cigarette smoke could be listed, such as polycyclic aromatic hydrocarbons that cause the formation of DNA adducts (7), these damaging chemicals are also found in exhausting gasses and roasted meat.

Strikingly, also normal cellular metabolism generates reactive oxygen species, including superoxide anions, hydrogen peroxide, and hydroxyl radicals, and these, in turn, can cause DNA strand breaks and several types of oxidized DNA bases, among which 8-Oxoguanine is the most abundant (8). Spontaneous changes in DNA can happen due to replication errors and lead to mismatching DNA bases, insertions, and deletions. Additionally, chemical bonds in DNA structure can degenerate due to spontaneous reactions, such as hydrolysis and alkylation under normal conditions. These can cause loss of DNA bases resulting in abasic sites and alkylation-induced deamination resulting in the conversion of coding bases to miscoding bases, such as cytosine to uracil (9).

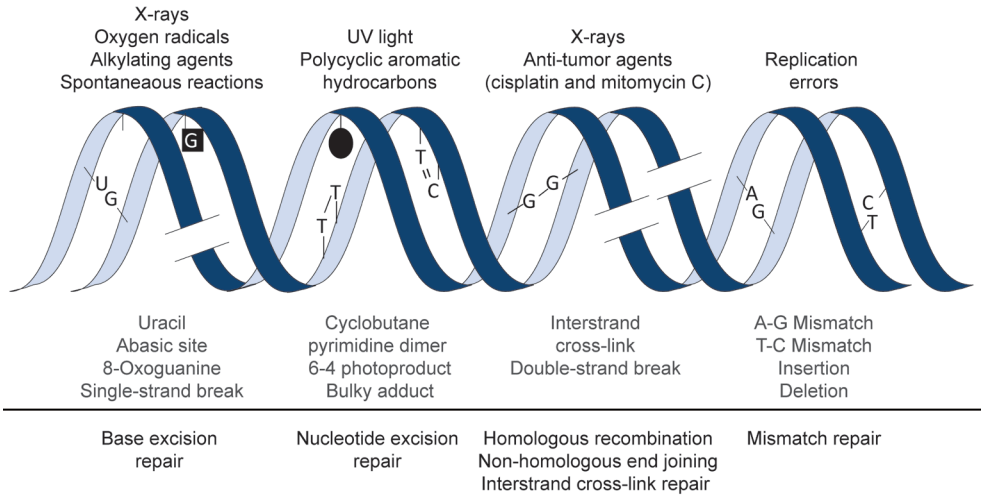

Figure 1. Common DNA damage and repair mechanisms. From top to bottom, the DNA damaging agents (top), the induced DNA lesions (middle), and the corresponding DNA repair mechanisms (bottom) to remove the lesions are listed. Figure adapted from Hoeijmakers (1).

DNA REPAIR

DNA damage is thus unavoidable and inherent to life but when not properly removed strongly impede the cellular homeostasis. Moreover, in contrast to other large polymeric biomolecules such as proteins and lipids, DNA cannot be discarded and resynthesized upon damage, as it is a unique molecule containing all the hereditary information, without any substitute. Fortunately, such detrimental outcomes can be prevented by the DNA damage response, which includes DNA damage signaling, cell-cycle checkpoint, and DNA damage tolerance pathways as well as different DNA repair mechanisms that can repair DNA damage specifically and efficiently. In mammals, several DNA repair mechanisms collectively remove most DNA lesions. The division of tasks among these diverse repair pathways is mainly determined by the type of lesion, their genomic location, and the phase of the cell cycle in which lesions are encountered. (Figure 1) (4,10,11). Below the main mammalian DNA repair mechanisms are shortly summarized as well as their biological impact, with a focus on nucleotide excision repair (NER), as this is the main topic of the research described in this thesis.

Homologous Recombination and Non-homologous End Joining

DNA double-strand breaks (DSBs) happen when the backbone of the two complementary DNA strands is broken at the same location. DSBs are induced by endogenous agents

such as reactive oxygen species (ROS) and collapsed replication forks and exogenous agents such as ionizing radiation and chemotherapeutic drugs. DSBs are highly toxic to the cells and can cause cell death or chromosomal changes such as deletions, translocations and fusions that could lead to cancer development (12). There are two main pathways that repair DSBs: homologous recombination (HR) and non-homologous end joining (NHEJ). HR accurately repairs DSBs by using the sister chromatid that is identical to broken DNA as a repair template. Therefore, HR can only take place during S and G2 phases of the cell cycle, when DNA replication has taken place and sister chromatids are present (13). In contrast, NHEJ can happen anytime during the whole cell cycle as it does not require a template. However, NHEJ repairs damaged DNA in a less accurate manner, as the main step in this process is simply joining (ligating) the two broken DNA ends. To allow ligation, chemically modified terminal nucleotides are processed or removed, which can cause loss or inaccurate insertion of DNA bases in the repaired site (14). Defective DSB repair gives rise to a predisposition to breast and ovarium cancer as well as other severe diseases, such as ataxia telangiectasia and Nijmegen breakage syndrome which are characterized by immunodeficiency, chromosomal instability and predisposition to lymphomas (2,4).

Interstrand cross-link repair

Interstrand cross-links (ICLs) are lesions where opposite DNA strands are crosslinked to each other due to exposure to various endogenous metabolites (mainly aldehydes) and exogenous agents as well as some chemotherapeutic agents. ICLs block DNA strand separation which is necessary for vital cellular processes such as replication and transcription (15), ICLs are thus highly cytotoxic. ICL repair is a complex procedure that requires sequential excision of the lesion from each strand. To prevent DSB formations by these excisions, the different steps in this process are tightly controlled to occur in a timely and coordinated fashion, which is regulated by multiple so-called Fanconi anemia (FA) proteins. Strikingly, in addition to these FA proteins, the collective action of multiple DNA repair pathways, including translesion synthesis, HR, and nucleotide excision repair is necessary (15). Defective repair of ICLs can cause a severe disease named Fanconi Anemia (FA), which is characterized by bone marrow failure, congenital anomalies, and a high risk for developing acute myeloid leukemia (16).

Mismatch Repair

Mismatch repair (MMR) removes mismatching DNA bases that are erroneously incorporated during replication by DNA polymerases, and small insertion or deletion loops of a few nucleotides that are introduced by slippage during DNA replication and recombination (2). MMR ensures the repair of these lesions by specialized mismatch-recognizing proteins and their excision, specifically from the nascent DNA strand, followed by the resynthesis of the excised DNA (17). Defects in MMR cause genome wide instability and significantly increase mutations which can lead to the development of cancer, such as hereditary non-polyposis colorectal cancer (HNPCC).

Base Excision Repair

Base excision repair (BER) removes lesions that only slightly distort the DNA helix such as those caused by endogenous deamination, oxidation, and alkylation as well as DNA single-strand breaks (SSBs). In BER, damaged bases are recognized and removed by a set of different DNA glycosylases, each specific for certain types of base damages. The removal of damaged bases from the DNA backbone generates an abasic site, also known as an apurinic/apyrimidinic (AP) site, which is further processed by AP-endonuclease to create a single strand nick and end-processing enzymes, to create DNA polymerase-competent ends. The remaining gap is filled in by either short-patch repair or long-patch repair. In short-patch repair, a single nucleotide is replaced and in long-patch repair 2-10 nucleotides are replaced (18). Defects in BER are associated with the development of cancer and neurodegenerative disorders (19).

Nucleotide Excision Repair

Nucleotide excision repair (NER) is a highly versatile DNA repair pathway that removes a broad range of DNA lesions, including the UV light-induced cyclobutane pyrimidine dimers (CPDs) and 6-4 photoproducts (6-4PPs) and multiple bulky DNA adducts, which all have in common that they locally disrupt base-pairing. These helix-destabilizing DNA lesions are detected by one of the two NER sub-pathways that vary in their method of damage recognition. Global genome NER (GG-NER) recognizes lesions throughout the whole genome and transcription-coupled NER (TC-NER) detects lesions in actively transcribed genes. After the recognition, both pathways converge to the steps of damage verification, dual excision, gap filling DNA synthesis, and ligation (Figure 2) (20).

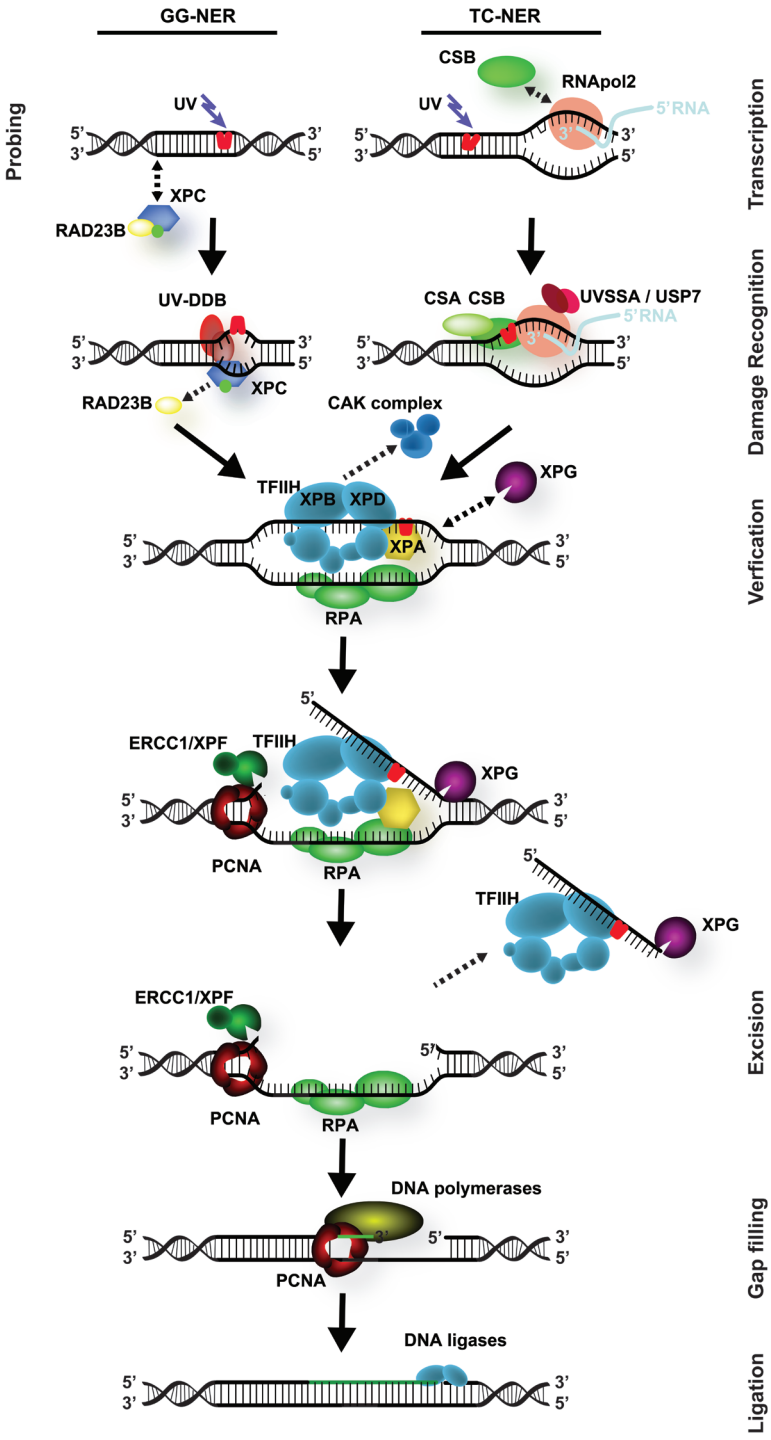
GG-NER
TC-NER
Probing
UV
CSB
RNApol2
5'RNA
XPC
RAD23B
UV-DDB
CSA CSB
UVSSA / USP7
CAK complex
TFIIH
XPB XPD
XPG
XPA
RPA
ERCC1/XPF
PCNA
DNA polymerases
DNA ligases
Transcription
Damage Recognition
Verfication
Excision
Gap filling
Ligation

Figure 2. Nucleotide Excision Repair (NER) pathway. Schematic representation of the NER pathway. In global genome NER (GG-NER, on the left), XPC, which is in a heterotrimeric complex with RAD23B and centrin2, probes the entire genome and recognizes lesions with the help of UV-DDB complex. Once XPC binds to damage, RAD23B is dissociated from the complex. Transcription-coupled NER (TC-NER, on the right) is initiated when elongating Pol II is stalled due to lesions in actively transcribed genes. During transcription, CSB probes Pol II whether it can forward-translocate on the DNA. When Pol II is blocked by a lesion, CSB binds to Pol II and recruits CSA, and UVSSA recruits USP7 to stabilize CSB. Once the lesion is recognized, TFIIH is recruited and CAK sub-complex of TFIIH is released. XPB and XPD, the helicase subunits of TFIIH, unwind the DNA around the lesion and verify the lesion together with XPA. This is followed by the recruitment of the ERCC1/XPF and XPG endonucleases to the 5' and 3' of the lesion respectively and this completes the pre-incision complex assembly. Afterwards, the DNA strand around the lesion is cut by the endonucleases in a coordinated manner and a DNA fragment of 22-30 nucleotides is released together with TFIIH and XPG. Eventually, the DNA is restored back to its original state via gap filling synthesis by PCNA and DNA polymerase (δ, ε or ϰ), and ligation by DNA ligase 1 or XRCC1/DNA ligase 3.

Global genome NER

In GG-NER, XPC is the main DNA damage sensor (21), which is part of a heterotrimeric complex with RAD23B and centrin2 (22,23). XPC probes the entire genome (24) and does not directly detect the lesion but instead detects damage-induced DNA helix distortions such as those caused by 6-4PP lesions (25). This is why GG-NER can recognize and repair a broad range of lesions. To detect mildly helix-destabilizing UV-induced CPD lesions, XPC requires the UV-DDB complex, formed by DDB1 and DDB2 (26,27). UV-DDB binds to UV-induced lesions, stabilizes the DNA in a conformation in which CPD is flipped out, and thereby creating helix-destabilization which thus facilitates CPD detection by XPC (28). UV-DDB also improves the detection of 6-4PP lesions (29). DDB1 and DDB2 are also part of an E3-ubiquitin ligase complex with CUL4A/B and RBX1, namely $CRL4^{DDB2}$ (30). Upon UV damage, XPC and DDB2, are ubiquitylated by the $CRL4^{DDB2}$ complex with different outcomes. DDB2 is ubiquitylated by K48-linked chains and thereby targeted for proteasomal degradation (31,32), while XPC gains a higher affinity to the damaged DNA *in vitro* (33). Recently it was shown that DDB2 ubiquitylated by $CRL4^{DDB2}$ is extracted from damaged chromatin by VCP/p97 segragase to facilitate its proteasomal degradation (34). Additionally, XPC was suggested to be protected from proteasomal degradation by USP7 mediated de-ubiquitylation (35). In addition to ubiquitylation, XPC is also modified by small ubiquitin-like modifier (SUMO) upon UV damage (36-38). This DDB2- and XPA-dependent modification protects XPC from proteasomal degradation (37,38). SUMOylated XPC is modified with K63-linked ubiquitin chains by the

SUMO-targeted ubiquitin ligase RNF111 (39). Recently we showed that RNF111-dependent XPC ubiquitylation results in the release of XPC from the damage, which is necessary for the incorporation of the downstream NER endonucleases XPG and ERCC1/XPF, thereby enabling efficient repair (40).

Transcription-coupled NER

During transcription, elongating RNA polymerase II (Pol II) is stalled when it encounters a transcription-blocking lesion (TBL). Lesion-stalling of Pol II stabilizes its transient interaction with the TC-NER-specific SWI/SNF-like ATPase CSB (41-43). A recent cryo-EM study of the yeast homolog of CSB, Rad26, revealed important insights into how TC-NER can distinguish between paused and stalled Pol II (44). This study showed that Rad26 binds upstream of Pol II and pushes it forward by translocating 3' to 5' direction, similar to the translocation activity of human CSB (45). Although Rad26 enables Pol II forward translocation over natural pause sites or less bulky lesions, it cannot push Pol II over bulky TBLs, such as CPDs (44). This prolongs the interaction of Rad26 with Pol II and highly likely triggers TC-NER initiation. Due to Rad26-DNA and Rad26-Pol II interaction interfaces and core domain of Rad26 being highly conserved between yeast and humans, a similar role for CSB in human TC-NER was proposed (44,46,47). Once TBLs are recognized by CSB (41,44,48), CSB recruits CSA (49) which is part of an E3-ubiquitin ligase complex with DDB1, Cul4A and Roc1 (30,50). Upon UV irradiation, this complex targets CSB for proteasomal degradation by ubiquitylation (51). The deubiquitylating enzyme USP7 is recruited by UVSSA to counteract this degradation and stabilize CSB (52,53), to ensure CSB can coordinate TC-NER complex formation.

Despite all these insights, how exactly these TC-NER factors are recruited to TBLs and form a TC-NER machinery is not known. In **Chapter 4**, by studying quantitative accumulation kinetics in live cells, we showed that UVSSA accumulates at TBLs independently of CSA and CSB. Utilizing UVSSA deletion mutants, we showed that the DUF2043 domain is involved in the recruitment of UVSSA to TBLs and the VHS domain is involved in the interaction of UVSSA with CSA. Using these mutants together with quantitative interaction proteomics, we identified the H2A/H2B chaperone FACT subunit Spt16 to interact with UVSSA via its DUF2043 domain. Using various imaging approaches, we demonstrated that Spt16 recruitment to TBLs takes place in early TC-NER independently of UVSSA and facilitates damage removal

and consecutive transcription restart. Our results uncover Spt16 as a TC-NER regulator and reveal insights into the recruitment of TC-NER factors to TBLs.

Lesion verification

Upon damage detection, XPC in GG-NER (54,55) and UVSSA in TC-NER recruits the general transcription factor II H (TFIIH) to the lesion by a common mechanism, via their interaction with P62 subunit of TFIIH (56). The TFIIH multi-protein complex is composed of ten subunits and is an important player for both transcription and NER (57,58). The trimeric CDK-activating kinase (CAK) sub-complex of TFIIH is required for transcription initiation but inhibitory for NER and thus dissociates after TFIIH is recruited by XPC to the lesion (59). TFIIH contains two helicases, namely XPB and XPD, which are essential for unwinding the DNA around the lesion (57,58). Additionally, XPB facilitates the lesion recruitment of TFIIH via its ATPase activity (60) and XPD verifies the lesion with the assistance of XPA (61-63), via its 5' – 3' unwinding activity (64). XPA is recently described to assist conformational change of TFIIH from a transcription active state to a NER active state by facilitating the release of the CAK sub-complex, re-orienting XPB and XPD helicases and removing a DNA binding inhibitory "plug" element from XPD, which enables lesion verification by XPD (65). Also, the single-stranded binding protein RPA is recruited and it coats the undamaged strand to protect it from endonucleases (66).

Dual incision and gap filling

The emerging NER complex licenses the recruitment of the structure-specific NER endonucleases for the dual incision. This process is highly coordinated since it is crucial that it takes place accurately to prevent the generation of undesirable ssDNA gaps which could induce DNA damage signaling pathways (20). XPA recruits the ERCC1/XPF endonuclease (67,68) and the XPG endonuclease is recruited either as a separate protein or as a TFIIH-interacting factor (69-71). RPA positions ERCC1/XPF and XPG on the 5' and 3' of the lesion respectively (66) and this completes the assembly of the pre-incision complex. ERCC1/XPF and XPG endonucleases coordinately incise the damaged strand around the lesion. The presence of XPG is necessary for the 5' incision by ERCC1/XPF and this leads to the 3' incision by XPG (72). Subsequently, a DNA fragment of a 22-30 nucleotides is released with TFIIH (73). The resulting gap is filled by the concerted activity of PCNA, RFC, and DNA polymerase (δ, ε or κ) (74), and sealed by DNA ligase 1 or XRCC1/DNA ligase 3 mediated ligation (75), restoring the

DNA back to its original state. These steps are carried out by DNA Pol ε and DNA ligase 1 in replicating cells, and DNA Pol δ or κ and XRCC1/DNA ligase 3 in non-replicating cells (74,75).

It is essential that each reaction step is tightly regulated in this multi-protein pathway, to ensure the proper and timely transition between the consecutive reaction steps. As explained above for GG-NER and TC-NER, post-translational modifications have been shown to be crucial for accurately orchestrating successive NER reaction steps (20,76-78). Additionally, transpiring in a complex chromatin environment, NER is affected by other activities such as DNA replication (79), RNA transcription (80), or chromatin remodeling (20,81,82). Therefore, it is highly likely that additional regulatory procedures are required to ensure that NER can efficiently progress in this dynamic setting.

To gain a deeper understanding of the regulation of NER, we aimed to detect new NER interactors and describe the functional relevance of these interactions. In **Chapter 2 and 3**, using quantitative interaction proteomics, we focused on interactors of TFIIH since this central NER factor plays important roles in various NER stages, namely DNA unwinding around the lesion, lesion verification and incision complex assembly (20). Additionally, although the incised lesion-containing oligonucleotide is described to be released together with TFIIH and XPG (73,83), the mechanism of this release is not known. In contrast, bacterial NER is known to utilize the helicase UvrD to release the endonuclease UvrC and the lesion-containing oligonucleotide upon incision (84,85), which enables repair synthesis by DNA polymerase I (84,86). In **Chapter 2**, using SILAC-based quantitative proteomics in combination with two different pull-down approaches, namely native and cross-linking IP, we examined the UV-induced TFIIH interaction network in detail. Our approach was validated by the identification of known TFIIH interactors and interestingly our results suggest that once engaged in NER, the TFIIH complex might harbor multiple XPD subunits. Most importantly, we detected a novel UV-induced TFIIH interactor, HLTF.

HLTF is not an unknown protein in DNA damage response. It is the closest human orthologue of the yeast protein Rad5 which is described to be involved in post-replication repair mechanisms (PRR), including template switching (TS) and translesion synthesis (TLS) (87). Similar to Rad5, HLTF harbors a 3'-OH ssDNA end binding HIRAN domain, SWI/SNF helicase domain, and a ubiquitin ligase RING domain (88-91).

HLTF is reported to use its RING domain as a ubiquitin ligase to induce PCNA polyubiquitylation (89,92). Its SWI/SNF helicase domain has been indicated to act as a dsDNA translocase to reverse stalled replication forks (90) and clear DNA-bound proteins (91). Its HIRAN domain has been described to promote its fork reversal activity by recruiting HLTF to replication forks via its 3'-OH ssDNA end binding activity (88,93).

In **Chapter 3**, we showed that HLTF is recruited to a TFIIH-containing NER intermediate where the double incision has already taken place, but gap-filling synthesis still has to occur. By depleting RAD18, which is necessary for the functioning of HLTF in PRR (89,92,94), we confirmed that HLTF has a distinct role in NER. Results obtained by an *in vivo* excision assay (83,95,96) and γH2AX signaling staining (97,98) suggested that HLTF activity is necessary for the removal of the incised DNA fragment. Using a set of HLTF domain mutants, we revealed that the RING domain is dispensable for the role of HLTF in NER, suggesting that the HLTF-mediated PCNA modification (89,92) is not relevant for NER. We found that the HIRAN domain is responsible for the recruitment of HLTF to NER intermediates. In line with 3'-OH ssDNA end binding activity of the HIRAN domain (88,93), we showed that HLTF interacts with 3'-OH at the dsDNA/ssDNA junction bound by XPF-ERCC1. Both HIRAN and SWI/SNF helicase domain mutants led to increased TFIIH accumulation at local UV damage while only SWI/SNF helicase domain mutant caused an increased HLTF accumulation at local UV damage which was completely abrogated for the HIRAN domain mutant. Considering all these observations, we suggest that the SWI/SNF helicase domain is responsible for enabling 3'-to-5' directional protein displacement once positioned by HIRAN at 3'-OH site, created by XPF-ERCC1 incision. Overall, we represent HLTF as a new NER factor that releases the incised lesion-containing oligonucleotide and this way facilitates gap filling, similar to UvrD in bacterial NER (84-86).

Clinical consequences of NER defects

Inherited mutations in NER genes can lead to severe and rather heterogeneous clinical consequences, ranging from developmental defects and severe cancer predisposition to neurodevelopmental defects and premature ageing, illustrating the clinical significance of NER (20). It is remarkable to note that defects in a single pathway can result in such diverse clinical outcomes. This can be explained by the fact that NER detects a broad range of lesions via two separate sub pathways, GG-NER and TC-NER, and is

a complex repair pathway with many players involved, some of which have additional functions beyond NER.

Defects in GG-NER pathway

GG-NER is responsible for the detection of UV-induced lesions throughout the entire genome. Lesions that are not repaired due to inherited defects in GG-NER can be bypassed by translesion DNA polymerases. Although lesion bypass enables cell survival, these polymerases are error-prone and result in genome-wide accumulation of mutations which lead to cancer development (99). Xeroderma pigmentosum (XP) patients with defective XPC and XPE (UV-DDB) genes have more than 1000-fold increased susceptibility to develop UV light-induced skin cancer and an increased risk for developing internal tumors. Additionally, they exhibit mild hypersensitivity to UV radiation, with hypopigmentation and hyperpigmentation in their skin (100).

Defects in TC-NER pathway

As transcription is a vital mechanism for cells, defects in TC-NER can lead to serious consequences such as premature cell death and accelerated aging (3,101). Interestingly, there are surprising differences in the phenotype of patients with mutations in the TC-NER proteins, UVSSA, CSA, and CSB. Mutations in UVSSA gene (52,53,102) lead to a mild and rare disorder, namely UV-sensitive syndrome ($UV^{S}S$), which is characterized by mild hypersensitivity to UV radiation, with freckling and telangiectasia (103). In contrast, patients of Cockayne syndrome (CS), which is caused by mutations in CSA and CSB genes, exhibit much severe clinical phenotypes such as neurological and developmental abnormalities, and premature aging on top of the UV hypersensitivity (104). CS patients have an average life expectancy of 12 years (105).

The strong contrast between $UV^{S}S$ and CS is surprising, especially considering that in both conditions TC-NER activity (106) and transcription restart (52,107) are abrogated, resulting in the complete absence of TC-NER mediated TBL removal. Yet, both CSA and CSB are described to facilitate the removal of Pol II stalled on TBLs via proteasomal degradation (108). Therefore, even if UVSSA is mutated, CSA and CSB can still remove Pol II and this could expose TBLs to the activity of other repair pathways, such as GG-NER (20,47). According to this hypothesis, although GG-NER would remove 6–4PPs efficiently, it would remove CPDs very slowly, explaining the UV-sensitivity phenotype of $UV^{S}S$. Additionally, CSB is also involved in other repair pathways than TC-NER,

including transcription-coupled BER (109-112), transcription-coupled homologous recombination (113,114) and inter-strand crosslink repair (115,116) and therefore defects in CSB highly likely leads to accumulation of a wider range of DNA damage, compared to UVSSA-deficiency.

Defects in core NER pathway

When core NER pathway factors XPB, XPD, ERCC1/XPF, and XPG are defective, GG-NER and TC-NER are both affected (117,118). Therefore patients with mutations in these genes exhibit either classical XP features or a clinical condition known as XP-CS complex, in which characteristics of both XP and CS syndromes are observed (47). Additionally, mutations in TFIIH members XPB, XPD, and TTDA can lead to trichothiodystrophy (TTD). TTD mutations hamper TFIIH activity not only in NER but also in transcription initiation during the final differentiation phase of skin, hair, and nail cells (119-121). As a result, TTD patients do not only exhibit typical characteristics of CS but also scaly skin, brittle hair, and nails (122).

Photo-reactivation

In addition to NER, in most species there exists an alternative pathway to remove UV-induced lesions by direct reversal, namely photo-reactivation (PR). This process has been preserved throughout evolution in basically all branches of life, from bacteria to non-placental mammals (123,124). Surprisingly, placental mammals have lost this repair pathway and fully rely on NER for UV-lesion removal. While NER is a complex mechanism requiring the coordinated action of at least 30 proteins (20), PR removes the UV light induced CPD and 6-4PP lesions by direct enzymatic reversal mediated by damage specific photolyases (PL)s using the energy of visible light.

There are two types of PLs, each responsible for the repair of one type of UV-induced lesions, namely CPD and 6-4PP PL (125,126). These PLs recognize and bind to CPD or 6-4PP lesions with high specificity, causing flipping out of the lesion into the active-site of the PL and creating a high affinity enzyme-substrate complex (127,128). In the presence of near-UV/blue light (300–500 nm), the PLs catalytically reverse the lesions to the original bases by a photo-induced electron transfer reaction. In the case of CPD PL, first, a 300-500 nm photon is adsorbed by the chromophore MTHF. Second, the excitation energy is transferred to flavin (FADH–). Third, flavin transfers an electron to the cyclobutane ring, splitting the pyrimidine dimer and restoring the bases. Finally,

flavin is restored back to its catalytically active form with a back electron transfer (128-130). In the case of 6-4PP PL, PR takes place with a similar mechanism with one important difference. Upon binding, 6-4PP PL first thermally converts the 6-4PP to an oxetane intermediate. This resembles the cyclobutane ring and is broken by photo-induced electron transfer (131-133). For both PLs, the entire reaction takes ~1 ns (128).

In **Chapter 5**, we exploited the damage recognition and binding ability of CPD and 6-4PP PLs, by tagging them with mCherry fluorescent protein. These fluorescently-tagged PLs precisely detect UV-induced DNA damage without interfering with NER activity. Utilizing fluorescence recovery after photo-bleaching (FRAP) (134,135), we developed a highly sensitive new method to quantify UV-induced DNA damage and repair kinetics in real time, in living cells. Moreover, we developed a live-cell repair method using the 405 nm laser which enables immediate DNA damage removal in a lesion specific manner. Overall, we present fluorescently-tagged PLs as a powerful tool to detect, quantify, and repair UV-induced DNA damage, which could be used in living cells to investigate the behavior of NER proteins.

REFERENCES

1. Lindahl, T. and Barnes, D.E. (2000) Repair of endogenous DNA damage. *Cold Spring Harbor symposia on quantitative biology*, **65**, 127-133.
2. Hoeijmakers, J.H. (2001) Genome maintenance mechanisms for preventing cancer. *Nature*, **411**, 366-374.
3. Hoeijmakers, J.H. (2009) DNA damage, aging, and cancer. *The New England journal of medicine*, **361**, 1475-1485.
4. Jackson, S.P. and Bartek, J. (2009) The DNA-damage response in human biology and disease. *Nature*, **461**, 1071-1078.
5. Ward, J.F. (1988) DNA damage produced by ionizing radiation in mammalian cells: identities, mechanisms of formation, and reparability. *Progress in nucleic acid research and molecular biology*, **35**, 95-125.
6. Scharer, O.D. (2005) DNA interstrand crosslinks: natural and drug-induced DNA adducts that induce unique cellular responses. *Chembiochem : a European journal of chemical biology*, **6**, 27-32.
7. Wogan, G.N., Hecht, S.S., Felton, J.S., Conney, A.H. and Loeb, L.A. (2004) Environmental and chemical carcinogenesis. *Seminars in cancer biology*, **14**, 473-486.
8. De Bont, R. and van Larebeke, N. (2004) Endogenous DNA damage in humans: a review of quantitative data. *Mutagenesis*, **19**, 169-185.
9. Lindahl, T. (1993) Instability and decay of the primary structure of DNA. *Nature*, **362**, 709-715.
10. Ciccia, A. and Elledge, S.J. (2010) The DNA damage response: making it safe to play with knives. *Molecular cell*, **40**, 179-204.
11. Giglia-Mari, G., Zotter, A. and Vermeulen, W. (2011) DNA damage response. *Cold Spring Harbor perspectives in biology*, **3**, a000745.
12. Shrivastav, M., De Haro, L.P. and Nickoloff, J.A. (2008) Regulation of DNA double-strand break repair pathway choice. *Cell research*, **18**, 134-147.
13. Moynahan, M.E. and Jasin, M. (2010) Mitotic homologous recombination maintains genomic stability and suppresses tumorigenesis. *Nature reviews. Molecular cell biology*, **11**, 196-207.
14. Lieber, M.R. (2010) The mechanism of double-strand DNA break repair by the nonhomologous DNA end-joining pathway. *Annual review of biochemistry*, **79**, 181-211.
15. Clauson, C., Scharer, O.D. and Niedernhofer, L. (2013) Advances in

understanding the complex mechanisms of DNA interstrand cross-link repair. *Cold Spring Harbor perspectives in biology*, **5**, a012732.

16. Auerbach, A.D. (2009) Fanconi anemia and its diagnosis. *Mutation research*, **668**, 4-10.
17. Jiricny, J. (2013) Postreplicative mismatch repair. *Cold Spring Harbor perspectives in biology*, **5**, a012633.
18. Krokan, H.E. and Bjoras, M. (2013) Base excision repair. *Cold Spring Harbor perspectives in biology*, **5**, a012583.
19. Wallace, S.S. (2014) Base excision repair: a critical player in many games. *DNA repair*, **19**, 14-26.
20. Marteijn, J.A., Lans, H., Vermeulen, W. and Hoeijmakers, J.H. (2014) Understanding nucleotide excision repair and its roles in cancer and ageing. *Nature reviews. Molecular cell biology*, **15**, 465-481.
21. Sugasawa, K., Ng, J.M., Masutani, C., Iwai, S., van der Spek, P.J., Eker, A.P., Hanaoka, F., Bootsma, D. and Hoeijmakers, J.H. (1998) Xeroderma pigmentosum group C protein complex is the initiator of global genome nucleotide excision repair. *Molecular cell*, **2**, 223-232.
22. Masutani, C., Sugasawa, K., Yanagisawa, J., Sonoyama, T., Ui, M., Enomoto, T., Takio, K., Tanaka, K., van der Spek, P.J., Bootsma, D. *et al.* (1994) Purification and cloning of a nucleotide excision repair complex involving the xeroderma pigmentosum group C protein and a human homologue of yeast RAD23. *The EMBO journal*, **13**, 1831-1843.
23. Araki, M., Masutani, C., Takemura, M., Uchida, A., Sugasawa, K., Kondoh, J., Ohkuma, Y. and Hanaoka, F. (2001) Centrosome protein centrin 2/caltractin 1 is part of the xeroderma pigmentosum group C complex that initiates global genome nucleotide excision repair. *The Journal of biological chemistry*, **276**, 18665-18672.
24. Hoogstraten, D., Bergink, S., Ng, J.M., Verbiest, V.H., Luijsterburg, M.S., Geverts, B., Raams, A., Dinant, C., Hoeijmakers, J.H., Vermeulen, W. *et al.* (2008) Versatile DNA damage detection by the global genome nucleotide excision repair protein XPC. *Journal of cell science*, **121**, 2850-2859.
25. Gillet, L.C. and Scharer, O.D. (2006) Molecular mechanisms of mammalian global genome nucleotide excision repair. *Chemical reviews*, **106**, 253-276.
26. Wakasugi, M., Kawashima, A., Morioka, H., Linn, S., Sancar, A., Mori, T., Nikaido, O. and Matsunaga, T. (2002) DDB accumulates at DNA damage sites

immediately after UV irradiation and directly stimulates nucleotide excision repair. *The Journal of biological chemistry*, **277**, 1637-1640.

27. Fitch, M.E., Nakajima, S., Yasui, A. and Ford, J.M. (2003) In vivo recruitment of XPC to UV-induced cyclobutane pyrimidine dimers by the DDB2 gene product. *The Journal of biological chemistry*, **278**, 46906-46910.
28. Scrima, A., Konickova, R., Czyzewski, B.K., Kawasaki, Y., Jeffrey, P.D., Groisman, R., Nakatani, Y., Iwai, S., Pavletich, N.P. and Thoma, N.H. (2008) Structural basis of UV DNA-damage recognition by the DDB1-DDB2 complex. *Cell*, **135**, 1213-1223.
29. Moser, J., Volker, M., Kool, H., Alekseev, S., Vrieling, H., Yasui, A., van Zeeland, A.A. and Mullenders, L.H. (2005) The UV-damaged DNA binding protein mediates efficient targeting of the nucleotide excision repair complex to UV-induced photo lesions. *DNA repair*, **4**, 571-582.
30. Groisman, R., Polanowska, J., Kuraoka, I., Sawada, J., Saijo, M., Drapkin, R., Kisselev, A.F., Tanaka, K. and Nakatani, Y. (2003) The ubiquitin ligase activity in the DDB2 and CSA complexes is differentially regulated by the COP9 signalosome in response to DNA damage. *Cell*, **113**, 357-367.
31. Matsuda, N., Azuma, K., Saijo, M., Iemura, S., Hioki, Y., Natsume, T., Chiba, T., Tanaka, K. and Tanaka, K. (2005) DDB2, the xeroderma pigmentosum group E gene product, is directly ubiquitylated by Cullin 4A-based ubiquitin ligase complex. *DNA repair*, **4**, 537-545.
32. Rapic-Otrin, V., McLenigan, M.P., Bisi, D.C., Gonzalez, M. and Levine, A.S. (2002) Sequential binding of UV DNA damage binding factor and degradation of the p48 subunit as early events after UV irradiation. *Nucleic acids research*, **30**, 2588-2598.
33. Sugasawa, K., Okuda, Y., Saijo, M., Nishi, R., Matsuda, N., Chu, G., Mori, T., Iwai, S., Tanaka, K., Tanaka, K. *et al.* (2005) UV-induced ubiquitylation of XPC protein mediated by UV-DDB-ubiquitin ligase complex. *Cell*, **121**, 387-400.
34. Puumalainen, M.R., Lessel, D., Ruthemann, P., Kaczmarek, N., Bachmann, K., Ramadan, K. and Naegeli, H. (2014) Chromatin retention of DNA damage sensors DDB2 and XPC through loss of p97 segregase causes genotoxicity. *Nature communications*, **5**, 3695.
35. He, J., Zhu, Q., Wani, G., Sharma, N., Han, C., Qian, J., Pentz, K., Wang, Q.E. and Wani, A.A. (2014) Ubiquitin-specific protease 7 regulates nucleotide excision repair through deubiquitinating XPC protein and preventing XPC protein from

undergoing ultraviolet light-induced and VCP/p97 protein-regulated proteolysis. *The Journal of biological chemistry*, **289**, 27278-27289.

36. Silver, H.R., Nissley, J.A., Reed, S.H., Hou, Y.M. and Johnson, E.S. (2011) A role for SUMO in nucleotide excision repair. *DNA repair*, **10**, 1243-1251.
37. Wang, Q.E., Praetorius-Ibba, M., Zhu, Q., El-Mahdy, M.A., Wani, G., Zhao, Q., Qin, S., Patnaik, S. and Wani, A.A. (2007) Ubiquitylation-independent degradation of Xeroderma pigmentosum group C protein is required for efficient nucleotide excision repair. *Nucleic acids research*, **35**, 5338-5350.
38. Wang, Q.E., Zhu, Q., Wani, G., El-Mahdy, M.A., Li, J. and Wani, A.A. (2005) DNA repair factor XPC is modified by SUMO-1 and ubiquitin following UV irradiation. *Nucleic acids research*, **33**, 4023-4034.
39. Poulsen, S.L., Hansen, R.K., Wagner, S.A., van Cuijk, L., van Belle, G.J., Streicher, W., Wikstrom, M., Choudhary, C., Houtsmuller, A.B., Marteijn, J.A. *et al.* (2013) RNF111/Arkadia is a SUMO-targeted ubiquitin ligase that facilitates the DNA damage response. *The Journal of cell biology*, **201**, 797-807.
40. van Cuijk, L., van Belle, G.J., Turkyilmaz, Y., Poulsen, S.L., Janssens, R.C., Theil, A.F., Sabatella, M., Lans, H., Mailand, N., Houtsmuller, A.B. *et al.* (2015) SUMO and ubiquitin-dependent XPC exchange drives nucleotide excision repair. *Nature communications*, **6**, 7499.
41. van den Boom, V., Citterio, E., Hoogstraten, D., Zotter, A., Egly, J.M., van Cappellen, W.A., Hoeijmakers, J.H., Houtsmuller, A.B. and Vermeulen, W. (2004) DNA damage stabilizes interaction of CSB with the transcription elongation machinery. *The Journal of cell biology*, **166**, 27-36.
42. Tantin, D., Kansal, A. and Carey, M. (1997) Recruitment of the putative transcription-repair coupling factor CSB/ERCC6 to RNA polymerase II elongation complexes. *Molecular and cellular biology*, **17**, 6803-6814.
43. van Gool, A.J., Citterio, E., Rademakers, S., van Os, R., Vermeulen, W., Constantinou, A., Egly, J.M., Bootsma, D. and Hoeijmakers, J.H. (1997) The Cockayne syndrome B protein, involved in transcription-coupled DNA repair, resides in an RNA polymerase II-containing complex. *The EMBO journal*, **16**, 5955-5965.
44. Xu, J., Lahiri, I., Wang, W., Wier, A., Cianfrocco, M.A., Chong, J., Hare, A.A., Dervan, P.B., DiMaio, F., Leschziner, A.E. *et al.* (2017) Structural basis for the initiation of eukaryotic transcription-coupled DNA repair. *Nature*, **551**, 653-657.

45. Selby, C.P. and Sancar, A. (1997) Cockayne syndrome group B protein enhances elongation by RNA polymerase II. *Proceedings of the National Academy of Sciences of the United States of America*, **94**, 11205-11209.
46. Geijer, M.E. and Marteijn, J.A. (2018) What happens at the lesion does not stay at the lesion: Transcription-coupled nucleotide excision repair and the effects of DNA damage on transcription in cis and trans. *DNA repair*, **71**, 56-68.
47. Lans, H., Hoeijmakers, J.H.J., Vermeulen, W. and Marteijn, J.A. (2019) The DNA damage response to transcription stress. *Nature reviews. Molecular cell biology*.
48. Selby, C.P. and Sancar, A. (1997) Human transcription-repair coupling factor CSB/ERCC6 is a DNA-stimulated ATPase but is not a helicase and does not disrupt the ternary transcription complex of stalled RNA polymerase II. *The Journal of biological chemistry*, **272**, 1885-1890.
49. Fousteri, M., Vermeulen, W., van Zeeland, A.A. and Mullenders, L.H. (2006) Cockayne syndrome A and B proteins differentially regulate recruitment of chromatin remodeling and repair factors to stalled RNA polymerase II in vivo. *Molecular cell*, **23**, 471-482.
50. Fischer, E.S., Scrima, A., Bohm, K., Matsumoto, S., Lingaraju, G.M., Faty, M., Yasuda, T., Cavadini, S., Wakasugi, M., Hanaoka, F. *et al.* (2011) The molecular basis of CRL4DDB2/CSA ubiquitin ligase architecture, targeting, and activation. *Cell*, **147**, 1024-1039.
51. Groisman, R., Kuraoka, I., Chevallier, O., Gaye, N., Magnaldo, T., Tanaka, K., Kisselev, A.F., Harel-Bellan, A. and Nakatani, Y. (2006) CSA-dependent degradation of CSB by the ubiquitin-proteasome pathway establishes a link between complementation factors of the Cockayne syndrome. *Genes & development*, **20**, 1429-1434.
52. Schwertman, P., Lagarou, A., Dekkers, D.H., Raams, A., van der Hoek, A.C., Laffeber, C., Hoeijmakers, J.H., Demmers, J.A., Fousteri, M., Vermeulen, W. *et al.* (2012) UV-sensitive syndrome protein UVSSA recruits USP7 to regulate transcription-coupled repair. *Nature genetics*, **44**, 598-602.
53. Zhang, X., Horibata, K., Saijo, M., Ishigami, C., Ukai, A., Kanno, S., Tahara, H., Neilan, E.G., Honma, M., Nohmi, T. *et al.* (2012) Mutations in UVSSA cause UV-sensitive syndrome and destabilize ERCC6 in transcription-coupled DNA repair. *Nature genetics*, **44**, 593-597.
54. Yokoi, M., Masutani, C., Maekawa, T., Sugasawa, K., Ohkuma, Y. and Hanaoka,

F. (2000) The xeroderma pigmentosum group C protein complex XPC-HR23B plays an important role in the recruitment of transcription factor IIH to damaged DNA. *The Journal of biological chemistry*, **275**, 9870-9875.

55. Bernardes de Jesus, B.M., Bjoras, M., Coin, F. and Egly, J.M. (2008) Dissection of the molecular defects caused by pathogenic mutations in the DNA repair factor XPC. *Molecular and cellular biology*, **28**, 7225-7235.
56. Okuda, M., Nakazawa, Y., Guo, C., Ogi, T. and Nishimura, Y. (2017) Common TFIIH recruitment mechanism in global genome and transcription-coupled repair subpathways. *Nucleic acids research*, **45**, 13043-13055.
57. Tapias, A., Auriol, J., Forget, D., Enzlin, J.H., Scharer, O.D., Coin, F., Coulombe, B. and Egly, J.M. (2004) Ordered conformational changes in damaged DNA induced by nucleotide excision repair factors. *The Journal of biological chemistry*, **279**, 19074-19083.
58. Compe, E. and Egly, J.M. (2012) TFIIH: when transcription met DNA repair. *Nature reviews. Molecular cell biology*, **13**, 343-354.
59. Coin, F., Oksenych, V., Mocquet, V., Groh, S., Blattner, C. and Egly, J.M. (2008) Nucleotide excision repair driven by the dissociation of CAK from TFIIH. *Molecular cell*, **31**, 9-20.
60. Oksenych, V., Bernardes de Jesus, B., Zhovmer, A., Egly, J.M. and Coin, F. (2009) Molecular insights into the recruitment of TFIIH to sites of DNA damage. *The EMBO journal*, **28**, 2971-2980.
61. Camenisch, U., Dip, R., Schumacher, S.B., Schuler, B. and Naegeli, H. (2006) Recognition of helical kinks by xeroderma pigmentosum group A protein triggers DNA excision repair. *Nature structural & molecular biology*, **13**, 278-284.
62. Li, C.L., Golebiowski, F.M., Onishi, Y., Samara, N.L., Sugasawa, K. and Yang, W. (2015) Tripartite DNA Lesion Recognition and Verification by XPC, TFIIH, and XPA in Nucleotide Excision Repair. *Molecular cell*, **59**, 1025-1034.
63. Marteijn, J.A., Hoeijmakers, J.H. and Vermeulen, W. (2015) Check, Check ...Triple Check: Multi-Step DNA Lesion Identification by Nucleotide Excision Repair. *Molecular cell*, **59**, 885-886.
64. Sugasawa, K., Akagi, J., Nishi, R., Iwai, S. and Hanaoka, F. (2009) Two-step recognition of DNA damage for mammalian nucleotide excision repair: Directional binding of the XPC complex and DNA strand scanning. *Molecular cell*, **36**, 642-653.
65. Kokic, G., Chernev, A., Tegunov, D., Dienemann, C., Urlaub, H. and Cramer, P.

(2019) Structural basis of TFIIH activation for nucleotide excision repair. *Nature communications*, **10**, 2885.

66. de Laat, W.L., Appeldoorn, E., Sugasawa, K., Weterings, E., Jaspers, N.G. and Hoeijmakers, J.H. (1998) DNA-binding polarity of human replication protein A positions nucleases in nucleotide excision repair. *Genes & development*, **12**, 2598-2609.
67. Tsodikov, O.V., Ivanov, D., Orelli, B., Staresincic, L., Shoshani, I., Oberman, R., Scharer, O.D., Wagner, G. and Ellenberger, T. (2007) Structural basis for the recruitment of ERCC1-XPF to nucleotide excision repair complexes by XPA. *The EMBO journal*, **26**, 4768-4776.
68. Orelli, B., McClendon, T.B., Tsodikov, O.V., Ellenberger, T., Niedernhofer, L.J. and Scharer, O.D. (2010) The XPA-binding domain of ERCC1 is required for nucleotide excision repair but not other DNA repair pathways. *The Journal of biological chemistry*, **285**, 3705-3712.
69. Dunand-Sauthier, I., Hohl, M., Thorel, F., Jaquier-Gubler, P., Clarkson, S.G. and Scharer, O.D. (2005) The spacer region of XPG mediates recruitment to nucleotide excision repair complexes and determines substrate specificity. *The Journal of biological chemistry*, **280**, 7030-7037.
70. Zotter, A., Luijsterburg, M.S., Warmerdam, D.O., Ibrahim, S., Nigg, A., van Cappellen, W.A., Hoeijmakers, J.H., van Driel, R., Vermeulen, W. and Houtsmuller, A.B. (2006) Recruitment of the nucleotide excision repair endonuclease XPG to sites of UV-induced dna damage depends on functional TFIIH. *Molecular and cellular biology*, **26**, 8868-8879.
71. Ito, S., Kuraoka, I., Chymkowitch, P., Compe, E., Takedachi, A., Ishigami, C., Coin, F., Egly, J.M. and Tanaka, K. (2007) XPG stabilizes TFIIH, allowing transactivation of nuclear receptors: implications for Cockayne syndrome in XP-G/CS patients. *Molecular cell*, **26**, 231-243.
72. Staresincic, L., Fagbemi, A.F., Enzlin, J.H., Gourdin, A.M., Wijgers, N., Dunand-Sauthier, I., Giglia-Mari, G., Clarkson, S.G., Vermeulen, W. and Scharer, O.D. (2009) Coordination of dual incision and repair synthesis in human nucleotide excision repair. *The EMBO journal*, **28**, 1111-1120.
73. Kemp, M.G., Reardon, J.T., Lindsey-Boltz, L.A. and Sancar, A. (2012) Mechanism of release and fate of excised oligonucleotides during nucleotide excision repair. *The Journal of biological chemistry*, **287**, 22889-22899.
74. Ogi, T., Limsirichaikul, S., Overmeer, R.M., Volker, M., Takenaka, K., Cloney,

R., Nakazawa, Y., Niimi, A., Miki, Y., Jaspers, N.G. *et al.* (2010) Three DNA polymerases, recruited by different mechanisms, carry out NER repair synthesis in human cells. *Molecular cell*, **37**, 714-727.

75. Moser, J., Kool, H., Giakzidis, I., Caldecott, K., Mullenders, L.H. and Fousteri, M.I. (2007) Sealing of chromosomal DNA nicks during nucleotide excision repair requires XRCC1 and DNA ligase III alpha in a cell-cycle-specific manner. *Molecular cell*, **27**, 311-323.
76. van Cuijk, L., Vermeulen, W. and Marteijn, J.A. (2014) Ubiquitin at work: the ubiquitous regulation of the damage recognition step of NER. *Experimental cell research*, **329**, 101-109.
77. Dijk, M., Typas, D., Mullenders, L. and Pines, A. (2014) Insight in the multilevel regulation of NER. *Experimental cell research*, **329**, 116-123.
78. Dantuma, N.P. and van Attikum, H. (2016) Spatiotemporal regulation of posttranslational modifications in the DNA damage response. *The EMBO journal*, **35**, 6-23.
79. Novarina, D., Amara, F., Lazzaro, F., Plevani, P. and Muzi-Falconi, M. (2011) Mind the gap: keeping UV lesions in check. *DNA repair*, **10**, 751-759.
80. Steurer, B. and Marteijn, J.A. (2017) Traveling Rocky Roads: The Consequences of Transcription-Blocking DNA Lesions on RNA Polymerase II. *Journal of molecular biology*, **429**, 3146-3155.
81. Lans, H., Marteijn, J.A. and Vermeulen, W. (2012) ATP-dependent chromatin remodeling in the DNA-damage response. *Epigenetics & chromatin*, **5**, 4.
82. Mandemaker, I.K., Vermeulen, W. and Marteijn, J.A. (2014) Gearing up chromatin: A role for chromatin remodeling during the transcriptional restart upon DNA damage. *Nucleus*, **5**, 203-210.
83. Hu, J., Choi, J.H., Gaddameedhi, S., Kemp, M.G., Reardon, J.T. and Sancar, A. (2013) Nucleotide excision repair in human cells: fate of the excised oligonucleotide carrying DNA damage in vivo. *The Journal of biological chemistry*, **288**, 20918-20926.
84. Orren, D.K., Selby, C.P., Hearst, J.E. and Sancar, A. (1992) Post-incision steps of nucleotide excision repair in Escherichia coli. Disassembly of the UvrBC-DNA complex by helicase II and DNA polymerase I. *The Journal of biological chemistry*, **267**, 780-788.
85. Manelyte, L., Guy, C.P., Smith, R.M., Dillingham, M.S., McGlynn, P. and Savery, N.J. (2009) The unstructured C-terminal extension of UvrD interacts

with UvrB, but is dispensable for nucleotide excision repair. *DNA repair*, **8**, 1300-1310.

86. Husain, I., Van Houten, B., Thomas, D.C., Abdel-Monem, M. and Sancar, A. (1985) Effect of DNA polymerase I and DNA helicase II on the turnover rate of UvrABC excision nuclease. *Proceedings of the National Academy of Sciences of the United States of America*, **82**, 6774-6778.
87. Unk, I., Hajdu, I., Blastyak, A. and Haracska, L. (2010) Role of yeast Rad5 and its human orthologs, HLTF and SHPRH in DNA damage tolerance. *DNA repair*, **9**, 257-267.
88. Kile, A.C., Chavez, D.A., Bacal, J., Eldirany, S., Korzhnev, D.M., Bezsonova, I., Eichman, B.F. and Cimprich, K.A. (2015) HLTF's Ancient HIRAN Domain Binds 3' DNA Ends to Drive Replication Fork Reversal. *Molecular cell*, **58**, 1090-1100.
89. Unk, I., Hajdu, I., Fatyol, K., Hurwitz, J., Yoon, J.H., Prakash, L., Prakash, S. and Haracska, L. (2008) Human HLTF functions as a ubiquitin ligase for proliferating cell nuclear antigen polyubiquitination. *Proceedings of the National Academy of Sciences of the United States of America*, **105**, 3768-3773.
90. Blastyak, A., Hajdu, I., Unk, I. and Haracska, L. (2010) Role of double-stranded DNA translocase activity of human HLTF in replication of damaged DNA. *Molecular and cellular biology*, **30**, 684-693.
91. Achar, Y.J., Balogh, D. and Haracska, L. (2011) Coordinated protein and DNA remodeling by human HLTF on stalled replication fork. *Proceedings of the National Academy of Sciences of the United States of America*, **108**, 14073-14078.
92. Motegi, A., Liaw, H.J., Lee, K.Y., Roest, H.P., Maas, A., Wu, X., Moinova, H., Markowitz, S.D., Ding, H., Hoeijmakers, J.H. *et al.* (2008) Polyubiquitination of proliferating cell nuclear antigen by HLTF and SHPRH prevents genomic instability from stalled replication forks. *Proceedings of the National Academy of Sciences of the United States of America*, **105**, 12411-12416.
93. Achar, Y.J., Balogh, D., Neculai, D., Juhasz, S., Morocz, M., Gali, H., Dhe-Paganon, S., Venclovas, C. and Haracska, L. (2015) Human HLTF mediates postreplication repair by its HIRAN domain-dependent replication fork remodelling. *Nucleic acids research*, **43**, 10277-10291.
94. Masuda, Y., Mitsuyuki, S., Kanao, R., Hishiki, A., Hashimoto, H. and Masutani, C. (2018) Regulation of HLTF-mediated PCNA polyubiquitination by RFC and PCNA monoubiquitination levels determines choice of damage tolerance

pathway. *Nucleic acids research*, **46**, 11340-11356.

95. Choi, J.H., Gaddameedhi, S., Kim, S.Y., Hu, J., Kemp, M.G. and Sancar, A. (2014) Highly specific and sensitive method for measuring nucleotide excision repair kinetics of ultraviolet photoproducts in human cells. *Nucleic acids research*, **42**, e29.
96. Choi, J.H., Kim, S.Y., Kim, S.K., Kemp, M.G. and Sancar, A. (2015) An Integrated Approach for Analysis of the DNA Damage Response in Mammalian Cells: NUCLEOTIDE EXCISION REPAIR, DNA DAMAGE CHECKPOINT, AND APOPTOSIS. *The Journal of biological chemistry*, **290**, 28812-28821.
97. Overmeer, R.M., Moser, J., Volker, M., Kool, H., Tomkinson, A.E., van Zeeland, A.A., Mullenders, L.H. and Fousteri, M. (2011) Replication protein A safeguards genome integrity by controlling NER incision events. *The Journal of cell biology*, **192**, 401-415.
98. Hanasoge, S. and Ljungman, M. (2007) H2AX phosphorylation after UV irradiation is triggered by DNA repair intermediates and is mediated by the ATR kinase. *Carcinogenesis*, **28**, 2298-2304.
99. Lange, S.S., Takata, K. and Wood, R.D. (2011) DNA polymerases and cancer. *Nature reviews. Cancer*, **11**, 96-110.
100. DiGiovanna, J.J. and Kraemer, K.H. (2012) Shining a light on xeroderma pigmentosum. *The Journal of investigative dermatology*, **132**, 785-796.
101. Ljungman, M. and Lane, D.P. (2004) Transcription - guarding the genome by sensing DNA damage. *Nature reviews. Cancer*, **4**, 727-737.
102. Nakazawa, Y., Sasaki, K., Mitsutake, N., Matsuse, M., Shimada, M., Nardo, T., Takahashi, Y., Ohyama, K., Ito, K., Mishima, H. *et al.* (2012) Mutations in UVSSA cause UV-sensitive syndrome and impair RNA polymerase IIo processing in transcription-coupled nucleotide-excision repair. *Nature genetics*, **44**, 586-592.
103. Spivak, G. (2005) UV-sensitive syndrome. *Mutation research*, **577**, 162-169.
104. Laugel, V. (2013) Cockayne syndrome: the expanding clinical and mutational spectrum. *Mechanisms of ageing and development*, **134**, 161-170.
105. Karikkineth, A.C., Scheibye-Knudsen, M., Fivenson, E., Croteau, D.L. and Bohr, V.A. (2017) Cockayne syndrome: Clinical features, model systems and pathways. *Ageing research reviews*, **33**, 3-17.
106. Wienholz, F., Zhou, D., Turkyilmaz, Y., Schwertman, P., Tresini, M., Pines, A., van Toorn, M., Bezstarosti, K., Demmers, J.A.A. and Marteijn, J.A. (2019) FACT subunit Spt16 controls UVSSA recruitment to lesion-stalled RNA Pol II

and stimulates TC-NER. *Nucleic acids research*, **47**, 4011-4025.

107. Mayne, L.V. and Lehmann, A.R. (1982) Failure of RNA synthesis to recover after UV irradiation: an early defect in cells from individuals with Cockayne's syndrome and xeroderma pigmentosum. *Cancer research*, **42**, 1473-1478.
108. Bregman, D.B., Halaban, R., van Gool, A.J., Henning, K.A., Friedberg, E.C. and Warren, S.L. (1996) UV-induced ubiquitination of RNA polymerase II: a novel modification deficient in Cockayne syndrome cells. *Proceedings of the National Academy of Sciences of the United States of America*, **93**, 11586-11590.
109. Menoni, H., Hoeijmakers, J.H. and Vermeulen, W. (2012) Nucleotide excision repair-initiating proteins bind to oxidative DNA lesions in vivo. *The Journal of cell biology*, **199**, 1037-1046.
110. Banerjee, D., Mandal, S.M., Das, A., Hegde, M.L., Das, S., Bhakat, K.K., Boldogh, I., Sarkar, P.S., Mitra, S. and Hazra, T.K. (2011) Preferential repair of oxidized base damage in the transcribed genes of mammalian cells. *The Journal of biological chemistry*, **286**, 6006-6016.
111. Guo, J., Hanawalt, P.C. and Spivak, G. (2013) Comet-FISH with strand-specific probes reveals transcription-coupled repair of 8-oxoGuanine in human cells. *Nucleic acids research*, **41**, 7700-7712.
112. Stevnsner, T., Muftuoglu, M., Aamann, M.D. and Bohr, V.A. (2008) The role of Cockayne Syndrome group B (CSB) protein in base excision repair and aging. *Mechanisms of ageing and development*, **129**, 441-448.
113. Batenburg, N.L., Thompson, E.L., Hendrickson, E.A. and Zhu, X.D. (2015) Cockayne syndrome group B protein regulates DNA double-strand break repair and checkpoint activation. *The EMBO journal*, **34**, 1399-1416.
114. Teng, Y., Yadav, T., Duan, M., Tan, J., Xiang, Y., Gao, B., Xu, J., Liang, Z., Liu, Y., Nakajima, S. *et al.* (2018) ROS-induced R loops trigger a transcription-coupled but BRCA1/2-independent homologous recombination pathway through CSB. *Nature communications*, **9**, 4115.
115. Enoiu, M., Jiricny, J. and Scharer, O.D. (2012) Repair of cisplatin-induced DNA interstrand crosslinks by a replication-independent pathway involving transcription-coupled repair and translesion synthesis. *Nucleic acids research*, **40**, 8953-8964.
116. Iyama, T., Lee, S.Y., Berquist, B.R., Gileadi, O., Bohr, V.A., Seidman, M.M., McHugh, P.J. and Wilson, D.M., 3rd. (2015) CSB interacts with SNM1A and promotes DNA interstrand crosslink processing. *Nucleic acids research*, **43**, 247-

258.

117. Natale, V. and Raquer, H. (2017) Xeroderma pigmentosum-Cockayne syndrome complex. *Orphanet journal of rare diseases*, **12**, 65.
118. Kashiyama, K., Nakazawa, Y., Pilz, D.T., Guo, C., Shimada, M., Sasaki, K., Fawcett, H., Wing, J.F., Lewin, S.O., Carr, L. *et al.* (2013) Malfunction of nuclease ERCC1-XPF results in diverse clinical manifestations and causes Cockayne syndrome, xeroderma pigmentosum, and Fanconi anemia. *American journal of human genetics*, **92**, 807-819.
119. Theil, A.F., Nonnekens, J., Steurer, B., Mari, P.O., de Wit, J., Lemaitre, C., Marteijn, J.A., Raams, A., Maas, A., Vermeij, M. *et al.* (2013) Disruption of TTDA results in complete nucleotide excision repair deficiency and embryonic lethality. *PLoS genetics*, **9**, e1003431.
120. de Boer, J., Andressoo, J.O., de Wit, J., Huijmans, J., Beems, R.B., van Steeg, H., Weeda, G., van der Horst, G.T., van Leeuwen, W., Themmen, A.P. *et al.* (2002) Premature aging in mice deficient in DNA repair and transcription. *Science*, **296**, 1276-1279.
121. Vermeulen, W., Rademakers, S., Jaspers, N.G., Appeldoorn, E., Raams, A., Klein, B., Kleijer, W.J., Hansen, L.K. and Hoeijmakers, J.H. (2001) A temperature-sensitive disorder in basal transcription and DNA repair in humans. *Nature genetics*, **27**, 299-303.
122. Kraemer, K.H., Patronas, N.J., Schiffmann, R., Brooks, B.P., Tamura, D. and DiGiovanna, J.J. (2007) Xeroderma pigmentosum, trichothiodystrophy and Cockayne syndrome: a complex genotype-phenotype relationship. *Neuroscience*, **145**, 1388-1396.
123. Dulbecco, R. (1949) Reactivation of ultra-violet-inactivated bacteriophage by visible light. *Nature*, **163**, 949.
124. Thompson, C.L. and Sancar, A. (2002) Photolyase/cryptochrome blue-light photoreceptors use photon energy to repair DNA and reset the circadian clock. *Oncogene*, **21**, 9043-9056.
125. Sancar, G.B. (1990) DNA photolyases: physical properties, action mechanism, and roles in dark repair. *Mutation research*, **236**, 147-160.
126. Todo, T., Takemori, H., Ryo, H., Ihara, M., Matsunaga, T., Nikaido, O., Sato, K. and Nomura, T. (1993) A new photoreactivating enzyme that specifically repairs ultraviolet light-induced (6-4)photoproducts. *Nature*, **361**, 371-374.
127. Husain, I., Sancar, G.B., Holbrook, S.R. and Sancar, A. (1987) Mechanism of

damage recognition by Escherichia coli DNA photolyase. *The Journal of biological chemistry*, **262**, 13188-13197.

128. Sancar, A. (2008) Structure and function of photolyase and in vivo enzymology: 50th anniversary. *The Journal of biological chemistry*, **283**, 32153-32157.
129. Huang, Y., Baxter, R., Smith, B.S., Partch, C.L., Colbert, C.L. and Deisenhofer, J. (2006) Crystal structure of cryptochrome 3 from Arabidopsis thaliana and its implications for photolyase activity. *Proceedings of the National Academy of Sciences of the United States of America*, **103**, 17701-17706.
130. Wang, H., Saxena, C., Quan, D., Sancar, A. and Zhong, D. (2005) Femtosecond dynamics of flavin cofactor in DNA photolyase: radical reduction, local solvation, and charge recombination. *The journal of physical chemistry. B*, **109**, 1329-1333.
131. Kim, S.T., Malhotra, K., Smith, C.A., Taylor, J.S. and Sancar, A. (1994) Characterization of (6-4) photoproduct DNA photolyase. *The Journal of biological chemistry*, **269**, 8535-8540.
132. Todo, T., Ryo, H., Yamamoto, K., Toh, H., Inui, T., Ayaki, H., Nomura, T. and Ikenaga, M. (1996) Similarity among the Drosophila (6-4)photolyase, a human photolyase homolog, and the DNA photolyase-blue-light photoreceptor family. *Science*, **272**, 109-112.
133. Zhao, X., Liu, J., Hsu, D.S., Zhao, S., Taylor, J.S. and Sancar, A. (1997) Reaction mechanism of (6-4) photolyase. *The Journal of biological chemistry*, **272**, 32580-32590.
134. Houtsmuller, A.B. and Vermeulen, W. (2001) Macromolecular dynamics in living cell nuclei revealed by fluorescence redistribution after photobleaching. *Histochemistry and cell biology*, **115**, 13-21.
135. Vermeulen, W. (2011) Dynamics of mammalian NER proteins. *DNA repair*, **10**, 760-771.

Chapter 4

FACT subunit Spt16 controls UVSSA recruitment to lesion-stalled RNA Pol II and stimulates TC-NER

Franziska Wienholz[1], Di Zhou[1,#], Yasemin Turkyilmaz[1,#], Petra Schwertman[1], Maria Tresini[1], Alex Pines[1], Marvin van Toorn[1], Karel Bezstarosti[2], Jeroen A. Demmers[2] and Jurgen A. Marteijn[1,*]

[1] Department of Molecular Genetics, Oncode Institute, Erasmus MC, Wytemaweg 80, 3015 CN Rotterdam, the Netherlands.
[2] Proteomics Centre, Erasmus University Medical Center, P.O. Box 1738, 3000 DR, Rotterdam, the Netherlands.
[#] These authors contributed equally

Published: Nucleic Acids Research, Volume 47, Issue 8, 07 May 2019, Pages 4011–4025, https://doi.org/10.1093/nar/gkz055

ABSTRACT

Transcription-coupled nucleotide excision repair (TC-NER) is a dedicated DNA repair pathway that removes transcription-blocking DNA lesions (TBLs). TC-NER is initiated by the recognition of lesion-stalled RNA Polymerase II (Pol II) by the joint action of the TC-NER factors CSA, CSB and UVSSA. However, the exact recruitment mechanism of these factors toward TBLs remains elusive. Here, we study the recruitment mechanism of UVSSA using live-cell imaging and show that UVSSA accumulates at TBLs independent of CSA and CSB. Furthermore, using UVSSA deletion mutants, we could separate the CSA interaction function of UVSSA from its DNA damage recruitment activity, which is mediated by the UVSSA VHS and DUF2043 domains, respectively. Quantitative interaction proteomics showed that the Spt16 subunit of the histone chaperone FACT interacts with UVSSA, which is mediated by the DUF2043 domain. Spt16 is recruited to TBLs, independently of UVSSA, to stimulate UVSSA recruitment and TC-NER-mediated repair. Spt16 specifically affects UVSSA, as Spt16 depletion did not affect CSB recruitment, highlighting that different chromatin-modulating factors regulate different reaction steps of the highly orchestrated TC-NER pathway.

INTRODUCTION

Eukaryotic gene transcription by RNA Polymerase II (Pol II) is crucial for proper cell function. However, different types of DNA lesions can damage the Pol II template, thereby severely impeding or even stalling the progression of elongating Pol II. These transcription-blocking DNA lesions (TBLs) can originate from endogenous or exogenous sources; for example, metabolic byproducts may induce oxidative DNA damage or UV-light induces helix-distorting lesions such as CPDs (1-3). TBLs pose a direct problem for cellular homeostasis due to a lack of newly synthesized RNA or to the formation of mutant RNA molecules. In addition, prolonged stalling of Pol II may result in collisions with advancing replication forks and may induce R-loop formation (4). TBLs can therefore cause genome instability, severe cellular dysfunction, premature cell death, and senescence, which finally may result in DNA damage induced, accelerated aging (5-7).

To overcome these cytotoxic TBLs, cells are endowed with transcription-coupled nucleotide excision repair (TC-NER). TC-NER is a dedicated branch of the nucleotide excision repair pathway that specifically repairs TBLs in the transcribed strand of active genes, thereby resolving lesions that stall RNA Pol II and subsequently allowing transcription to restart (4,8). The importance of TC-NER is best shown by its causative link with the Cockayne Syndrome (CS) and the UV-sensitivity syndrome ($UV^{S}S$) (6,9,10). CS is caused by mutations in *CSA* and *CSB (11,12),* while mutations in *UVSSA* give rise to $UV^{S}S$ (13-15). Despite a similar deficiency in the repair of UV-induced TBLs, the CS and $UV^{S}S$ phenotypes are strikingly different (6,9,10). CS is characterized by photosensitivity, growth failure, progressive neurodevelopmental defects, and premature aging (10,16), while $UV^{S}S$ has a far less severe phenotype, which is restricted to cutaneous photosensitivity, such as freckling and pigmentation abnormalities (9).

The recognition of lesion-stalled Pol II by Cockayne Syndrome protein B (CSB) is assumed to be the initiating signal for TC-NER (17-19). In unperturbed conditions, the transcription elongation factor CSB transiently interacts with elongating Pol II; however, this interaction becomes more stable when Pol II is stalled at a TBL (18,20). In line with this, recent cryo-EM studies of Rad26, the yeast homolog of CSB, show that it binds DNA upstream of Pol II, where it has a key role in lesion recognition (19). Through its ATPase activity, Rad26 facilitates forward translocation of Pol II over naturally occurring pause sites or less bulky lesions. However, Rad26 cannot translocate Pol II over bulky TBLs (19). This prolonged binding of CSB to lesion-stalled Pol II

is thought to be one of the first steps in the assembly of the TC-NER complex, as for example shown by the CSB-dependent CSA translocation to the nuclear matrix following UV-induced DNA damage (21). CSA forms an E3-ubiquitin ligase complex with DDB1, Cul4A, ROC1/Rbx1 (22,23), and is involved in the ubiquitylation and subsequent degradation of CSB upon UV irradiation (24). The UV-induced degradation of CSB is counteracted by the deubiquitylating enzyme USP7, which is recruited by the TC-NER factor UV-Stimulated Scaffold Protein A (UVSSA) (13,14). Furthermore, UVSSA plays a role in the restoration of the hypo-phosphorylated form of Pol II (Pol IIa) (13) and in UV-induced ubiquitin modifications of Pol II (15), but both effects might be indirect. Recently, it was suggested that UVSSA also plays an important role in the recruitment of the transcription factor II H (TFIIH) via a direct interaction with P62 (15,25). TFIIH subsequently unwinds a stretch of approximately 30 nucleotides surrounding the damage site and is, in combination with XPA and RPA, responsible for damage verification and the orientation of the XPF/ERCC1 and XPG endonucleases, thereby playing an important role in the DNA strand specificity. Following excision of the damaged DNA, the resulting single-stranded gap is filled by DNA synthesis and sealed by DNA ligases (6).

Despite significant advances, the regulation and recruitment mechanisms of TC-NER factors to lesion-stalled Pol II is thus far not fully understood and such understanding is required for proper comprehension of the TC-NER mechanism and its disease etiology. For example, the exact recruitment mechanism of UVSSA remains under debate. Like CSB, UVSSA has affinity for Pol II in unperturbed conditions (14,18,26), and it has been suggested that this interaction is stabilized following DNA damage (13). Although UVSSA interacts with CSA (27), UVSSA accumulation at sites of UV-induced DNA damage is a CSA- and CSB-independent process (14). In contrast, the UV-induced UVSSA translocation to chromatin observed in cell fractionation assays was shown to depend on CSA (27).

To increase our understanding of the spatiotemporal build-up of the TC-NER complex and its molecular mechanism, we compared the accumulation kinetics of different TC-NER factors in living cells and studied the UVSSA recruitment in TC-NER-deficient cells in a quantitative manner. Our analysis showed that UVSSA recruitment to DNA damage occurs in a CSA- and CSB-independent manner. In addition, UVSSA deletion mutants showed that UVSSA binding to CSA and recruitment to TBLs are mediated

by distinct domains; the Vps/Hrs/STAM (VHS) domain and the domain of unknown function 2043 (DUF2043), respectively. Using these separation-of-function mutants of UVSSA, in combination with quantitative interaction proteomics, we identified the Spt16 subunit of the H2A/H2B chaperone FACT (facilitates chromatin transcription) to be involved in the UVSSA recruitment. Spt16 is recruited early in the TC-NER reaction in a UVSSA-independent manner, thereby stimulating excision of the TBLs and subsequent transcription restart after DNA damage removal. Our work establishes Spt16 as an important regulator of TC-NER-mediated repair and provides new insights into the different mechanisms involved in the recognition of lesion-stalled Pol II and how the remodeling of chromatin fine-tunes the regulation of the different stages of TC-NER.

MATERIALS AND METHODS

Plasmid constructs

GFP-tagged UVSSA deletion mutants of the DUF2043 and NLS domains amino acids 495-709 (ΔDUF), DUF2043 domain amino acids 495-605 (ΔDUFonly), C-terminal NLS amino acids 645-709 (ΔNLS) and VHS domain amino acid 1-152 (ΔVHS) domain were made by PCR amplification on pLenti CMV Hygro vector (28), containing either full length C1-UVSSA construct or N2-UVSSA (for ΔVHS) construct, with Phusion High-Fidelity DNA polymerase (M0530, New England Biosciences) using the following primers: ΔDUF Forward 5'-CACCATGGTGAGCAAGGGCGAG-3', ΔDUF Reverse 5'-CTATGCTGCCAGCTTCTGGGCCTC-3', ΔVHS Forward 5'-CACCATGTTTCAAGACACGAATGCTCGGAGT-3', ΔVHS Reverse 5'-TTACTTGTACAGCTCGTCCAT-3', ΔNLS Forward 5'-CACCATGGTGAGCAAGGGCGAG-3' and ΔNLS Reverse 5'-GCTGTACCTGGATGAGCCGAGAT-3'. PCR products were gel purified, to prevent contamination of later PCR reactions with template DNA and subsequently subcloned into pENTR™/D-TOPO® vector using pENTR™ directional TOPO® Cloning kit (Invitrogen). To generate the ΔDUFonly mutant the following primers were used to amplify the complete GFP-UVSSA construct in pENTR4-GFP-C1 (w392-1) lacking the DUF2043 domain: ΔDUFonly Forward 5'-phos-AGGGCTCGTGAGCAGCGGCG-3' ΔDUFonly Reverse 5'-phos-TGCTGCCAGCTTCTGGGCCTCC-3'. The obtained PCR fragment was used in a subsequent T4 ligation reaction to reassemble the ΔDUFonly mutant in pENTR4-GFP-C1. All constructs were cloned by recombination into the pLenti CMV Hygro destination vector (Addgene, plasmid ID: #17454) using

the Gateway LR Clonase II Enzyme Mix (Invitrogen).

Cell line generation

Full length GFP-UVSSA (14) or UVSSA deletion mutants (GFP-UVSSA ΔDUF, ΔDUFonly, ΔNLS and UVSSA ΔVHS-GFP) expressing cell lines were generated by lentiviral transduction of the indicated constructs. To that end, third-generation lentiviruses were made in HEK293T cells and were used to transduce UV^{S}S-A (TA24) SV40-immortalized cells. Fibroblasts originating from NER patients (SV40 transformed) were complemented with the respective deficient NER protein as described: GFP-CSB in CS-B (CS1AN) (18), CSA-Flag-GFP in CS-A (CS3BE) (29), XPC-GFP in XP-C (XP4PA) (30), GFP-XPA in XP-A (XP20S) (31), GFP-XPB in XP-B (XPCS2BA) (32). Vh10 (hTert) cells stably expressing GFP-DDB2 were described before (33). The generation of U2OS cells stably expressing GFP-tagged Spt16 or SSRP1 was described before (34), UV^{S}S-A (TA24) cells expressing GFP-tagged Spt16 were generated in a similar approach. TA24 GFP-Spt16 cells were complemented with FLAG-tagged UVSSA by lentiviral transduction. Gateway LR Clonase (Invitrogen) was used to recombine UVSSA-Flag from pENTR4 no ccDB (686-1, Addgene, plasmid ID: #17424) (14) to pLenti CMV Puro Dest (w118-1, Addgene, plasmid ID: #17452). The generated, rescued cell line was subjected to a combination of selection by Puromycin (2.5 μg/ml) for UVSSA-Flag and Hygromycin (5μg/ml) for Spt16-GFP. GFP-H2A (34) was stably expressed in HeLa cells (34) or in UV^{S}S-A (TA24) cells by transfection using X-treme Gene HP (Roche) according to the manufactures protocol. Cells stably expressing GFP-H2A were selected using 0.5 mg/ml G418 and FACS sorting.

Cell culture

TA24 (UV^{S}S-A), CS1AN (CS-B), CS3BE (CS-A), XP4PA (XP-C), XP20S (XP-A), XPCS2BA (XP-B), HeLa, Vh10 and U2OS cell lines were cultured in a 1:1 ratio of DMEM and Ham's F10 (Invitrogen) containing 10 % fetal calf serum (FCS, Biowest) and antibiotics at 37 °C and 5 % CO_2. For SILAC labelling, cells were cultured for 2 weeks in DMEM without lysine, arginine or leucine (AthenaES) supplemented with antibiotics, 10 % dialyzed FCS (Invitrogen) and 105 μg/ml leucine (Sigma) and either 73 μg/ml light [$^{12}C_6$]-lysine and 42 μg/ml [$^{12}C_6$,$^{14}N_4$]-arginine (Sigma) or with heavy [$^{13}C_6$]-lysine and [$^{13}C_6$,$^{15}N_4$]-arginine (Cambridge Isotope Laboratories) at 37°C and 5% CO_2.

RNA interference

Transient siRNA-mediated knock-down was achieved using Lipofectamine RNAiMAX (Invitrogen) transfection, according to the manufacturer's instruction. The siRNA oligonucleotides used, (Thermo Fisher Scientific) were as follows: CTRL (D-001210-05-20) 5'-UGGUUUACAUGUCGACUAA-3', Spt16 (L-009517-00) 5'-AGUCUAAUGUGUCCUAUAA-3', 5'-GCAUAUACCAUCGCUGUAA-3', 5'-ACACGGAUGUGCAGUUCUA-3', 5'-GUACAGCAAUUGGCGGAAA-3', SSRP1 (L-011783-00), 5'-GCUCUGGGCCAUGGACUUA-3', 5'-GGAGUUCAACGACGUCUAU-3', 5'-CGAUGAAUAUGCUGACUCU-3', 5'-AAGAAGAACUAGCCAGUAC-3', UVSSA (J-0243197-23-0002) 5'-GCUCGUGGAUCCAGCGCUU-3', Nap1 L1 (L-017274-01-0005), 5'-UAACCAUAGUUCAUCGAAAUU-3', 5'-GCGUAUAAUCCCAAGAUCAUU-3', 5'-GUUAAGGCAUAUUGAGUUAUU-3', 5'-GGAACGAGAUGCUAUACU-3'

Clonogenic survival assay

Cells were seeded in triplicate in 6-well plates (300 cells/well) and treated with a single dose of the indicated UV-C dose (254 nm; Philips TUV lamp) 1 day after seeding. After 1 week, colonies were fixed and stained in 50 % methanol, 7 % acetic acid and 0.1 % Coomassie blue and subsequently counted with the Gelcount (Oxford Optronix, Software Version 1.1.2.0). The survival was plotted as the mean percentage of colonies detected following the indicated UV-C dose compared to the mean number of colonies from the non-irradiated samples.

Live-cell confocal laser-scanning microscopy

Confocal laser-scanning microscopy images were obtained with a Leica SP5 confocal microscope using a 100x quartz objective for local UV-damage induction. Local DNA damage infliction for kinetic studies of GFP-tagged protein accumulation was performed using a 266 nm UV-C (2 mW pulsed (7.8 kHz) diode pumped solid-state laser (Rapp OptoElectronic, Hamburg) as described previously (14,35). Briefly, cells were grown on quartz cover slips and were imaged and irradiated through a 100 x 1.2 NA Ultrafluar quartz objective. During microscopy, cells were kept at 37 °C and 5% CO_2. Images were acquired using the LAS AF software (Leica) and the fluorescence intensity at the damage area was recorded over time, background corrected and normalized to pre-damage

fluorescence levels to quantify accumulation kinetics. H2A exchange on UV-C induced DNA damage was performed as described previously (34). In short, half of the nucleus was photobleached by a 488nm laser and local UV-C damage was subsequently induced in the bleached area. The recovery of fluorescence, representing histone exchange, on the UV-C damaged area and non-damaged area was quantified. Fluorescence intensities were background corrected and the fluorescence on the UV-C damaged area was normalised to the fluorescence for the non-damaged area. The indicated number of cells originate from at least 2 experiments and the results were pooled and plotted as the mean fluorescence intensity ± SEM.

Immunofluorescence

Cells were grown on 24-mm coverslips and fixed using 2% paraformaldehyde supplemented with triton X-100. Subsequently cells were permeabilized with PBS containing 0.1% triton X-100. Coverslips were washed with PBS containing 0.15% glycine and 0.5% BSA and incubated with primary antibody, FLAG M2 (1:1000) for 1–2 h at room temperature. Cells were washed three times and two times for 10 min with 0.1% triton X-100 and once with PBS containing 0.15% glycine and 0.5% BSA. To visualize primary antibodies, coverslips were incubated for 1 h with secondary antibodies labelled with ALEXA fluorochrome 594 (Invitrogen). Again cells were washed with 0.1% Triton X-100 and PBS+. Subsequently coverslips were embedded in Dapi-containing Vectashield mounting medium (Vector Laboratories). Images were obtained using a Zeiss LSM700 microscope equipped with a 63 × oil Plan-apochromat 1.4 NA oil immersion lens (Carl Zeiss Microimaging Inc.).

TC-NER specific Unscheduled DNA Synthesis (UDS)

The amplified UDS assay was performed as described (36). Briefly, XP186LV, XPC-deficient cells, seeded on 24-mm coverslips 4 days prior to the experiment were transfected with siRNA 2 days later. 1 day following transfection the medium was replaced by low-serum containing medium (Ham's F10 supplemented with 0.5 % FCS) to reduce the number of cells in S-phase. For global UV-C irradiation (8 J/m^2), a 254 nm germicidal lamp (Philips) was used. Following irradiation, cells were labelled with medium (Ham's F10 supplemented with 0.5% dialyzed FCS) containing 5-ethynyl,2'-deoxyuridine (EdU, 20 μM, ThermoFisher Scientific) and 2'-Deoxy-5-fluorouridine (Floxuridine, 1 μM, Sigma-Aldrich) for 7 h. Subsequently, cells were fixed in 3.6 % formaldehyde (Sigma-Aldrich) in PBS with 0.5% Triton X-100 (Sigma-Aldrich). EdU incorporation

was visualized using a combination of the Click-iT reaction (Invitrogen) and Tyramide Signal Amplification (ThermoFisher Scientific). The Click-it reaction was performed as described in the manufactures protocol using Azide-PEG3-Biotin Conjugate (20 μM in DMSO, Jena Bioscience), 1x Click-it reaction buffer (ThermoFisher Scientific), Copper(III)sulphate (0.1 M), and 10x Reaction buffer additive (ThermoFisher Scientific). The tyramide-based amplification was conducted as described in the manufactures protocol by using the HRP-Streptavidin conjugate (500 μg/ml, ThermoFisher Scientific) and Alexa-Fluor 488 nm labeled tyramide (ThermoFisher Scientific). Cover slips were embedded in DAPI containing Vectashield mounting medium (VectorLaboratories) and sealed using nail polish, and visualized using a Zeiss LSM700 microscope equipped with a 40x oil Plan-Apochromat 40 0.6-1.3 numerical aperture (NA) oil immersion lens (Carl Zeiss Micro imaging Inc.). TCR-UDS signal was quantified by analyzing at least 6 fields for each condition Mean nuclear fluorescence signals were quantified using ImageJ software (Version 1.48) (37). Sample analysis was performed as described (36). The mean nuclear fluorescence signal ± standard error of the mean is shown.

In vivo cross-linking and immunoprecipitation

The cross-linked immunoprecipitation procedure has been described previously (14,34). Briefly, *in vivo* cross-linking was performed by adding 1 % formaldehyde to the culture medium for 10 min at 4 °C. Cross-linked cells were scrapped and chromatin was purified. Finally, the nuclear suspension was sonicated using the Bioruptor Sonicator (Diagenode) with 6 cycles of 30 s on and 60 s off. For immunoprecipitations, equal amounts of crosslinked chromatin from all samples were incubated in RIPA buffer with 30 μl GFP-Trap-A agarose bead slurry (ChromoTek), overnight at 4 °C. Beads were collected by centrifugation, washed 5 times with RIPA buffer and GFP-tagged proteins were de-crosslinked and eluted by incubation at 95 °C for 30 min in 2x Laemmli SDS sample buffer. Samples were analyzed by western blot and loaded to 4–15% Mini-PROTEAN TGX™ Precast Protein Gels (BioRad). Gels were fixed and stained by Roti-blue (Carl Roth GmbH) according to the manufacturer's protocol.

For native IP with Benzonase, cells were lysed in IP buffer (30 mM HEPES pH 7.5, 130 mM NaCl, 1 mM MgCl2, 0.5% Triton X-100 and protease inhibitor cocktail) during for 10 min at 4 °C. Subsequently, cells were sonicated using the Bioruptor Sonicator (Diagenode) with 10 cycles of 15 s on and 45 s off, and 500 U of Benzonase (Sigma) was added to the lysates. Following 1 h of incubation, the lysates were cleared

by centrifugation and the supernatants were subjected to immunoprecipation with GFP-Trap-A agarose beads overnight at 4 °C. Beads were collected by centrifugation, washed 5 times with IP buffer and GFP-tagged proteins were eluted by incubation at 95 °C for 5 min in 2x Laemmli SDS sample buffer.

Western blot and Antibodies

Lysates were separated by SDS–PAGE and transferred to a PVDF membrane (0.45 µm). Membranes were blocked with 5% milk in PBS for 1 h at room temperature and incubated with primary antibodies raised against GFP (Roche, 11814460001), CSA/ERCC8 (Abcam, ab137033), USP7 (Bethyl, A300-033A), Spt16, SSRP1 (Santa Cruz Biotechnology, sc-28734 and sc-74536, respectively), Spt16 (Abcam, Ab56855) or Tubulin (Sigma Aldrich, clone B-5-1-2). Secondary antibodies coupled to IRDyes (LI-COR) were used to visualize proteins using an Odyssey CLx infrared scanner (LiCor).

Mass spectrometry

SDS-PAGE gel lanes were cut into 2-mm slices and subjected to in-gel reduction with dithiothreitol, alkylation with iodoacetamide and digestion with trypsin (sequencing grade; Promega), as described previously (14). Nanoflow liquid chromatography tandem mass spectrometry (nLC-MS/MS) was performed on an EASY-nLC coupled to a Q Exactive mass spectrometer (Thermo) or to an Orbitrap Fusion Tribid mass spectrometer (Thermo), both operating in positive mode. Peptide mixtures were trapped on a ReproSil C18 reversed phase column (Dr Maisch; 1.5 cm × 100 µm) at a rate of 8 µl/min. Peptides were separated on a ReproSil-C18 reversed-phase column (Dr Maisch; 15 cm × 50 µm) using a linear gradient of 0–80% acetonitrile (in 0.1% formic acid) for 170 min at a rate of 200 nl/min. The elution was directly sprayed into the electrospray ionization (ESI) source of the mass spectrometer. Spectra were acquired in continuum mode; fragmentation of the peptides was performed in data-dependent mode by HCD (Q Exactive) or CID (Orbitrap Fusion).

Raw mass spectrometry data were analyzed using the MaxQuant software suite (version 1.4.1.2) (38). A false discovery rate of 0.01 for proteins and peptides and a minimum peptide length of 7 amino acids were set. The Andromeda search engine was used to search the MS/MS spectra against the Uniprot database (taxonomy: *Homo sapiens*, release June 2013). A maximum of two missed cleavages was allowed. The peptide tolerance was set to 10 ppm and the fragment ion tolerance was set to 20 mmu for HCD spectra

(Q Exactive) or to 0.6 Da for CID spectra (Orbitrap Fusion). The enzyme specificity was set to "trypsin", and cysteine carbamidomethylation was set as a fixed modification. SILAC protein ratios were calculated as the median of all peptide ratios assigned to the protein. In addition, a posterior error probability for each MS/MS spectrum below or equal to 0.1 was required. In case the identified peptides of two proteins were the same or the identified peptides of one protein included all peptides of another protein, these proteins were combined by MaxQuant and reported as one protein group. Before further statistical analysis, known contaminants and reverse hits were removed.

RESULTS

UVSSA accumulates independently of CSA and CSB on UV-C induced DNA damage

To acquire more insights into the recruitment mechanism of UVSSA, we first quantified its accumulation at sites of DNA damage and compared this to the recruitment kinetics of the other TC-NER initiating factors, CSA and CSB. For this purpose, we used TC-NER-deficient patient cell lines that are mutated in either CSA, CSB, or UVSSA and are functionally complemented by the stable expression of GFP-tagged versions of the respective full-length TC-NER factors (14,18,29) (Supplemental Figure 1A and B). Accumulation kinetics of these TC-NER factors at sites of local UV-C laser-induced (266 nm) DNA damage were determined using quantitative live-cell confocal imaging (35). GFP-UVSSA and GFP-CSB recruitment at sites of locally UV-induced DNA damage (LUD) was clearly visible and showed a similar, swift, 2-fold accumulation (Figure 1A and B). Interestingly, despite the fact that CSA is a crucial TC-NER factor (5) and has been shown to directly interact with both UVSSA and CSB (13,24,27) (Figure 2C), its accumulation at sites of LUD was barely detectable (Figure 1A and B). This might be explained by a transient binding of CSA to the TC-NER complex. Furthermore, the almost complete absence of CSA at LUD makes it unlikely that UVSSA recruitment to the TC-NER complex is mediated via a direct protein–protein interaction with CSA. In line with this assumption, we have previously shown that UVSSA accumulation can still be detected at sites of UV-C-induced DNA damage in the absence of functional CSA and CSB (14). However, as these experiments do not rule out that CSA or CSB might have more subtle effects on UVSSA recruitment kinetics, e.g., reduced accumulating rates or levels, we determined the accumulation of GFP-UVSSA in time in a quantitative manner in CSA- and CSB-deficient cells and compared this to that in TC-NER-proficient cells (complemented UV^{S}S-A patient cell

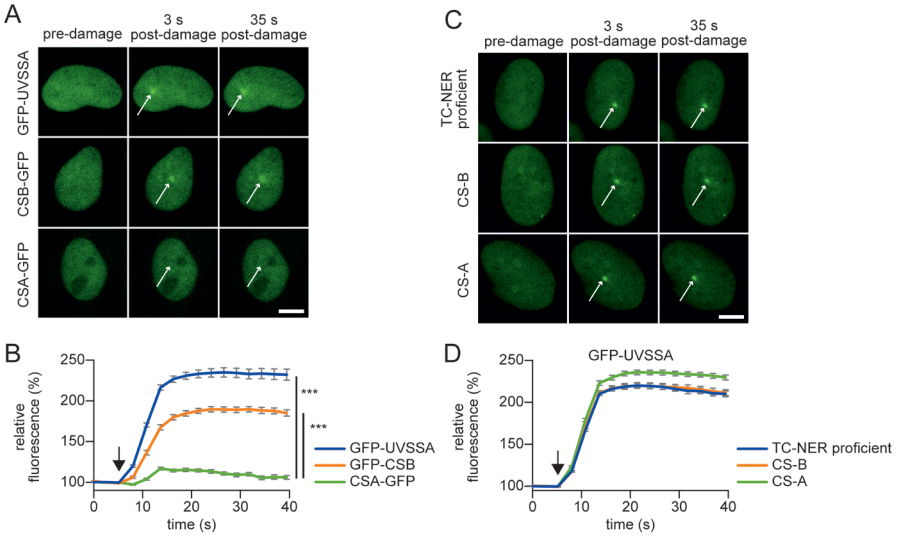

Figure 1: Accumulation kinetics of TC-NER factors reveal a CSA independent UVSSA recruitment. **(A)** Representative images of live cell imaging analysis of GFP-UVSSA, GFP-CSB or CSA-GFP at the indicated time points following local UV-C laser (266nm) induced damage (LUD) in a sub-nuclear region (indicated by a white arrow). Scale bar: 7.5 μm. **(B)** Relative accumulation of the indicated GFP-tagged TC-NER factors. GFP fluorescence intensity at LUD was quantified over time and normalised to pre-damage intensity set at 100 at t=0 (n = 25 cells of 2 independent experiments, mean ± SEM). The moment of damage induction is indicated with a black arrow. A one-way Anova test was performed and P-values <0.001 (***) are depicted. **(C)** Representative images of GFP-UVSSA accumulation at the indicated time points at LUD (indicated by a white arrow). GFP-UVSSA is expressed to functionally complement UVSS-A cells (TC-NER proficient cells) or GFP-UVSSA expressed in CS-A and CS-B cell lines. Scale bar: 7.5 μm. **(D)** Relative accumulation of GFP-UVSSA in the indicated cell lines. GFP fluorescence intensity at LUD of was quantified over time and normalised to pre-damage intensity set at 100 at t=0 (n = 30 cells, 2 independent experiments, mean ± SEM). The moment of damage induction is indicated with a black arrow.

line) (Figure 1C and D). GFP-UVSSA was recruited with the same kinetics in TC-NER-proficient cells as in CSA- or CSB-deficient cells, indicating that UVSSA accumulation is not influenced by CSA or CSB activities.

The VHS and DUF2043 domains of UVSSA have distinct functions and are both required for TC-NER

To gain insight into the mechanism of UVSSA recruitment to TBLs, we tested which domain of UVSSA is involved in this process. Therefore, we stably expressed two GFP-

tagged UVSSA deletion mutants in UVSSA-deficient TA24 cells, in which either the C-terminal DUF2043 domain (ΔDUF) or the N-terminal VHS domain (ΔVHS) (15) was deleted (Figure 2A). In contrast to expression of the full-length GFP-UVSSA (wt), cells expressing either ΔDUF or ΔVHS UVSSA mutants showed similar UV-hypersensitivity as UVSSA-deficient cells (Figure 2B), indicating that both the DUF2043 and VHS domains are essential for TC-NER. In line with previous data that mapped the CSA interaction domain to the N-terminus of UVSSA (27), immunoprecipitation experiments showed that the deletion of the N-terminal VHS domain resulted in the complete loss of CSA interaction, while this interaction remained unaffected in the ΔDUF mutant (Figure 2C and Supplemental Figure 2A). Of note, the ΔVHS mutant could still interact with the known UVSSA interaction partner USP7, indicating that the ΔVHS mutant is at least partially functional. Like the wt UVSSA, the ΔVHS mutant showed strict nuclear localization (Figure 2D). However, the ΔDUF mutant featured an additional cytoplasmic localization, which may have been caused by the deletion of the predicted C-terminal nuclear localization signal (NLS) (15). Despite its partial cytoplasmic localization, a significant fraction of the ΔDUF mutant remained present in the nucleus, in line with the retained interaction with the nuclear TC-NER factor CSA (21) (Figure 2C). Subsequently, we quantified the recruitment kinetics of these UVSSA mutants to DNA damage. While the ΔVHS mutant accumulated to the same level as wt UVSSA, the recruitment of the ΔDUF mutant to sites of local DNA damage was severely reduced (Figure 2D, E). To test whether the partial cytoplasmic localization of the ΔDUF mutant influences the UVSSA accumulation at DNA lesions, we generated two additional mutants in which either the DUF2043 domain alone (ΔDUFonly) or the C-terminal-predicted NLS domain (ΔNLS) was removed (Supplemental Figure 2B and C). In contrast to the ΔDUF mutant, the ΔDUFonly mutant was specially localized to the nucleus (Supplemental Figure 2D). However, deletion of the DUF2043 domain still severely reduced the accumulation of UVSSA at DNA damage (Supplemental Figure 2E). Deletion of the NLS alone (ΔNLS) did not affect the UVSSA accumulation. Surprisingly, this ΔNLS mutant was also localized mainly in the nucleus, suggesting that the region that is deleted in the ΔDUF mutant, located between the DUF2043 domain and the predicted NLS sequence, is important for the nuclear localization of UVSSA (Supplemental Figure 2B and D). Together our data show a clear separation-of-function of the UVSSA domains; the VHS domain is crucial for CSA interaction, while the DUF2043 domain plays an important role during the UVSSA recruitment to DNA damage. Importantly, in line with the unaffected UVSSA accumulation in CS-A

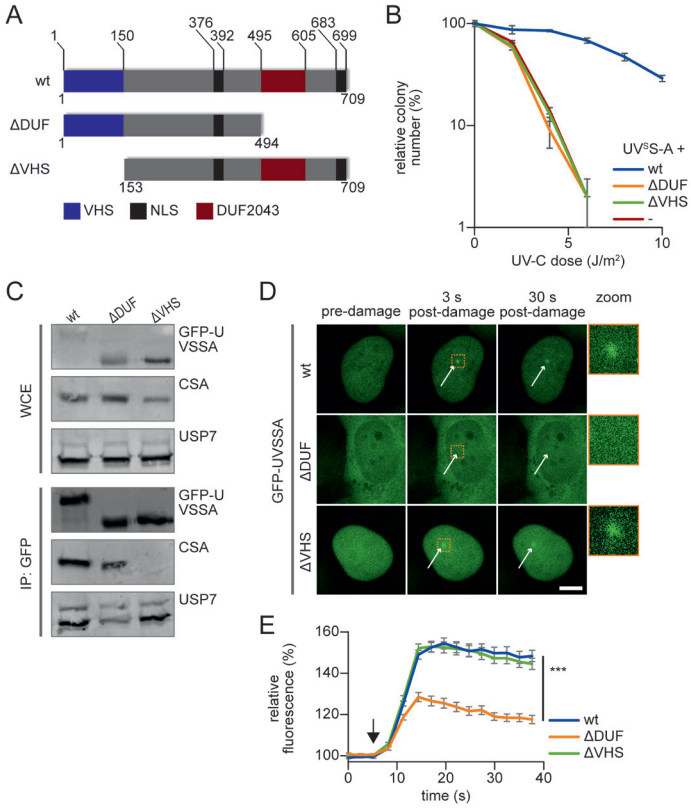

Figure 2: CSA interaction and recruitment to DNA damage is mediated by distinct UVSSA domains. **(A)** Schematic overview of the protein domains present in UVSSA and the used UVSSA deletion mutants that either lack the VHS domain (ΔVHS) or the DUF2043 domain (ΔDUF). NLS: nuclear localization signal. **(B)** UV sensitivity of UVSS-A cells (-) and UVSS-A cells complemented with GFP-UVSSA (wt), GFP-UVSSA ΔDUF (ΔDUF) or UVSSA ΔVHS-GFP (ΔVHS) was determined by their colony-forming ability, following irradiation with the indicated UV-C doses. The percentage of surviving colonies is plotted against the UV-C dose. The number of colonies counted at 0 J/m^2 is set as 100% survival. Data represents the experiment conducted in triplicate and error bars represent SEM. **(C)** Whole cell extracts (WCE) of UVSS-A patient cells stably expressing the indicated constructs were subjected to GFP immunoprecipitation. Western blot analysis of the immunoprecipitated proteins was performed using GFP, CSA or USP7 antibodies. WCE: whole-cell extract, IP: Immunoprecipitate. **(D)** Representative images of live cell imaging analysis of GFP-UVSSA or ΔDUF and ΔVHS mutants following local UV-C laser (266nm) induced damage (indicated by a white arrow). Scale bar: 7.5 μm. Right panel: 4x zoomed image to visualize accumulation at 3s post-damage induction. **(E)** GFP fluorescence intensity of the indicated constructs at LUD was quantified over time and normalised to pre-damage intensity set at 100 at t=0 (n = 30 cells of 2 independent experiments, mean ± SEM). A one-way Anova test was performed and P-values <0.001 (***) are depicted. The moment of damage induction is indicated with a black arrow.

cells, these data further show that UVSSA recruitment to TBLs is a CSA-independent process.

Identification of UVSSA-interacting proteins

To identify proteins that are involved in recruiting UVSSA to DNA damage, we set out to identify UVSSA-interacting proteins using SILAC-based quantitative interaction proteomics. UVSSA-containing protein complexes were isolated using GFP-nanotrap pulldowns (39) in UV^{S}S-A cells stably complemented with GFP-UVSSA. UV^{S}S-A cells expressing free GFP were used as a control for non-specific binding proteins. All experiments were conducted in duplicates with a label swap and only proteins identified in both independent experiments (forward and reverse) with a $\log_2$ SILAC ratio of GFP-UVSSA/GFP above 0.6 were considered as specific UVSSA-interacting proteins. Results were visualized by plotting the $\log_2$ SILAC ratios of proteins of the two independent experiments (Figure 3A and Supplemental Table 1). In total, 66 specific UVSSA interactors were identified (Figure 3A, indicated in blue and orange). The bait UVSSA was identified with the highest SILAC ratio followed by USP7, a known UVSSA interactor (13,14,40), confirming the validity of our approach. To identify biological processes associated with these UVSSA-interacting proteins, we performed a Gene Ontology (GO) enrichment analysis. As expected, the biological process of DNA repair was among the top enriched GO annotations (Figure 3B). In addition, several of the top enriched GO terms were proteins involved in chromatin remodeling, suggesting that UVSSA interactors are involved in this process. Chromatin remodeling has been shown to play an important role in TC-NER (41-43), for example by enhancing the recruitment of TC-NER factors to DNA damage (44).

To pinpoint which proteins, from the 66 identified UVSSA interactors, are involved in the recruitment of UVSSA to DNA damage, we hypothesized that these proteins would retain their interaction with the ΔVHS mutant (the mutant that can localize to DNA damage), but might have lost binding with the ΔDUF mutant (the mutant that is not recruited to damage). Therefore, we performed quantitative proteomics experiments to map which of the identified UVSSA interactors are lost in the respective UVSSA deletion mutants (Supplemental Table 2). We compared proteins interacting with GFP-UVSSA (wt) to proteins interacting with GFP-UVSSA ΔVHS (Figure 3C) or GFP-UVSSA (wt) to GFP-UVSSA ΔDUF (Figure 3D). Log_2 SILAC ratios around 0 indicate that proteins are equally bound to wt UVSSA as they are bound to the respective deletion mutant,

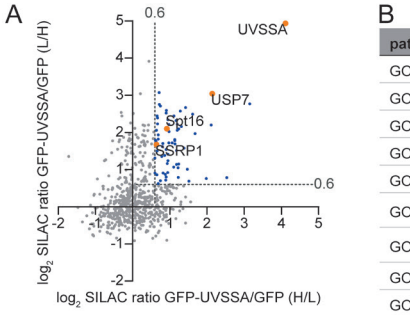

B

pathway ID	pathway description	GC	FDR
GO.0051276	chromosome organization	33	1.59E-24
GO.0032392	DNA geometric change	14	1.38E-19
GO.0032508	DNA duplex unwinding	12	3.55E-16
GO.0071103	DNA conformation change	17	3.64E-16
GO.0006281	DNA repair	19	7.23E-14
GO.0006974	cellular response to DNA damage stimulus	22	9.85E-14
GO.0006271	DNA strand elongation involved in DNA replication	9	1.29E-12
GO.0006259	DNA metabolic process	20	1.71E-11
GO.0006996	organelle organization	32	3.06E-09
GO.0006325	chromatin organization	17	7.03E-09

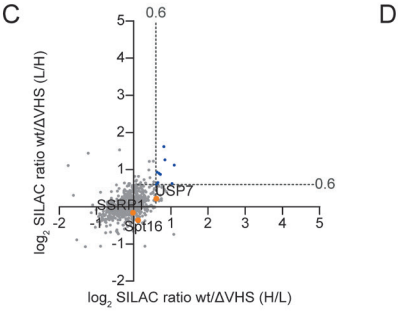

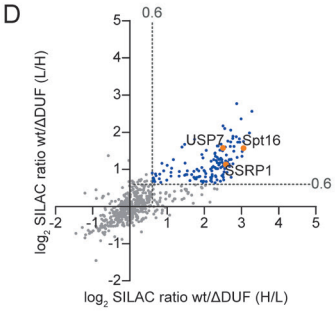

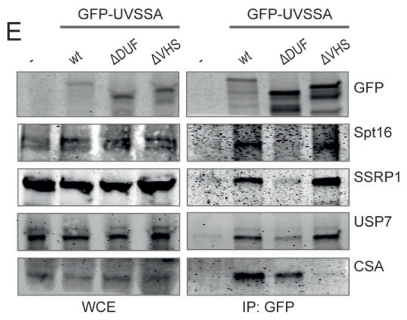

Figure 3: Quantitative interaction proteomics reveal UVSSA interaction partners and required UVSSA-domains. (A) Scatter plot of $\log_2$ SILAC ratios of proteins isolated by GFP-pulldown in UVSS-A cells stably expressing either GFP-UVSSA or GFP (non-specific binding control). The experiment was conducted in duplicate with a label swap. The $\log_2$ SILAC ratios of proteins identified in the forward experiment (GFP-UVSSA versus GFP, H/L, x-axis) are plotted against the $\log_2$ SILAC ratios of proteins identified in the reversed experiment (GFP-UVSSA versus GFP, L/H, y-axis). Proteins were classified as specific UVSSA interactors (marked in blue) when $\log_2$ SILAC ratio > 0.6 (indicated by grey dotted line) in both replicates. **(B)** GO-term analysis of the 66 proteins identified as specific interactors of UVSSA. A selection of the top 10 enriched biological process pathways is shown. GC: gene count, FDR: false discovery

rate. **(C)** Scatter plot of $\log_2$ SILAC ratios of proteins identified in the GFP-pulldowns of wt UVSSA versus ΔVHS, only proteins that were also identified in the GFP-UVSSA versus GFP proteomics experiment are depicted. The experiment was conducted in duplicate, including a label swap. The $\log_2$ SILAC ratios of proteins identified in the forward experiment (wt versus ΔVHS, H/L, x-axis) are plotted against the $\log_2$ SILAC ratio of proteins identified in the reversed experiment (wt versus ΔVHS, L/H, y-axis). The majority of proteins have similar binding ability to the ΔVHS mutant compared to the wt ($\log_2$ SILAC ratio < 0.6, proteins marked in grey). Proteins marked in blue represent proteins whose interaction with UVSSA is decreased in the absence of the VHS domain. **(D)** Scatter plot of $\log_2$ SILAC ratios of proteins identified in the GFP-pulldowns of wt UVSSA versus ΔDUF only proteins that were also identified in the GFP-UVSSA versus GFP proteomics experiment are depicted. The experiment was conducted in duplicate, including a label swap. The $\log_2$ SILAC ratios of proteins identified in the forward experiment (wt versus ΔDUF, H/L, x-axis) are plotted against the $\log_2$ SILAC ratio of proteins identified in the reversed experiment (wt versus ΔDUF, L/H, y-axis). Proteins marked in blue have a reduced interaction with UVSSAΔDUF compared to wt (proteins are marked in blue, $\log_2$ SILAC ratio > 0.6, grey dotted line marks the threshold). **(E)** Crosslinked nuclear extracts of UVSS-A patient cell line (TA24), stably expressing the indicated constructs were subjected to GFP immunoprecipitation. Non-complemented UVSS-A patient cell line (-) was used as negative binding control. WCE: whole-cell extract, IP: Immunoprecipitation. Western blot analysis of the co-immunoprecipitated proteins was performed for GFP, Spt16, SSRP1, USP7 and CSA.

while a positive $\log_2$ SILAC ratio indicates that the interaction with the tested deletion mutant is reduced compared to that with the wt UVSSA. Remarkably, only a few interactions were lost in the ΔVHS deletion mutant (Figure 3C, marked in blue), while numerous protein interactions with UVSSA were lost in the ΔDUF mutant (Figure 3D). This shows, in contrast to the interaction of the VHS domain with CSA (Figure 2C), that the majority of the identified UVSSA interactors depend on the DUF2043 domain.

Of the 66 proteins identified as UVSSA interactors (Figure 3A, indicated in blue), 45 proteins were detected in all three proteomic screens. The SILAC ratio of 25 of these proteins remained unchanged (SILAC ratio < 1.2) in the ΔVHS mutant, indicating that the interactions between those proteins and UVSSA were similar for the wt UVSSA and the ΔVHS mutant. Since we hypothesized that proteins involved in the UVSSA recruitment to DNA damage would bind specifically to the DUF2043 domain (Figure 3D, indicated in blue), we sorted these remaining 25 proteins with descending wt/ΔDUF SILAC ratios (Supplemental Table 2). Interestingly, both the Spt16 and SSRP1 subunits of the histone chaperone complex FACT were identified as UVSSA interactors whose binding was lost most upon deletion of the DUF2043 domain.

FACT complex interaction with UVSSA is mediated by the DUF2043 domain

The H2A/H2B histone chaperone FACT is an interesting interaction partner of UVSSA, as it was originally discovered as an essential factor for productive *in vitro* Pol II transcription on chromatinized DNA (45) and plays essential roles in histone H2A/H2B exchange during DNA transcription and replication (46,47). Interestingly, recent studies have shown that FACT is involved in several DNA repair pathways (34,48-53). More specifically, Spt16 was shown to stimulate histone H2A/H2B exchange at sites of UV-induced DNA damage and to play an important role during the cellular response to TBLs by facilitating efficient restart of transcription following DNA damage removal (34). However, its exact mode of action and whether Spt16 is involved in TC-NER remains thus far unknown.

To test whether the role of Spt16 in transcription restart might be mediated via its identified interaction with UVSSA, we first confirmed the interaction between the FACT complex and UVSSA. Cross-linked immunoprecipitation experiments verified the interaction of the FACT complex with UVSSA and, as expected, with the known UVSSA interaction-partners CSA (27) and USP7 (13,14,40) (Figure 3E). This identified UVSSA–Spt16 interaction is strongly reduced when immunoprecipitation experiments are performed without cross-linking in the presence of benzonase, which degrades DNA and RNA (Supplemental Figure 3A). This indicates that the UVSSA interacts with Spt16 in a very transient manner, or that this interaction depends on the presence of RNA or DNA. In line with our proteomics data, we confirmed that FACT binding is mediated by the DUF2043 domain of UVSSA, as upon immunoprecipitation of the ΔDUF mutant Spt16 and SSRP1 could not be detected, whereas the interaction was present in the wt and ΔVHS mutant. Of note, the USP7 interaction with ΔDUF was significantly reduced, in agreement with our proteomics data (Figure 3D). However, the USP7 interaction was not completely lost, indicating that in addition to the DUF2043 domain, other UVSSA domains are also involved (40).

Spt16 enables efficient UVSSA recruitment and stimulates TC-NER-mediated damage excision

The identified UVSSA interaction with the FACT subunits SSRP1 and Spt16, together with the previously identified role of Spt16 in transcription restart, indicate that the FACT complex is involved in the function of UVSSA at sites of DNA damage. To test this, we quantified the UVSSA accumulation to sites of DNA damage in cells following

siRNA-mediated knockdown of the FACT complex. Simultaneous knockdown of both FACT subunits significantly reduced the accumulation of UVSSA at LUD (Figure 4A and B). It is noteworthy that while knock down of Spt16 alone resulted in a comparable reduction of UVSSA accumulation, depletion of its canonical binding partner SSRP1, did not affect the accumulation of UVSSA, even though SSRP1 was efficiently depleted following siRNA transfection (Figure 4C). It should be noted, as is commonly observed for heterodimeric protein complexes, that siRNA-mediated knockdown of SSRP1 also results in the reduction of Spt16 protein levels, but not to the same extent as Spt16 knockdown itself (Supplemental Figure 3B). The remaining Spt16 protein levels after SSRP1 depletion are apparently sufficient to allow UVSSA recruitment. Furthermore, Spt16 knockdown also reduced the UVSSA accumulation in CSA-deficient patient cells (Supplemental Figure 3C and D), indicating that the residual UVSSA accumulation in TC-NER-proficient cells upon Spt16 depletion is not mediated by CSA.

To test whether Spt16 depletion specifically affects UVSSA recruitment, or whether its absence inhibits the TC-NER complex assembly in general, we tested whether Spt16 depletion has a similar effect on CSB recruitment. In contrast to UVSSA, siRNA-mediated depletion of FACT did not affect CSB accumulation on UV-induced DNA damage (Figure 4D and Supplemental Figure 3E). As CSB is recruited to lesion-stalled Pol II (18), the absence of an effect of UVSSA on CSB recruitment suggests that the effect of Spt16 on UVSSA accumulation is not caused by a general effect on transcription or chromatin state. In line with this, the depletion of another H2A/H2B chaperone, the nucleosome assembly protein 1-like 1 (NAP1L1), did not interfere with UVSSA accumulation (Figure 4E and Supplemental Figure 3F, G), indicating that UVSSA accumulation is not influenced by histone chaperones in general.

In accordance with the SSRP1-independent role of Spt16 in UVSSA recruitment, Spt16 was also shown to be specifically involved in transcription restart (34). This might suggest that the observed inhibition of transcription resumption is caused by a reduced UVSSA recruitment to sites of DNA damage, thereby inhibiting TC-NER efficiency and the subsequent transcription restart. To quantify TC-NER activity, we measured unscheduled DNA synthesis (UDS) by quantifying the DNA damage-induced EdU incorporation during gap-filling synthesis, which represents the last step of NER (36). To specifically quantify the TC-NER-mediated UDS, this assay was performed in non-cycling GG-NER-deficient cells (XP-C) and combined with a signal amplification step

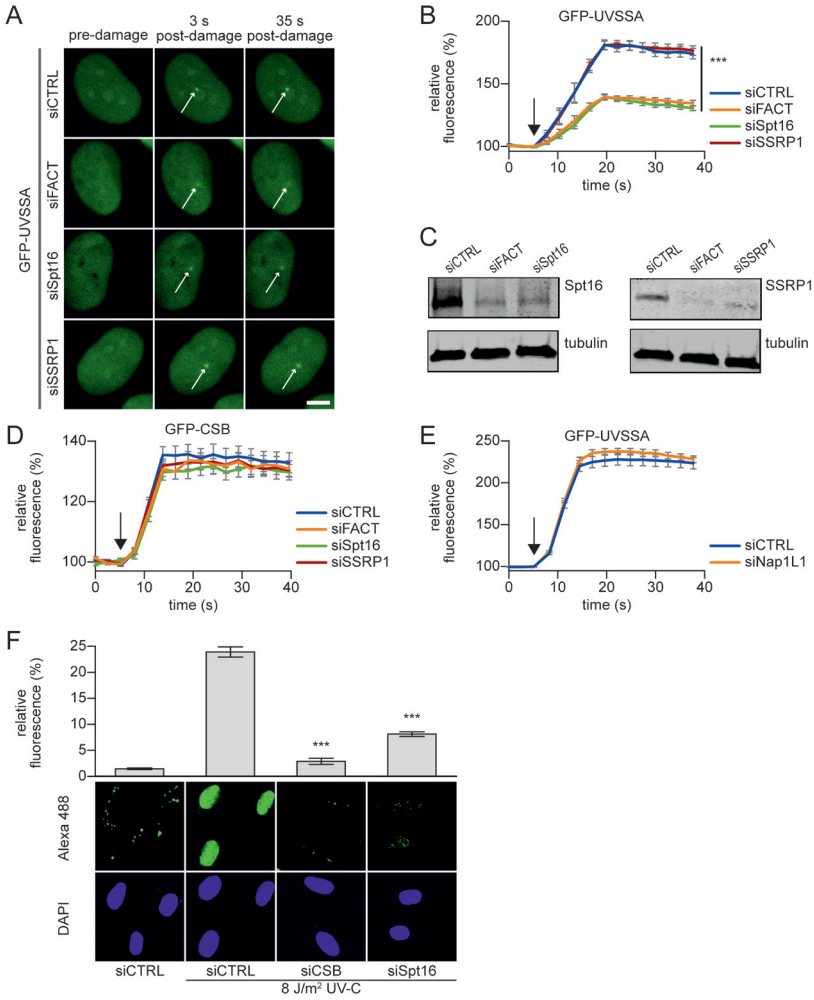

Figure 4: Spt16 mediates UVSSA accumulation on UV-C induced DNA damage. (A) Representative images of live-cell imaging analysis of GFP-UVSSA expressing cells transfected with the indicated siRNAs (CTRL is a non-targeting siRNA), following local UV-C laser (266nm) induced damage (indicated by a white arrow). Scale bar: 7.5 μm. **(B)** Relative GFP-UVSSA accumulation at sites of LUD in cells transfected with the indicated siRNA. GFP fluorescence intensity at LUD was measured over time using live-cell confocal imaging and normalised to pre-damage intensity set at 100 at t=0 (n = 30 cells of 2 independent, pooled experiments, mean ± SEM). A one-way Anova test was performed and P-values <0.001 (***) are depicted. The moment of damage induction is indicated with a black arrow. **(C)** siRNA transfected cells as used in the live-cell imaging experiments (A and B) were lysed directly after the experiment. Lysates were analysed by Western blot with the indicated antibodies. Tubulin was used as loading control. **(D)** Relative

GFP-CSB accumulation in CS-B (CS1AN) cells at sites of LUD in cells transfected with the indicated siRNA. GFP fluorescence intensity at LUD was measured over time using live-cell confocal imaging and normalised to pre-damage intensity set at 100 at t=0 (n > 25 cells of 2 independent experiments, mean ± SEM). The black arrow indicated the moment of damage induction. Representative images are shown in Supplemental Figure 1B. **(E)** Relative GFP-UVSSA accumulation at sites of LUD in control and NAP1L1 depleted cells. Representative images and knock down efficacy are shown in Supplemental Figure 1C and D respectively. GFP fluorescence intensity at LUD was measured over time using live-cell confocal imaging and normalised to pre-damage intensity set at 100 at t=0 (n > 30 cells, 2 independent experiments, mean ± SEM). The black arrow indicates the moment of damage induction. **(F)** XP186LV patient cells (XP-C; GG-NER-deficient) were transfected with non-targeting control (CTRL) siRNA and siRNA against CSB and Spt16. Cells were irradiated with UV-C (8 J/m^2) or mock-treated as indicated, and subsequently labelled for 7 h with EdU. The efficacy of the gap-filling synthesis was assessed by measuring the fluorescently labelled, incorporated EdU into the DNA. Amplified UDS signals were quantified (upper panel) by confocal microscopy measurement of the total nuclear fluorescence (Alexa-Fluor 488 nm, n>170 cells for each condition, two independent experiments, mean ± SEM) and representative images (lower panel) are shown. A two-tailed t-test was performed and P-values <0.001 (***) are depicted.

(36). In control siRNA-transfected cells, a clear UV-induced and TC-NER-specific UDS signal was observed, which was severely reduced following CSB depletion (Figure 4F). Interestingly, also upon siRNA-mediated knockdown of Spt16, the TC-NER-mediated UDS was significantly reduced. This indicates that Spt16 plays an important role in TC-NER by enhancing UVSSA recruitment, thereby subsequently stimulating transcription restart.

Spt16 function in TC-NER

Previously, we have shown that Spt16 stimulates accelerated exchange of histones H2A/H2B at sites of UV-induced damage (34). The identified interaction of Spt16 with UVSSA (Figure 3) together with the finding that both factors are recruited to DNA damage sites (14,34) (Figure 4A and 5D) prompted us to test whether UVSSA is involved in damage-induced accelerated exchange of histones H2A/H2B. Hence, we compared the UV-induced histone H2A exchange in UVSSA-proficient and -deficient cells. Histone exchange at DNA damage was determined in living cells by inducing local UV-C damage in a photobleached area of cells stably expressing GFP-H2A (34). Areas in the photobleached half of the nucleus that feature a higher histone exchange rate are characterized by an increased local GFP-H2A fluorescence due to eviction of photobleached GFP-H2A followed by incorporation of fluorescent (non-photobleached) GFP-H2A (Figure 5A). Histone exchange was quantified by comparing the recovery of GFP-H2A signal at sites of LUD with an undamaged region in the bleached part

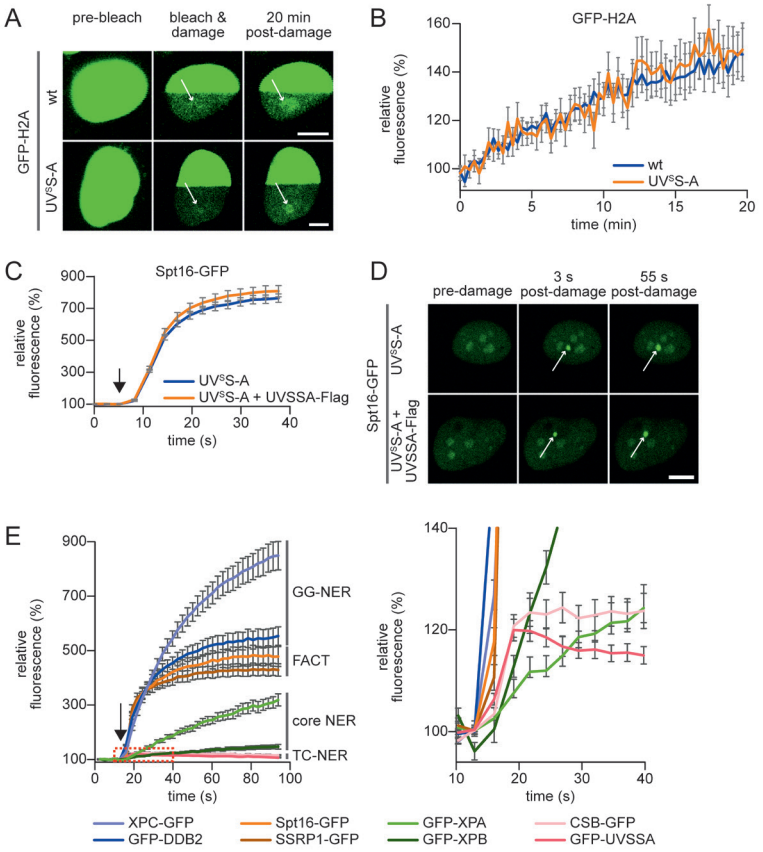

Figure 5: Spt16 is recruited to DNA damage early during TC-NER and independent of UVSSA. (A) Representative images of live-cell analysis of stable GFP-H2A expressing TC-NER proficient (HeLa cells, top panel) or UVSS-A (TA24 cells, lower panel) cells. Left panel, unbleached cells. After photobleaching half of the nucleus, (middle panel), local UV-damage (indicated with a white arrow) was inflicted with an UV-C (266 nm) laser in the bleached half of the nucleus. H2A-GFP exchange was imaged over time. Scale bar: 7.5 μm. **(B)** The recovery of fluorescence in damaged and undamaged areas of the photobleached half of the nucleus is quantified in time. GFP-H2A exchange rate at LUD is depicted, normalized to the undamaged area (n = 15 cells from 2 independent mean ± SEM). **(C)** Relative Spt16-GFP accumulation at sites of LUD in UVSS-A deficient and complemented cells. GFP fluorescence intensity at LUD was measured over time using live-cell confocal imaging and was normalised to pre-damage intensity at t=0, which was set to 100 (n = 30 cells, 2 independent experiments, mean ± SEM). The moment of damage induction is indicated with a black arrow. **(D)** Representative images of live-cell imaging analysis of Spt16-GFP expressed in either UVSS-A deficient or in UVSSA complemented (UVSSA-Flag) cells (lower panel). The white arrow indicates areas of UV-C laser (266 nm) induced DNA damage. Scale bar: 7.5 μm. **(E)** Quantification of the GFP fluorescence intensity of cells stably expressing the indicated GFP-tagged NER

proteins, GFP-tagged Spt16 or SSRP1. Cells subjected to local UV-C laser (266nm) induced DNA damage were imaged over time. All cells were imaged and damaged under the exact same conditions. Fluorescence at LUD was normalised to pre-damage fluorescence at t=0, which was set to 100 (n = 20 cells, 2 independent experiments, mean ± SEM). The moment of damage induction is indicated with a black arrow. Right graph shows zoomed graph of the indicated box, to clearly illustrate the kinetics of TC-NER factors. Representative images are shown in Supplemental Figure 2.

of the nucleus (Figure 5B). Both in UV^{S}S-A (TA24) and TC-NER-proficient cells (HeLa), a comparable UV-induced H2A exchange was observed. This indicates that the Spt16-mediated H2A exchange at sites of DNA damage is independent of UVSSA. Together with the Spt16-dependent UVSSA accumulation, this suggests that the Spt16 recruitment acts in parallel or prior to UVSSA recruitment. To verify this, we compared the accumulation of stably expressed GFP-Spt16 to LUD in UV^{S}S-A patient cells with UV^{S}S-A complemented cells (Figure 5C and D, Supplemental Figure 4A). No difference could be observed in Spt16 accumulation. Similar results were obtained in U2OS cells stably expressing Spt16-GFP in which UVSSA was depleted using siRNA (Supplemental Figure 4B and C). The observation that Spt16 enhances the UVSSA accumulation to TBLs (Figure 4B), but not vice-versa, indicates that the activity of Spt16 is needed prior to the UVSSA recruitment during TC-NER.

To test whether Spt16 is indeed a factor that is recruited at the early stages of the TC-NER reaction, we directly compared its recruitment with the accumulation kinetics of a panel of GFP-tagged NER factors that are active at different stages in the NER reaction (Figure 5E and Supplemental Figure 4D). In line with previous studies (14,54), the DNA damage-recognizing GG-NER factors XPC and DDB2 showed a swift and robust accumulation (>6-fold change), while the core NER factors (XPA and XPB) involved in the more downstream damage verification step of NER featured slower accumulation kinetics with a more modest accumulation (1.5–3-fold change). The TC-NER-specific CSB and UVSSA proteins showed a quick but very modest accumulation (~1.2-fold change). In line with a Spt16 recruitment upstream of UVSSA recruitment, Spt16 showed a very rapid accumulation. Remarkably, Spt16 showed a more pronounced accumulation (~5-fold change) than UVSSA and CSB (~1.2 fold) (Figure 5E), which might indicate a different mode of damage recruitment for Spt16 compared to TC-NER factors. Of note, even though not essential for UVSSA recruitment, SSRP1 showed similar accumulation as Spt16 (34).

Together, our data show that Spt16 functions as an early factor in the UV-DDR and plays an important role in the recruitment of UVSSA, thereby stimulating efficient transcription-coupled repair and subsequent transcription resumption.

DISCUSSION

Recognition of lesion-stalled Pol II is a crucial initiating step for damage removal by TC-NER and its tight regulation is expected to be critical for correct spatiotemporal formation of the TC-NER complex, remodeling of lesion-stalled Pol II, and for the subsequent recruitment of downstream NER factors enabling efficient excision of TBLs (8,55). To gain further insight into this regulation, we investigated in detail the spatiotemporal behavior of the TC-NER initiating proteins CSA, CSB and UVSSA. We found that in living cells, the accumulation kinetics of CSB and UVSSA were strikingly similar, which might suggest similar modes of recruitment. Both proteins have been reported to have affinity for Pol II in unperturbed conditions, and their interaction is stabilized or their affinity is increased when bound to lesion-stalled Pol II (14,18,19). Despite their highly similar recruitment kinetics, UVSSA was recruited in a CSB-independent manner. Conversely, while CSB accumulation is reduced in the absence of UVSSA (13,14), this is most likely caused not by a direct effect of UVSSA on the initial CSB recruitment but rather by the stabilization of CSB via the deubiquitylating activity of the UVSSA binding partner USP7 (13,14). Interestingly, even though the crucial TC-NER factor CSA has been shown to directly interact with both UVSSA (27) and CSB (24), it could hardly be detected at sites of UV-induced DNA damage. This absence might be explained by the fact that CSA binds transiently to the TC-NER complex. This is in line with the general highly dynamic nature of interactions of E3 ligases with their substrates. Furthermore, this suggests that, in contrast to CSB and UVSSA, CSA has no structural or scaffold-like function in the TC-NER complex. Of note, the expected short residence time of CSA on TBLs makes it unlikely that CSA is responsible for recruiting UVSSA to UV-induced DNA damage via a direct protein interaction, as previously suggested based on cellular fractionation assays (13,27).

In this study, we precisely determined the accumulation kinetics of different TC-NER factors in living cells and show that UVSSA accumulation is similar in TC-NER-proficient and CSA- and CSB-deficient cells, indicating that the recruitment of UVSSA to sites of DNA damage is not influenced by CSA or CSB. The CSA-independent accumulation of UVSSA was further shown by the use of UVSSA deletion mutants

lacking either the N-terminal VHS or the C-terminal DUF2043 domain. Of note, deletion of either domain resulted in a severe UV sensitivity and a reduced transcription resumption following irradiation (15). Interestingly, while deletion of the VHS domain resulted in the complete loss of CSA interaction (27), this mutant was recruited to DNA damage with exactly the same kinetics as full-length UVSSA. Conversely, deletion of the DUF2043 domain resulted in a severe reduction of UVSSA recruitment, without affecting the CSA interaction. These experiments show that the UVSSA recruitment at sites of TBLs can be separated from its interaction with CSA.

A plausible explanation for the apparent contradicting results on the role of CSA and CSB in the UVSSA recruitment (13,14,27,56) could be that the initial UVSSA recruitment to lesion-stalled Pol II, as determined in live-cell imaging experiments, is completely independent of CSA and CSB. However, the direct interaction between CSA and UVSSA, or another activity of CSA, might play an important role in the subsequent stabilization of the TC-NER complex. This complex-stabilizing function of CSA might explain the loss of UVSSA near TBLs in the absence of CSA (13,27), as weak or transient interactions might be lost during fractionation or immunoprecipitation assays. The CSA-independent UVSSA accumulation during live-cell experiments is also in line with previous studies. For example, the ATP-dependent chromatin remodeler SWI/SNF-related matrix-associated actin-dependent regulator of chromatin subfamily A member 5 (SMARCA5) stimulates CSB (and presumably CSA) recruitment to UV-induced DNA damage, but does not affect UVSSA recruitment (44). Furthermore, while CSA is dispensable for the recruitment of TFIIH to lesion-stalled Pol II (57), functional TFIIH is essential for the CSA translocation to damaged chromatin (58). This data, together with the recent suggestion that UVSSA recruits TFIIH (25), supports a model in which UVSSA is recruited prior to and independent of CSA. This model raises an interesting question regarding the physiological function of the observed CSA–UVSSA interaction that can be detected even in unperturbed conditions (13,15,27,29). A specific mutation in CSA (W361C), which abolishes the interaction with UVSSA, results in the development of UV^{S}S (27), indicating the importance of the CSA–UVSSA interaction for efficient TC-NER. It is tempting to speculate that the intrinsic affinity of UVSSA for CSA might be involved in the recruitment of the CRL4^{CSA} E3 ligase to DNA damage. Otherwise, as CSA has affinity for CSB as well (24), it may play an important role in the stabilization or proper conformation of the TC-NER complex.

To identify proteins involved in the recruitment of UVSSA, we performed interaction proteomics. Among the top interacting proteins were the established UVSSA binding partners USP7 and the DDB1 and CUL4B subunits of the $CRL4^{CSA}$ complex (13,14,27), showing the validity of our approach (Figure 3A). To identify factors involved in UVSSA recruitment, we assumed that their interaction would be dependent on the DUF2043 domain, which is crucial for its localization to TBLs. Interestingly, in addition to the loss of interaction with the FACT subunits Spt16 and SSRP1, many other interactions were lost upon deletion of the DUF2043 domain, suggesting that this domain is a hotspot for interactions. For example, our MS analysis shows that the DUF2043 domain is essential for the UVSSA interaction with the U2 and U5 snRNP splicing factors SF3B1, SF3B2, and PRPF8. The interactions with these U2 and U5 snRNPs might be explained by the affinity of UVSSA for elongating Pol II in both unperturbed or DNA damage conditions (14). These late-stage splicing factors have been shown to be displaced from the chromatin following TBL induction, thereby increasing R-loop formation and activation of ATM signaling (59). The identified interaction with these splicing factors might indicate a role for UVSSA in these transcription-coupled processes during the DNA damage response.

In this study, we focused on the role of Spt16 in the regulation of UVSSA and TC-NER, as we have previously identified this subunit of the H2A/H2B histone chaperone FACT to be involved in the UV-induced H2A/H2B exchange and to stimulate transcription restart following DNA damage (34). However, thus far, the exact mechanism of how Spt16 regulates TC-NER remains unknown. In line with the interaction of Spt16 being dependent on the DUF2043 domain of UVSSA, we found that Spt16 is required for the recruitment of UVSSA to damaged DNA. The ~50% reduction of UVSSA recruitment following SPT16 depletion, caused severe effects on the TC-NER-mediated repair, as shown by a strong impediment of the TC-NER-specific gap-filling synthesis. This reduced repair efficiency can explain the previously observed inhibition of transcription restart and UV sensitivity upon Spt16 knockdown (34). However, additional effects of Spt16 on the transcription restart process independent of repair, as shown for Dot1L (60), cannot be excluded. As Spt16 depletion (Figure 4B), or deletion of the DUF2043 domain (Figure 2E), does not result in a full loss of UVSSA recruitment at sites of DNA damage, it is likely that additional mechanisms and factors are involved in the recruitment of UVSSA.

The effects of Spt16 on UVSSA recruitment, as well as transcription restart and UV sensitivity (34), are independent of SSRP1, its canonical binding partner in the FACT complex. Despite being not essential for TC-NER, SSRP1 interacts with UVSSA and has similar accumulation kinetics at DNA damage sites as Spt16. Spt16 seems to be the driving force of the FACT accumulation, as the SSRP1 accumulation at UV-induced DNA damage depends on the presence of Spt16 (34). Together, this suggests that under normal conditions, the complete FACT heterodimer is present at sites of DNA damage, but in the absence of SSRP1, Spt16 can be recruited and function during TC-NER independently of SSRP1. Although, thus far, it remains unknown how Spt16 and SSRP1 are exactly recruited to sites of DNA damage, Spt16 accumulation occurs early during the repair reaction and independently of other TC-NER-initiating factors (Figure 5C-E) (34). In addition, Spt16 and SSRP1 showed, in comparative DNA damage accumulation experiments, a striking pattern. Similar to TC-NER factors, FACT accumulated almost instantaneously following DNA damage infliction. However, while CSB and UVSSA only showed a modest ~1,2-fold accumulation, FACT subunits showed a 5-fold accumulation, almost to the same extent as the highly efficient DNA damage-recognizing GG-NER factors DDB2 and XPC. This might suggest that Spt16 has, in addition to what is described for SSRP1 (50,53), damage-recognizing capabilities, either by directly recognizing the lesion, or indirectly, for example by sensing damage-induced transcription impediment. Furthermore, these differences in fold accumulation might indicate that a multitude of Spt16 molecules are present near TBLs compared to the TC-NER proteins CSB and UVSSA.

We found that H2A/H2B exchange at sites of DNA damage was independent of UVSSA. This indicates that UVSSA interaction with Spt16 is not needed to induce accelerated histone exchange at TBLs, but rather suggests that Spt16-mediated histone exchange mediates efficient UVSSA recruitment or, alternatively, that it is important for the stable incorporation of UVSSA in the TC-NER complex. However, this effect is not caused by a general inhibition of histone turnover, as knockdown of NAP1L1, another H2A/H2B chaperone, did not affect UVSSA recruitment (Figure 4E).

Although transcription and thus also TC-NER, occurs in a more open and therefore accessible chromatin state, several chromatin-remodeling enzymes were shown to be necessary for efficient repair and transcription restart (4,42). For example, Nap1L1 stimulates the ATP-dependent chromatin-remodeling activity of CSB (61). In addition,

in our UVSSA interaction screen, we also identified CHD4 as a putative TC-NER-involved chromatin remodeller (Supplemental table 1). While CHD4 has been reported to be involved in DDR (62,63), it is currently unknown whether it is involved in TC-NER. Thus far, the only two chromatin-modifying factors shown to influence accumulation of TC-NER factors are Spt16, which stimulates UVSSA recruitment, and the ATP-dependent chromatin remodeller SMARCA5, which facilitates recruitment of CSB (44). Interestingly, both factors act at specific TC-NER reaction steps; SMARCA5 does not affect UVSSA recruitment and Spt16 is not involved in the CSB recruitment. This suggests that the involvement of these chromatin modifiers in TC-NER is not restricted simply to making the chromatin accessible. The need for different chromatin-modifying enzymes for recruitment of CSB and UVSSA strengthens our observation that despite their similar accumulation kinetics, these TC-NER-initiating factors are independently recruited (14) to damaged chromatin. Furthermore, this suggests that both SMARCA5 and Spt16 stimulate specific changes in the chromatin, e.g., nucleosome sliding or histone exchange, that are important during different TC-NER reaction steps. In line with this notion, distinct functions for CSB and UVSSA during TC-NER have been described. CSB was suggested to stimulate Pol II forward translocation, analogous to the action of Mfd in prokaryotes (64), thereby discriminating between lesion-stalled Pol II and other non-forward translocating Pol II complexes, e.g., Pol II stalled on naturally occurring pause sites (19). UVSSA was shown to recruit TFIIH via a direct interaction with P62 in a similar manner as XPC recruits TFIIH in GG-NER (65). Collectively, these observations would suggest that SMARCA5 is involved in remodeling lesion-stalled Pol II, while Spt16 either recruits or allows TFIIH to properly function during the TC-NER reaction. In summary, this study provides important new insight into the regulation of TC-NER and, more specifically, into the assembly of the TC-NER complex. Furthermore, these results highlight that different chromatin-modulating factors regulate distinct steps of the highly orchestrated TC-NER pathway.

SUPPLEMENTAL TABLES

Supplemental Tables are available at NAR Online.

ACKNOWLEDGEMENTS

We thank the Optical Imaging Centre (OIC) of the Erasmus MC for support with microscopes and Dr. Arjan Theil for help with FACS sorting.

FUNDING

This work was funded by the Dutch organization for Scientific Research ZonMW TOP Grant (912.12.132), Horizon Zenith (935.11.042), Dutch organization for Scientific Research (NWO-ALW) VIDI (864.13.004) and Erasmus MC fellowship. This work is part of the Oncode Institute which is partly financed by the Dutch Cancer Society and was funded by a grant from the Dutch Cancer Society (KWF grant 10506).

CONFLICT OF INTEREST STATEMENT

None declared.

REFERENCES

1. Brueckner, F., Hennecke, U., Carell, T. and Cramer, P. (2007) CPD damage recognition by transcribing RNA polymerase II. *Science*, **315**, 859-862.
2. Shin, J.H., Xu, L. and Wang, D. (2016) RNA polymerase II acts as a selective sensor for DNA lesions and endogenous DNA modifications. *Transcription*, **7**, 57-62.
3. Vermeij, W.P., Hoeijmakers, J.H. and Pothof, J. (2014) Aging: not all DNA damage is equal. *Curr Opin Genet Dev*, **26**, 124-130.
4. Steurer, B. and Marteijn, J.A. (2017) Traveling Rocky Roads: The Consequences of Transcription-Blocking DNA Lesions on RNA Polymerase II. *J Mol Biol*, **429**, 3146-3155.
5. Hanawalt, P.C. and Spivak, G. (2008) Transcription-coupled DNA repair: two decades of progress and surprises. *Nat Rev Mol Cell Biol*, **9**, 958-970.
6. Marteijn, J.A., Lans, H., Vermeulen, W. and Hoeijmakers, J.H. (2014) Understanding nucleotide excision repair and its roles in cancer and ageing. *Nat Rev Mol Cell Biol*, **15**, 465-481.
7. Tornaletti, S. (2005) Transcription arrest at DNA damage sites. *Mutation research*, **577**, 131-145.
8. Spivak, G. (2016) Transcription-coupled repair: an update. *Arch Toxicol*, **90**, 2583-2594.
9. Spivak, G. (2005) UV-sensitive syndrome. *Mutation research*, **577**, 162-169.
10. Karikkineth, A.C., Scheibye-Knudsen, M., Fivenson, E., Croteau, D.L. and Bohr, V.A. (2017) Cockayne syndrome: Clinical features, model systems and pathways. *Ageing Res Rev*, **33**, 3-17.
11. Laugel, V. (2013) Cockayne syndrome: the expanding clinical and mutational spectrum. *Mech Ageing Dev*, **134**, 161-170.
12. Cleaver, J.E., Lam, E.T. and Revet, I. (2009) Disorders of nucleotide excision repair: the genetic and molecular basis of heterogeneity. *Nat Rev Genet*, **10**, 756-768.
13. Zhang, X., Horibata, K., Saijo, M., Ishigami, C., Ukai, A., Kanno, S., Tahara, H., Neilan, E.G., Honma, M., Nohmi, T. *et al.* (2012) Mutations in UVSSA cause UV-sensitive syndrome and destabilize ERCC6 in transcription-coupled DNA repair. *Nat Genet*, **44**, 593-597.
14. Schwertman, P., Lagarou, A., Dekkers, D.H., Raams, A., van der Hoek, A.C., Laffeber, C., Hoeijmakers, J.H., Demmers, J.A., Fousteri, M., Vermeulen, W.

et al. (2012) UV-sensitive syndrome protein UVSSA recruits USP7 to regulate transcription-coupled repair. *Nat Genet*, **44**, 598-602.

15. Nakazawa, Y., Sasaki, K., Mitsutake, N., Matsuse, M., Shimada, M., Nardo, T., Takahashi, Y., Ohyama, K., Ito, K., Mishima, H. *et al.* (2012) Mutations in UVSSA cause UV-sensitive syndrome and impair RNA polymerase IIo processing in transcription-coupled nucleotide-excision repair. *Nat Genet*, **44**, 586-592.
16. Spivak, G. (2004) The many faces of Cockayne syndrome. *Proceedings of the National Academy of Sciences of the United States of America*, **101**, 15273-15274.
17. Selby, C.P. and Sancar, A. (1997) Human transcription-repair coupling factor CSB/ERCC6 is a DNA-stimulated ATPase but is not a helicase and does not disrupt the ternary transcription complex of stalled RNA polymerase II. *J Biol Chem*, **272**, 1885-1890.
18. van den Boom, V., Citterio, E., Hoogstraten, D., Zotter, A., Egly, J.M., van Cappellen, W.A., Hoeijmakers, J.H., Houtsmuller, A.B. and Vermeulen, W. (2004) DNA damage stabilizes interaction of CSB with the transcription elongation machinery. *J Cell Biol*, **166**, 27-36.
19. Xu, J., Lahiri, I., Wang, W., Wier, A., Cianfrocco, M.A., Chong, J., Hare, A.A., Dervan, P.B., DiMaio, F., Leschziner, A.E. *et al.* (2017) Structural basis for the initiation of eukaryotic transcription-coupled DNA repair. *Nature*, **551**, 653-657.
20. Troelstra, C., van Gool, A., de Wit, J., Vermeulen, W., Bootsma, D. and Hoeijmakers, J.H. (1992) ERCC6, a member of a subfamily of putative helicases, is involved in Cockayne's syndrome and preferential repair of active genes. *Cell*, **71**, 939-953.
21. Kamiuchi, S., Saijo, M., Citterio, E., de Jager, M., Hoeijmakers, J.H. and Tanaka, K. (2002) Translocation of Cockayne syndrome group A protein to the nuclear matrix: possible relevance to transcription-coupled DNA repair. *Proceedings of the National Academy of Sciences of the United States of America*, **99**, 201-206.
22. Groisman, R., Polanowska, J., Kuraoka, I., Sawada, J., Saijo, M., Drapkin, R., Kisselev, A.F., Tanaka, K. and Nakatani, Y. (2003) The ubiquitin ligase activity in the DDB2 and CSA complexes is differentially regulated by the COP9 signalosome in response to DNA damage. *Cell*, **113**, 357-367.
23. Fischer, E.S., Scrima, A., Bohm, K., Matsumoto, S., Lingaraju, G.M., Faty, M., Yasuda, T., Cavadini, S., Wakasugi, M., Hanaoka, F. *et al.* (2011) The molecular basis of CRL4DDB2/CSA ubiquitin ligase architecture, targeting, and activation.

Cell, **147**, 1024-1039.

24. Groisman, R., Kuraoka, I., Chevallier, O., Gaye, N., Magnaldo, T., Tanaka, K., Kisselev, A.F., Harel-Bellan, A. and Nakatani, Y. (2006) CSA-dependent degradation of CSB by the ubiquitin-proteasome pathway establishes a link between complementation factors of the Cockayne syndrome. *Genes Dev*, **20**, 1429-1434.
25. Okuda, M., Higo, J., Komatsu, T., Konuma, T., Sugase, K. and Nishimura, Y.
26. de Boer, J. and Hoeijmakers, J.H. (2000) Nucleotide excision repair and human syndromes. *Carcinogenesis*, **21**, 453-460.
27. Fei, J. and Chen, J. (2012) KIAA1530 protein is recruited by Cockayne syndrome complementation group protein A (CSA) to participate in transcription-coupled repair (TCR). *J Biol Chem*, **287**, 35118-35126.
28. Campeau, E., Ruhl, V.E., Rodier, F., Smith, C.L., Rahmberg, B.L., Fuss, J.O., Campisi, J., Yaswen, P., Cooper, P.K. and Kaufman, P.D. (2009) A versatile viral system for expression and depletion of proteins in mammalian cells. *PLoS One*, **4**, e6529.
29. Pines, A., Dijk, M., Makowski, M., Meulenbroek, E.M., Vrouwe, M.G., van der Weegen, Y., Baltissen, M., French, P.J., van Royen, M.E., Luijsterburg, M.S. *et al.* (2018) TRiC controls transcription resumption after UV damage by regulating Cockayne syndrome protein A. *Nat Commun*, **9**, 1040.
30. Hoogstraten, D., Bergink, S., Ng, J.M., Verbiest, V.H., Luijsterburg, M.S., Geverts, B., Raams, A., Dinant, C., Hoeijmakers, J.H., Vermeulen, W. *et al.* (2008) Versatile DNA damage detection by the global genome nucleotide excision repair protein XPC. *J Cell Sci*, **121**, 2850-2859.
31. Rademakers, S., Volker, M., Hoogstraten, D., Nigg, A.L., Mone, M.J., Van Zeeland, A.A., Hoeijmakers, J.H., Houtsmuller, A.B. and Vermeulen, W. (2003) Xeroderma pigmentosum group A protein loads as a separate factor onto DNA lesions. *Mol Cell Biol*, **23**, 5755-5767.
32. Hoogstraten, D., Nigg, A.L., Heath, H., Mullenders, L.H.F., van Driel, R., Hoeijmakers, J.H.J., Vermeulen, W. and Houtsmuller, A.B. (2002) Rapid Switching of TFIIH between RNA Polymerase I and II Transcription and DNA Repair In Vivo. *Molecular Cell*, **10**, 1163-1174.
33. Pines, A., Vrouwe, M.G., Marteijn, J.A., Typas, D., Luijsterburg, M.S., Cansoy, M., Hensbergen, P., Deelder, A., de Groot, A., Matsumoto, S. *et al.* (2012) PARP1 promotes nucleotide excision repair through DDB2 stabilization and

recruitment of ALC1. *J Cell Biol*, **199**, 235-249.

34. Dinant, C., Ampatziadis-Michailidis, G., Lans, H., Tresini, M., Lagarou, A., Grosbart, M., Theil, A.F., van Cappellen, W.A., Kimura, H., Bartek, J. *et al.* (2013) Enhanced chromatin dynamics by FACT promotes transcriptional restart after UV-induced DNA damage. *Mol Cell*, **51**, 469-479.
35. Dinant, C., de Jager, M., Essers, J., van Cappellen, W.A., Kanaar, R., Houtsmuller, A.B. and Vermeulen, W. (2007) Activation of multiple DNA repair pathways by sub-nuclear damage induction methods. *J Cell Sci*, **120**, 2731-2740.
36. Wienholz, F., Vermeulen, W. and Marteijn, J.A. (2017) Amplification of unscheduled DNA synthesis signal enables fluorescence-based single cell quantification of transcription-coupled nucleotide excision repair. *Nucleic Acids Res*, **45**, e68.
37. Schindelin, J., Arganda-Carreras, I., Frise, E., Kaynig, V., Longair, M., Pietzsch, T., Preibisch, S., Rueden, C., Saalfeld, S., Schmid, B. *et al.* (2012) Fiji: an open-source platform for biological-image analysis. *Nat Methods*, **9**, 676-682.
38. Cox, J., Neuhauser, N., Michalski, A., Scheltema, R.A., Olsen, J.V. and Mann, M. (2011) Andromeda: a peptide search engine integrated into the MaxQuant environment. *J Proteome Res*, **10**, 1794-1805.
39. Rothbauer, U., Zolghadr, K., Muyldermans, S., Schepers, A., Cardoso, M.C. and Leonhardt, H. (2008) A versatile nanotrap for biochemical and functional studies with fluorescent fusion proteins. *Molecular & cellular proteomics : MCP*, **7**, 282-289.
40. Higa, M., Zhang, X., Tanaka, K. and Saijo, M. (2016) Stabilization of Ultraviolet (UV)-stimulated Scaffold Protein A by Interaction with Ubiquitin-specific Peptidase 7 Is Essential for Transcription-coupled Nucleotide Excision Repair. *J Biol Chem*, **291**, 13771-13779.
41. Lans, H., Marteijn, J.A. and Vermeulen, W. (2012) ATP-dependent chromatin remodeling in the DNA-damage response. *Epigenetics Chromatin*, **5**, 4.
42. Mandemaker, I.K., Vermeulen, W. and Marteijn, J.A. (2014) Gearing up chromatin: A role for chromatin remodeling during the transcriptional restart upon DNA damage. *Nucleus*, **5**, 203-210.
43. Czaja, W., Mao, P. and Smerdon, M.J. (2012) The emerging roles of ATP-dependent chromatin remodeling enzymes in nucleotide excision repair. *Int J Mol Sci*, **13**, 11954-11973.
44. Aydin, O.Z., Marteijn, J.A., Ribeiro-Silva, C., Rodriguez Lopez, A., Wijgers, N.,

Smeenk, G., van Attikum, H., Poot, R.A., Vermeulen, W. and Lans, H. (2014) Human ISWI complexes are targeted by SMARCA5 ATPase and SLIDE domains to help resolve lesion-stalled transcription. *Nucleic Acids Res*, **42**, 8473-8485.

45. Orphanides, G., LeRoy, G., Chang, C.H., Luse, D.S. and Reinberg, D. (1998) FACT, a factor that facilitates transcript elongation through nucleosomes. *Cell*, **92**, 105-116.
46. Tsunaka, Y., Fujiwara, Y., Oyama, T., Hirose, S. and Morikawa, K. (2016) Integrated molecular mechanism directing nucleosome reorganization by human FACT. *Genes Dev*, **30**, 673-686.
47. Winkler, D.D. and Luger, K. (2011) The histone chaperone FACT: structural insights and mechanisms for nucleosome reorganization. *J Biol Chem*, **286**, 18369-18374.
48. Gao, Y., Li, C., Wei, L., Teng, Y., Nakajima, S., Chen, X., Xu, J., Legar, B., Ma, H., Spagnol, S.T. *et al.* (2017) SSRP1 Cooperates with PARP and XRCC1 to Facilitate Single-Strand DNA Break Repair by Chromatin Priming. *Cancer research*, **77**, 2674-2685.
49. Charles Richard, J.L., Shukla, M.S., Menoni, H., Ouararhni, K., Lone, I.N., Roulland, Y., Papin, C., Ben Simon, E., Kundu, T., Hamiche, A. *et al.* (2016) FACT Assists Base Excision Repair by Boosting the Remodeling Activity of RSC. *PLoS Genet*, **12**, e1006221.
50. Yarnell, A.T., Oh, S., Reinberg, D. and Lippard, S.J. (2001) Interaction of FACT, SSRP1, and the high mobility group (HMG) domain of SSRP1 with DNA damaged by the anticancer drug cisplatin. *J Biol Chem*, **276**, 25736-25741.
51. Oliveira, D.V., Kato, A., Nakamura, K., Ikura, T., Okada, M., Kobayashi, J., Yanagihara, H., Saito, Y., Tauchi, H. and Komatsu, K. (2014) Histone chaperone FACT regulates homologous recombination by chromatin remodeling through interaction with RNF20. *J Cell Sci*, **127**, 763-772.
52. Keller, D.M. and Lu, H. (2002) p53 serine 392 phosphorylation increases after UV through induction of the assembly of the CK2.hSPT16.SSRP1 complex. *J Biol Chem*, **277**, 50206-50213.
53. Krohn, N.M., Stemmer, C., Fojan, P., Grimm, R. and Grasser, K.D. (2003) Protein kinase CK2 phosphorylates the high mobility group domain protein SSRP1, inducing the recognition of UV-damaged DNA. *J Biol Chem*, **278**, 12710-12715.
54. Marteijn, J.A., Bekker-Jensen, S., Mailand, N., Lans, H., Schwertman, P.,

Gourdin, A.M., Dantuma, N.P., Lukas, J. and Vermeulen, W. (2009) Nucleotide excision repair-induced H2A ubiquitination is dependent on MDC1 and RNF8 and reveals a universal DNA damage response. *J Cell Biol*, **186**, 835-847.

55. Marteijn, J.A., Hoeijmakers, J.H. and Vermeulen, W. (2015) Check, Check ...Triple Check: Multi-Step DNA Lesion Identification by Nucleotide Excision Repair. *Mol Cell*, **59**, 885-886.
56. Schwertman, P., Vermeulen, W. and Marteijn, J.A. (2013) UVSSA and USP7, a new couple in transcription-coupled DNA repair. *Chromosoma*, **122**, 275-284.
57. Fousteri, M. and Mullenders, L.H. (2008) Transcription-coupled nucleotide excision repair in mammalian cells: molecular mechanisms and biological effects. *Cell Res*, **18**, 73-84.
58. Saijo, M., Hirai, T., Ogawa, A., Kobayashi, A., Kamiuchi, S. and Tanaka, K. (2007) Functional TFIIH is required for UV-induced translocation of CSA to the nuclear matrix. *Mol Cell Biol*, **27**, 2538-2547.
59. Tresini, M., Warmerdam, D.O., Kolovos, P., Snijder, L., Vrouwe, M.G., Demmers, J.A., van, I.W.F., Grosveld, F.G., Medema, R.H., Hoeijmakers, J.H. *et al.* (2015) The core spliceosome as target and effector of non-canonical ATM signalling. *Nature*, **523**, 53-58.
60. Oksenych, V., Zhovmer, A., Ziani, S., Mari, P.O., Eberova, J., Nardo, T., Stefanini, M., Giglia-Mari, G., Egly, J.M. and Coin, F. (2013) Histone methyltransferase DOT1L drives recovery of gene expression after a genotoxic attack. *PLoS Genet*, **9**, e1003611.
61. Cho, I., Tsai, P.F., Lake, R.J., Basheer, A. and Fan, H.Y. (2013) ATP-dependent chromatin remodeling by Cockayne syndrome protein B and NAP1-like histone chaperones is required for efficient transcription-coupled DNA repair. *PLoS Genet*, **9**, e1003407.
62. Burd, C.J., Kinyamu, H.K., Miller, F.W. and Archer, T.K. (2008) UV radiation regulates Mi-2 through protein translation and stability. *J Biol Chem*, **283**, 34976-34982.
63. O'Shaughnessy, A. and Hendrich, B. (2013) CHD4 in the DNA-damage response and cell cycle progression: not so NuRDy now. *Biochem Soc Trans*, **41**, 777-782.
64. Pani, B. and Nudler, E. (2017) Mechanistic insights into transcription coupled DNA repair. *DNA Repair (Amst)*, **56**, 42-50.
65. Okuda, M., Nakazawa, Y., Guo, C., Ogi, T. and Nishimura, Y. (2017) Common

TFIIH recruitment mechanism in global genome and transcription-coupled repair subpathways. *Nucleic Acids Res*, **45**, 13043-13055.

SUPPLEMENTAL FIGURES

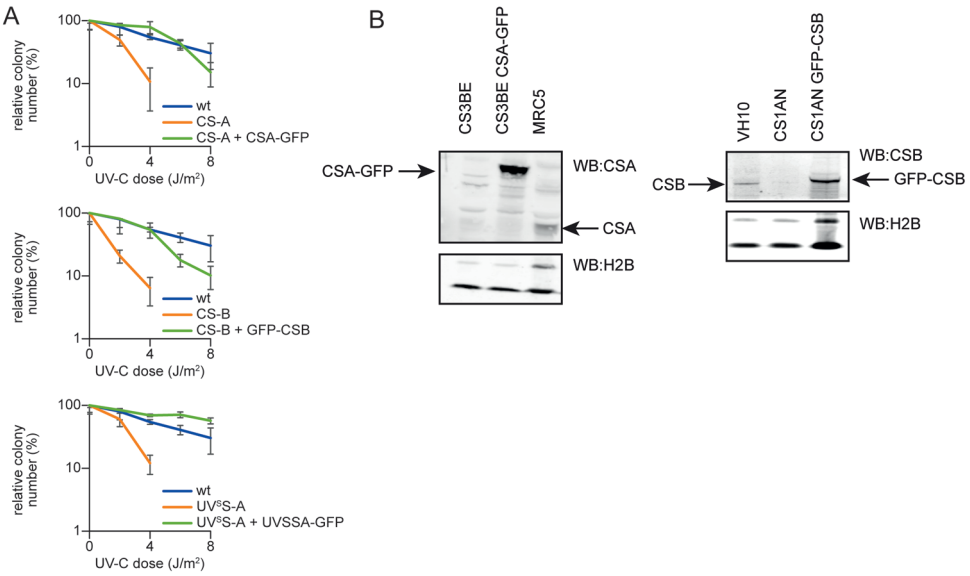

Supplemental Figure 1.

(A) Colony survival of wt (VH10), with top panel: CS-A (CS3BE) and CS-A cells complemented with CSA-GFP (CS3BE + CSA-GFP), middle panel: CS-B (CS1AN) and CS-B cells complemented with GFP-CSB, lower panel: UVSS-A (TA24) and UVSS-A cells complemented with UVSSA-GFP following irradiation with the indicated UV dose. The percentage of surviving cells, normalized to undamaged conditions is set at 100% and is plotted against the applied UV-C (J/m^2) dose. Data represent two pooled, independent experiments ± standard deviation. **(B)** Left panel: CSA expression in TC-NER proficient MRC5 cells and CSA deficient CS3BE cells with or without expression of CSA-GFP. Right panel: CSB expression in TC-NER proficient VH10 cells and CSB deficient CS1AN cells with or without expression of GFP-CSB. H2B staining is used as loading control.

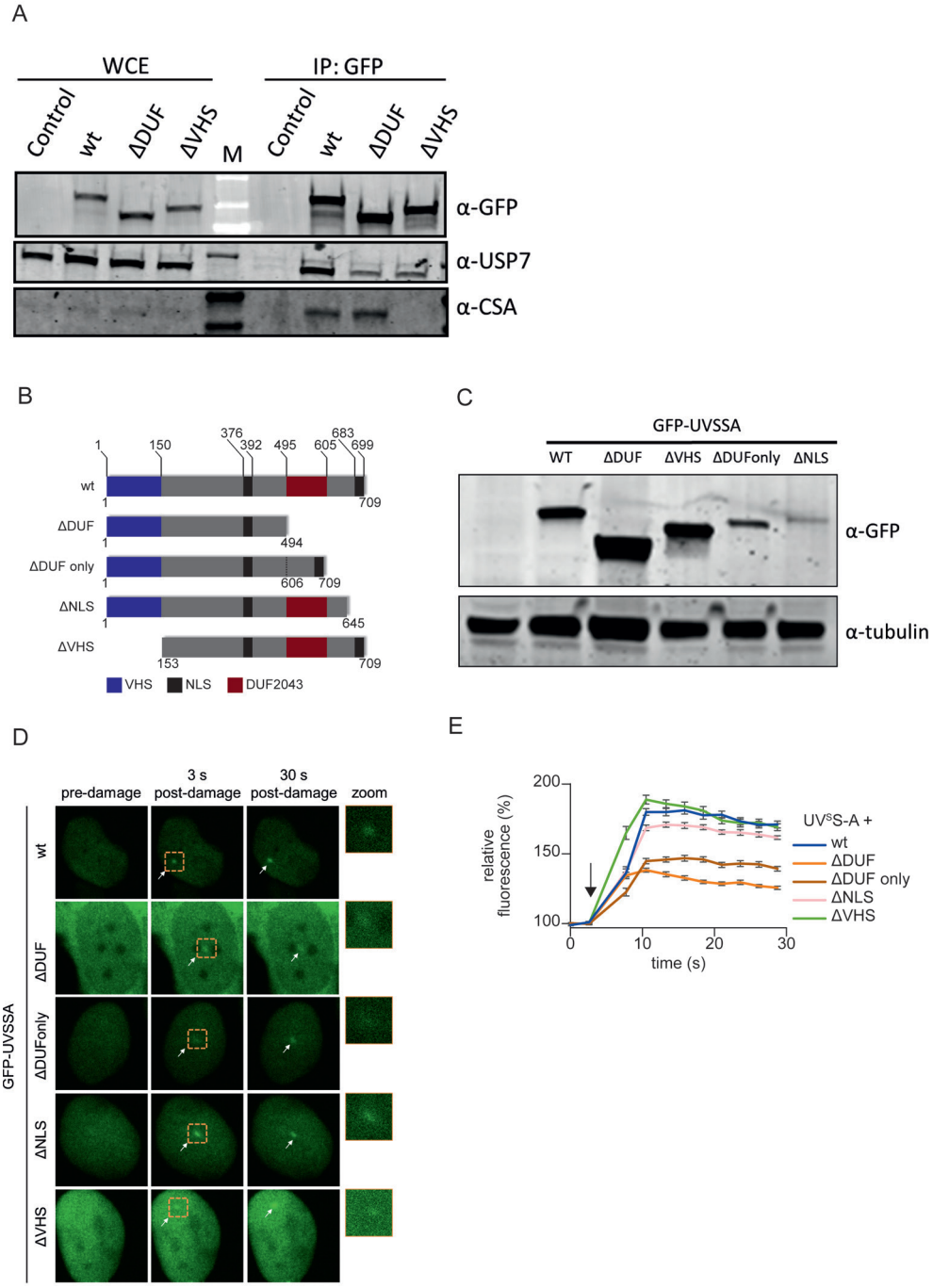
A
WCE
IP: GFP
Control
wt
ΔDUF
ΔVHS
M
Control
wt
ΔDUF
ΔVHS
α-GFP
α-USP7
α-CSA
B
1
150
376
392
495
605
683
699
wt
1
709
ΔDUF
1
494
ΔDUF only
1
606
709
ΔNLS
1
645
ΔVHS
153
709
VHS
NLS
DUF2043
C
GFP-UVSSA
WT
ΔDUF
ΔVHS
ΔDUFonly
ΔNLS
α-GFP
α-tubulin
D
pre-damage
3 s post-damage
30 s post-damage
zoom
GFP-UVSSA
wt
ΔDUF
ΔDUFonly
ΔNLS
ΔVHS
E
relative fluorescence (%)
200
150
100
0
10
20
30
time (s)
UVˢS-A +
wt
ΔDUF
ΔDUF only
ΔNLS
ΔVHS

Supplemental Figure 2.

(A) Whole cell extracts (WCE) of UVSS-A patient cells, or UVSS-A cells stably expressing the indicated GFP-UVSSA constructs were subjected to GFP immunoprecipitation. Western blot analysis of the immunoprecipitated proteins was performed using GFP, CSA or USP7 antibodies. WCE: whole-cell extract, IP: Immunoprecipitate. M: indicates protein marker. **(B)** Schematic overview of the protein domains present in UVSSA and the used UVSSA deletion mutants. NLS: nuclear localization signal. **(C)** Western blot analysis of the expression of the indicated GFP-UVSSA constructs in UVSS-A patient cells. Tubulin is used as loading control. **(D)** Representative images of live cell imaging analysis of GFP-UVSSA wt or the indicated mutants following local UV-C laser (266nm) induced damage (indicated by a white arrow). Right panel: 4x zoomed image to visualize accumulation at 3s post-damage induction. **(E)** GFP fluorescence intensity of the indicated constructs at LUD was quantified over time and normalised to pre-damage intensity set at 100 at t=0 (n=18 cells of 2 independent experiments, mean ± SEM). The moment of damage induction is indicated with a black arrow.

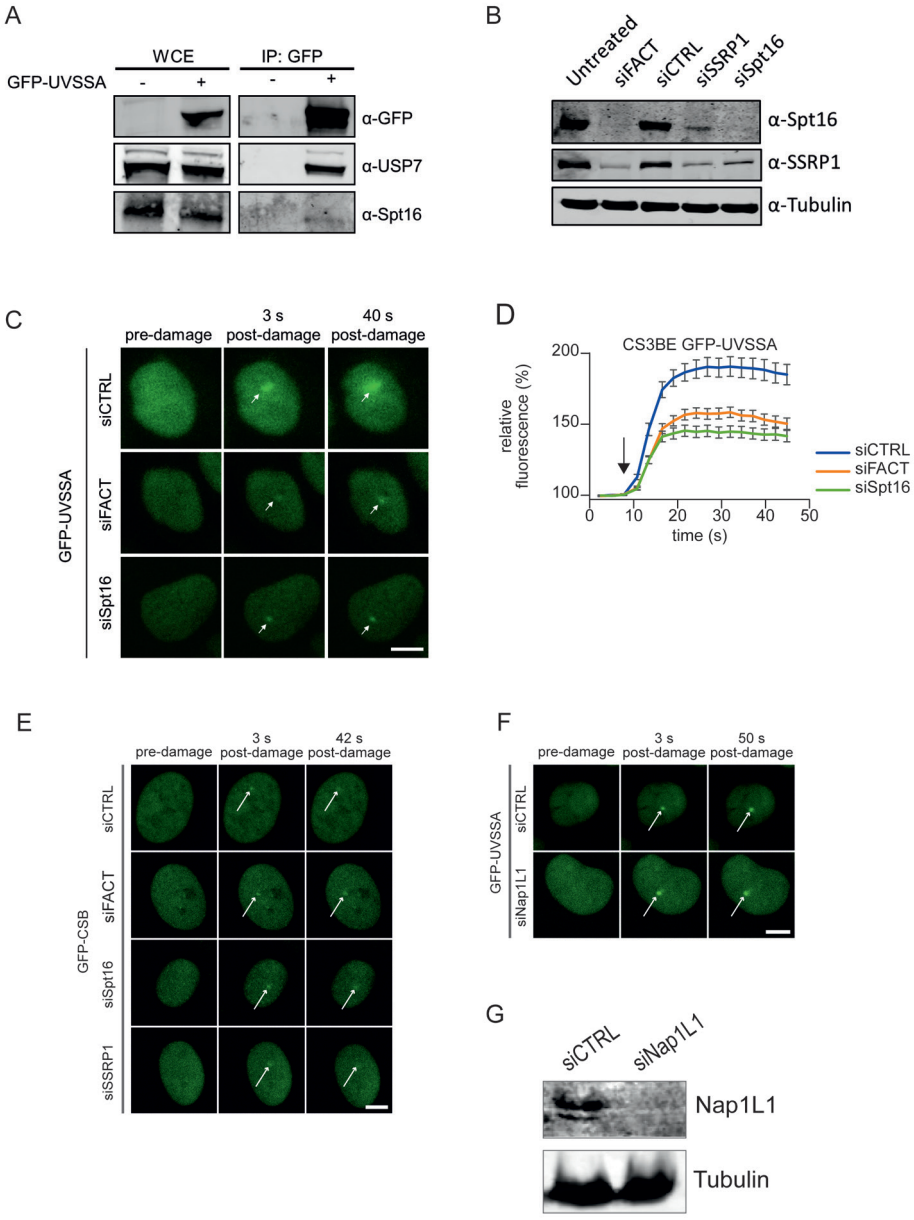
A
WCE
IP: GFP
GFP-UVSSA
- + - +
α-GFP
α-USP7
α-Spt16
B
Untreated
siFACT
siCTRL
siSSRP1
siSpt16
α-Spt16
α-SSRP1
α-Tubulin
C
pre-damage
3 s post-damage
40 s post-damage
GFP-UVSSA
siCTRL
siFACT
siSpt16
D
CS3BE GFP-UVSSA
relative fluorescence (%)
200
150
100
0 10 20 30 40 50
time (s)
siCTRL
siFACT
siSpt16
E
pre-damage
3 s post-damage
42 s post-damage
GFP-CSB
siCTRL
siFACT
siSpt16
siSSRP1
F
pre-damage
3 s post-damage
50 s post-damage
GFP-UVSSA
siCTRL
siNap1L1
G
siCTRL
siNap1L1
Nap1L1
Tubulin

Supplemental Figure 3.

(A) Benzonase treated whole cell extracts (WCE) of UVSS-A patient cells, or UVSS-A cells stably expressing GFP-UVSSA were subjected to GFP immunoprecipitation under non-crosslinked conditions. Western blot analysis of the immunoprecipitated proteins was performed using GFP, Spt16 or USP7 antibodies. WCE: whole-cell extract, IP: Immunoprecipitate. **(B)** Transfected cells with the indicated siRNAs were lysed and analysed by Western blot with the indicated antibodies. Tubulin was used as loading control. **(C)** Representative images of live-cell imaging analysis of GFP-UVSSA expressing CS-A cells (CS3BE) transfected with the indicated siRNAs (CTRL is a non-targeting siRNA), following local UV-C laser (266nm) induced damage (indicated by a white arrow). **(D)** Relative GFP-UVSSA accumulation at sites of LUD in cells transfected with the indicated siRNA. GFP fluorescence intensity at LUD was measured over time using live-cell confocal imaging and normalised to pre-damage intensity set at 100 at t=0 (n = 16 cells of 2 independent, pooled experiments, mean ± SEM). The moment of damage induction is indicated with a black arrow. **(E)** Representative images of the accumulation of CSB in CS-B (CS1AN) cells upon local DNA damage induction using a UV-C (266nm) laser. Cells were transfected with the indicated siRNAs (siFACT: combination of both siSpt16 and siSSRP1. siCTRL: is a non-targeting siRNA). GFP fluorescence intensity at LUD (indicated by a white arrow) was measured over time using live-cell confocal imaging. Scale bar: 7.5 μm. **(F)** Representative images of the accumulation of UVSS-A cells stably expressing GFP-UVSSA, transfected with CTRL or Nap1L1 siRNA. GFP fluorescence intensity was measured over time at LUD (indicated by a white arrow) using live-cell confocal imaging. Scale bar: 7.5 μm. **(G)** Knock down efficacy of Nap1L1 was determined by Western blotting using Nap1L1 antibody, tubulin is used as loading control.

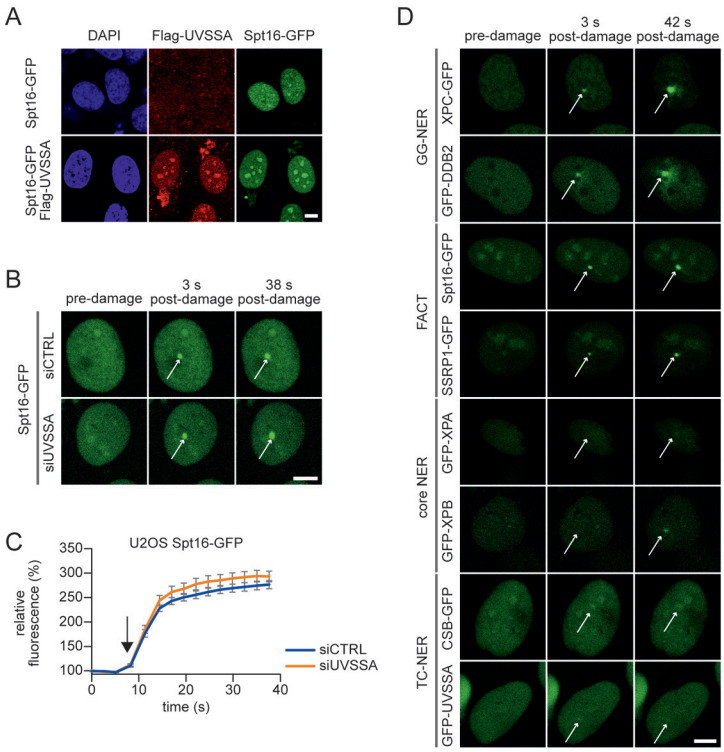

Supplemental Figure 4.

(A) UVSS-A (TA24) stably expressing Spt16-GFP (top panel) or Spt16-GFP and Flag-UVSSA (bottom panel) were subjected to immunofluorescence to determine expression of Flag-UVSSA in all cells (Alexa-Fluor 594). Nuclei were visualized by DAPI staining. **(B)** Representative images of U2OS cells stably expressing Spt16-GFP, transfected with indicated siRNA's. Spt16-GFP accumulation (indicated by a white arrow) upon local exposure to UV-C (266nm) laser-induced DNA damage was measured by monitoring GFP fluorescence intensity over time using live-cell confocal imaging. Scale bar: 7.5 μm. **(C)** Quantification of the GFP fluorescence intensity at LUD was normalised to pre-damage fluorescence at t=0, which was set to 100 (n = 30 cells of 2 independent experiments were pooled, mean ± SEM). The moment of damage induction is indicated with a black arrow. **(D)** Representative images of damage accumulation plotted in Figure 5E. Cells stably expressing the indicated GFP-tagged proteins were followed over time after UV-C laser (266nm) induced DNA damage (indicated by a white arrow). All cells expressing GFP tagged-NER factors, Spt16-GFP or SSRP1-GFP were imaged and damaged under the exact same conditions. Scale bar: 7.5 μm.

Chapter 5

Fluorescently-labelled CPD and 6-4PP photolyases: new tools for live-cell DNA damage quantification and laser-assisted repair

Barbara Steurer[1,#], Yasemin Turkyilmaz[1,#], Marvin van Toorn[1], Wessel van Leeuwen[1], Paula Escudero-Ferruz[1], Jurgen A. Marteijn[1]

[1] Department of Molecular Genetics, Oncode Institute, Erasmus MC, Wytemaweg 80, 3015 CN Rotterdam, the Netherlands.
[#] These authors contributed equally

Published: Nucleic Acids Research, Volume 47, Issue 7, 23 April 2019, Pages 3536–3549, https://doi.org/10.1093/nar/gkz035

ABSTRACT

UV light induces cyclobutane pyrimidine dimers (CPDs) and pyrimidine-pyrimidone (6-4) photoproducts (6-4PPs), which can result in carcinogenesis and aging, if not properly repaired by nucleotide excision repair (NER). Assays to determine DNA damage load and repair rates are invaluable tools for fundamental and clinical NER research. However, most current assays to quantify DNA damage and repair cannot be performed in real time. To overcome this limitation, we made use of the damage recognition characteristics of CPD and 6-4PP photolyases (PLs). Fluorescently-tagged PLs efficiently recognize UV-induced DNA damage without blocking NER activity, and therefore can be used as sensitive live-cell damage sensors. Importantly, FRAP-based assays showed that PLs bind to damaged DNA in a highly sensitive and dose-dependent manner, and can be used to quantify DNA damage load and to determine repair kinetics in real time. Additionally, PLs can instantly reverse DNA damage by 405 nm laser-assisted photo-reactivation during live-cell imaging, opening new possibilities to study lesion-specific NER dynamics and cellular responses to damage removal. Our results show that fluorescently-tagged PLs can be used as a versatile tool to sense, quantify and repair DNA damage, to study NER kinetics and UV-induced DNA damage response in living cells.

INTRODUCTION

Our genome is continuously exposed to various types of DNA damage. If not repaired correctly, DNA lesions may result in mutations, cellular senescence or cell death, which can eventually lead to various pathological conditions including carcinogenesis and aging [1]. To counteract these deleterious effects of DNA damage, cells have evolved a variety of mechanisms, including several DNA repair pathways [2]. Nucleotide excision repair (NER) is one of the most versatile DNA repair pathways, as it removes a wide variety of DNA helix-destabilizing lesions. Prominent examples of NER substrates are the UV-induced cyclobutane pyrimidine dimers (CPDs) and pyrimidine-pyrimidone (6-4) photoproducts (6-4PPs). The biological importance of NER is illustrated by the severe clinical symptoms of human disorders caused by inherited NER defects, including the cancer-prone xeroderma pigmentosum (XP) syndrome or the premature aging disorder Cockayne's syndrome (CS) [3].

NER is initiated by two sub-pathways that differ in their mode of damage recognition. Global genome NER (GG-NER) detects lesions in the entire genome, by the main DNA damage binding protein XPC [4]. XPC recognizes DNA-helix distortions such as induced by 6-4PP lesions, but needs the activity of the UV-DDB complex, composed of DDB1 and DDB2, to detect mildly helix-destabilizing CPD lesions [5, 6]. Transcription-coupled NER (TC-NER) is initiated when DNA damage located in the actively transcribed strand blocks elongating RNA polymerase II, which results in the recruitment of the TC-NER factors CSA, CSB, and UVSSA [7, 8]. Once the DNA lesion is recognized, general transcription factor II H (TFIIH) is recruited [9, 10] to unwind the DNA surrounding the damage [11] and to verify the lesion together with XPA [12, 13]. The endonucleases XPG and ERCC1/XPF subsequently remove a ~30 nucleotide long fragment of DNA around the lesion [14]. Finally, the DNA is restored back to its original state by DNA synthesis and ligation steps [15, 16].

Recent studies have shown that NER is a tightly regulated, multistep pathway that requires many proteins and post-translational modifications for the efficient and accurate transition between the successive reaction steps [3, 17-19]. Additionally, as NER takes place in the complex chromatin and nuclear environment, many factors involved in chromatin remodeling [3, 20, 21], transcription [22], or replication [23] influence NER activity, and most likely many other involved factors are awaiting their discovery. Therefore, assays to quantify DNA damage and repair rates are invaluable tools

to investigate the roles of such factors and to obtain new fundamental insights into the molecular mechanism of NER. Moreover, assays to detect impairments or deficiencies in NER activity have been crucial for the diagnosis of NER-deficient patients and can be used as indicators for predispositions to mutations, the onset of cancer, or DNA damage-induced aging [24-27].

Over the years, several assays were developed to quantitatively monitor UV-induced DNA damage and NER-mediated repair. Traditionally NER activity is measured by determining the rate of UV-induced DNA repair synthesis, the last step of the NER reaction [28-30], or by determining the levels of CPDs in the DNA in time using T4 endonuclease V [31]. Over the years several other assays have been developed to monitor upstream NER activity, including UV-damage removal [32], NER-induced incisions [33] or quantification of excision products [34]. TC-NER is often determined indirectly by quantifying the recovery of RNA synthesis (RRS) [35, 36], or by using host cell reactivation assays [37]. Alternatively, TC-NER can be measured in a direct manner by strand-specific repair assays [38], or by more recently developed single-cell assays, such as the modified COMET-FISH procedure [39], or the TC-NER specific UDS assay [40]. Direct detection and quantification of UV-induced DNA damage and its removal in time can be accomplished using antibodies specifically recognizing CPD or 6-4PP lesions in combination with immunofluorescence or ELISA procedures [32]. Although proven to be useful in studying UV-induced DNA repair, these assays depend highly on the quality of the antibodies and have specific limitations. For instance, antibody-based detection of CPD or 6-4PP lesions requires DNA denaturation, to allow DNA damage recognition by these antibodies. For example in immunofluorescence experiments, this denaturation may interfere with co-staining of other proteins of interest. Importantly, most of these assays require cell fixation, which makes them incompatible with live-cell applications, and therefore can only provide endpoint measurements. To overcome these issues, measurements of the DNA damage binding kinetics of fluorescently-tagged NER factors can be used to evaluate repair activity in living cells [41-43]. However, these binding kinetics do not provide a direct measurement of DNA damage quantities, as the DNA damage-induced binding of the NER proteins is not influenced exclusively by the DNA damage load, but can also be regulated by post-translational modifications or chromatin remodelers [42, 44-49].

While NER is the only mechanism to repair UV-induced DNA damage in placental

mammals, an alternative damage removal mechanism known as photo-reactivation (PR) remained preserved through evolution in other branches of life, ranging from bacteria to non-placental mammals, [50, 51]. In contrast to NER-mediated repair, which is a complex mechanism that requires the activity of at least 30 proteins [3], PR is the direct reversal of CPD or 6-4PP lesions by one single damage specific photolyase (PL). PLs recognize the helix distortions created by CPD and 6-4PPs and bind to them through moderately strong ionic interactions. These interactions further destabilize the distorted DNA helix and lead to a flipping out of the DNA lesion into the active site of the PL, forming a highly stable complex [52, 53]. In contrast to the binding of PLs to DNA lesions, which is independent of light, the catalytic reversal of pyrimidine dimers to the original bases requires the absorption of a photon. Catalysis by PLs is achieved by light-initiated cycloconversion of the cyclobutane ring joining the two pyrimidines, which encompasses first the adsorption of a 333-500 nm photon by the chromophore MTHF, second the energy transfer from the blue light photon to the Flavin cofactor (FADH-), and third the electron transfer from FADH- to the cyclobutane ring, which splits the pyrimidine dimer and forms a flavin radical (FADH·). The catalytic cycle is completed when the electron is transferred back to the cofactor, restoring catalytically active, fully reduced FADH- [53-55]. The entire reaction takes ~1 ns for both types of PLs [53]. The repair-independent binding of PLs to CPDs or 6-4PPs and their very fast damage removal makes PLs an attractive tool to study UV-induced damage and its repair. However thus far, PLs have mainly been used to test the specific cellular responses to either CPD or 6-4PP after removing the other type of lesion by PR [56-59].

Here we show, that fluorescently labelled PLs provide a versatile and sensitive tool to locate, quantify and repair UV-induced DNA damage in real time in living cells. Fluorescence recovery after photobleaching (FRAP)-based mobility studies of PLs allow to quantitatively determine DNA damage load, as well as repair kinetics. Furthermore, we show that PLs can be activated by the 405 nm laser light during live cell imaging experiments to photo reactivate DNA damage, which facilitates studying the behavior of NER factors and the DNA damage response upon DNA repair in living cells.

MATERIAL AND METHODS

Cell Lines and Constructs

VH10 hTERT immortalized human fibroblasts, XP4PA SV40 immortalized XP-C

fibroblasts and HCT116 human colon cancer cells were cultured in DMEM/F10 and RPMI/F10 media, respectively, containing 10% FCS and 1% penicillin-streptomycin in a humidified incubator at 37°C and 5% CO_2. To generate a lentiviral 6-4PP-PL-mCherry-3xNLS-HA expression vector, *Arabidopsis thaliana* 6-4PP-PL cDNA [60], missing the first 57 nucleotides corresponding to a mitochondrial localization signal, was first cloned into pENTR/D-TOPO vector (Invitrogen). mCherry-3xNLS-HA was ordered as gBlocks Gene Fragment (Integrated DNA technologies) and ligated to the C-terminal of 6-4PP-PL cDNA in the pENTR/D-TOPO vector, using AscI and EcoRI. Then 6-4PP-PL-mCherry-3xNLS-HA was cloned into pLenti CMV Puro DEST using Gateway cloning (Invitrogen). CPD-PL-mCherry [48], or 6-4PP-PL-mCherry-3xNLS-HA expressing lentiviral vectors were used to make the corresponding lentiviruses using the third generation system [61]. GFP-DDB2 expressing VH10 cells [44], or GFP-XPC expressing HCT116 cells were transduced with the generated lentiviruses and cells stably expressing CPD-PL-mCherry or 6-4PP-PL-mCherry-3xNLS-HA were selected with puromycin.

GFP-XPC expressing HCT116 cells were generated by a CRISPR/Cas9 mediated knock-in strategy where HCT116 cells were co-transfected with a lentiCRISPR v2 vector containing an XPC guide RNA (5'-GCTCGGAAACGCGCGGCCGG-3') targeting right after the XPC start codon and, a linearized homology-directed repair (HDR) template. GFP-XPC DDB2^{-}/- HCT116 cells were generated by transfection of GFP-XPC HCT116 cells with a lentiCRISPR v2 vector containing a DDB2 guide RNA (5'-TATTACGCCCCAGGAACAAG-3'). The HDR template to generate a GFP-XPC knock-in was generated in a single PCR step using 200 bp primers. The primers were designed in a way that 30 bp of each primer anneals to the FLAG-GFP construct and the remaining 170 bp anneals to the human genomic XPC sequence. Furthermore, the PAM sequence was mutated by 5 silent mutations which were introduced in the region targeted by the XPC gRNA to prevent Cas9 cutting the integrated HDR template. The following primers were used to generate the HDR template: forward primer (5' CCGCAGTTTTTTAGTGGCCACGGGTATGGGGT GGAGCTTCCTTTAGGGGCGTGACTAGGCCTCCAACGAAG GGGCGTGGCCAAGCGCACCGCCTCGGGGGCGGGG CCGGCGTTCTAGCGCATCGCGGCCGGGTGCGTCACTCG CGAAGTGGAATTTGCCCAGACAAGCAACATGGA CTACAAGGACGACGATGACAAGGTG-3'), reverse primer

(5'-GCCTCTGGGCCTCCTCCGCCCACCGGCGGCGT CTCCCGCGAAGCCCGCTGGGCCTCGCTCTCACCCTCCTCCTC C T C C T C A C G C C G G G C C T T G C T C T T G G C C T T G G ATTTCTGGCTGCGCAGTTCGCGTCCCCGCGGCTCCCCGCCTG C G G C T C T C T T C C G A G C G A G A T G C T T G T A C A G C TCGTCCATGCCGAGAGTGAT-3'). The PCR generated template was cloned into pCR-Blunt II-TOPO vector and then the vector was digested with EcoRI to generate the linearized GFP-XPC construct.

Transfected HCT116 cells were selected by puromycin for 2 days and stable GFP-XPC expressing cells were FACS sorted. Then single cell clones were picked and clones were selected using genotyping, and western blotting to check for expression of the full-length GFP-XPC protein and the concomitant loss of wild type XPC expression.

RNA interference

Cells were transfected with the indicated siRNAs (150 pmol) using RNAiMax (Thermo Fisher Scientific) 48-72h prior to the experiment, according to manufacturer's protocol. The siRNAs were purchased from Dharmacon: control (siGENOME Non_Targeting siRNA#5, D-001210-05) and XPF (siGENOME ERCC4 siRNA, M-019946-00).

Inflication of UV-induced DNA damage

Cells were washed with PBS, and after PBS removal the cells were exposed to UV-C light from a 254 nm germicidal lamp (Philips). Local UV-C damage was inflicted through an isopore membrane filter (Millipore) with a pore size of 5 μm [62].

Photo-reactivation

After PBS wash, cells were covered with a thin layer of HBSS (Thermofisher) and then placed at a distance of 10 cm under white-light tubes (General Electric Lightning Polylux LX F36W/840) for 10 minutes at 37°C. Mock-treated samples were covered with aluminum foil during photo-reactivation (PR).

Western blotting

Cells were lysed in 2x sample buffer and boiled for 10 minutes at 95°C. The proteins were subsequently separated by SDS-PAGE and transferred to PVDF membranes

(0.45 μm). Membranes were blocked with 5% BSA in PBS-T (PBS containing 0.05% Tween 20) for 1 hour at room temperature (RT) and blotted with the following primary antibodies: CPD-PL and 6-4PP-PL (rabbit polyclonal, 1:500) [58, 59], RFP mCherry (rat monoclonal, 1:1000, 5F8, Chromotek), DDB2 (rabbit monoclonal, 1:1000, EPR981, abcam), Ku70 (goat polyclonal, 1:1000, M-19, sc-1487, Santa Cruz), tubulin (mouse monoclonal, 1:3000, B-5-1-2, sc-23948, Santa Cruz), XPC (rabbit polyclonal, 1:1000, A301-122A, Bethyl) or XPF (mouse monoclonal, 1:500, 3F2/3, sc-136153, Santa Cruz). After five times washing with PBS-T, the membranes were blotted with the following corresponding secondary antibodies from Sigma Aldrich: CF™ 680 Goat anti-Rabbit IgG (1:5000) and CF™ 770 Goat anti-Mouse IgG (1:5000). The blots were imaged with the Odyssey CLx Infrared Imaging System (LI-COR Biosciences).

Immunofluorescence

Cells were grown on 24 mm coverslips and fixed in 2% paraformaldehyde containing PBS Triton X-100 (0.1%). After five times washing with PBS Triton X-100, the coverslips were blocked in PBS+ (PBS containing 0.15% glycine and 0.5% BSA). A denaturation step of 5 minutes using freshly diluted NaOH (0.07M) in PBS was performed to make DNA lesions accessible for the CPD (mouse monoclonal, 1:1000, TDM-2, Cosmo Bio) or 6-4PP (mouse monoclonal, 1:300, 64M2, Cosmo Bio) primary antibodies. Following an incubation of 1-2h at RT with primary antibodies diluted in PBS+, the coverslips were washed with PBS Triton X-100 five times and PBS+ once. Then the coverslips were incubated with 488, 555 or 639 Alexa Fluor secondary antibody conjugates (Invitrogen) diluted in PBS+ for 1h at RT. After the coverslips were washed again as described above, they were embedded in Vectashield Mounting Medium with DAPI (Vector Laboratories). The coverslips were imaged using a LSM 700 microscope equipped with a Plan-Apochromat 40x/1.3 NA oil immersion lens (Carl Zeiss MicroImaging Inc.). The ImageJ software [63] was used to quantify the CPD and 6-4PP signals in the generated images. The DAPI signal was used to determine the nuclei and the mean fluorescence intensities measured in the nuclei were used to plot the graphs. For CPD and 64PP removal assay cells were globally UV irradiated with 10J/m^2 and 16 10J/m^2 respectively, and fixed after the indicated time points. CPD and 6-4PP staining was performed as described above. Fluorescence levels were quantified in at least 70 cells per sample by measuring the background-corrected overall nuclear fluorescence, which was set at 100% for 0 h after UV irradiation.

Colony survival assay

Cells were seeded in triplicate in 6-well plates (300 cells/well) and next day treated with the indicated UV-C doses. After a week, the colonies were fixed and stained with 0.1% Brilliant Blue R (Sigma), and counted using GelCount (Oxford Optronix Ltd.).

Live cell confocal laser-scanning microscopy

All live cell imaging experiments were performed at 37°C and 5% CO_2 using a Leica SP5 laser-scanning confocal microscope with a 63×/1.4 NA HCX PL APO CS oil immersion objective. Fluorescence recovery after photobleaching (FRAP) experiments were performed as described previously [42], in short; a narrow strip (512 x 16 pixels at zoom 9) along the nucleus was bleached 94 ms with 100% power of 488 nm laser for the GFP and 42 ms with 100% power of 561 nm laser for the mCherry signal. The signal in this strip was measured pre-bleach for 3.6 s and post-bleach for 20 s every 400 ms with 0.2% power of the 488 nm laser for GFP-XPC. FRAP of the mCherry-tagged PLs was performed by measuring pre-bleach for 2.5 s and post-bleach for 20 s every 100 ms with 3% power of the 561 nm laser for the mCherry signal of the PLs. To analyze fluorescence recovery, measured fluorescence intensities were first background corrected, then normalized to the average pre-bleach fluorescence signal which was set at 1. Immobile fractions were calculated using the following formula: Immobile fraction (%) = 1 – ((average fluorescence intensity of UV-C irradiated cells – the first post-bleach data point) / (average fluorescence intensity of mock-treated cells–the first post-bleach data point)). The average fluorescence intensities are calculated over the measurements of the last 10 s. For local repair during live cell imaging experiments, the fluorescence intensity of PL-mCherry was monitored every 2.585 s, both inside and outside the local damage within the nucleus (at zoom 10). PR was performed by exposure of the DNA damage to 5 frames of 5% 405 nm laser light. The power output of the 405 nm laser was measured to be 0.063 mW at 10% laser power. Data were corrected for background fluorescence signal outside the cell and normalized to average fluorescence signal at the local damage before PR, which was set at 1.

RESULTS

Generation and characterization of CPD-PL and 6-4PP-PL-expressing cells

To develop a method to quantify UV-induced DNA damage and its repair kinetics directly in living cells, we first tested whether the ability of PLs to specifically detect UV-

induced lesions could be exploited to generate live cell damage markers by fluorescently labeling them. For this purpose, we generated lentiviral vectors [64] expressing *Potorous tridactylis* CPD-PL [58] or *Arabidopsis thaliana* 6-4PP-PL [65] tagged with mCherry fluorescent protein at their C-terminus. In addition, 3 NLS sequences were added after the mCherry-tag of the 6-4PP PL to ensure nuclear expression. These lentiviruses were used to transduce GFP-DDB2 expressing VH10 (hTERT immortalized human fibroblast) cells [44] to stably express either CPD PL-mCherry or 6-4PP PL-mCherry (referred as CPD-PL or 6-4PP-PL, respectively). Western blot analysis showed that the generated VH10 cell lines express full-length PL-mCherry fusion proteins (Figure 1A). To be able to use these PL-mCherry proteins as UV damage markers, it is important that PL expression does not interfere with NER-mediated repair of UV-induced lesions. As shown by UV colony survival experiments, both CPD-PL and 6-4PP-PL-expressing cells showed a similar UV sensitivity as wild type (WT) VH10 cells (Figure 1B), indicating that the expression of these fusion proteins does not affect endogenous DNA repair activity. To corroborate this, we compared the kinetics of 6-4PP and CPD removal in PL-expressing cells and WT VH10 cells (Supplementary Figure S1A and B). This revealed that the endogenous repair of CPDs and 6-4PPs by NER was similar in PL-expressing cells and in wild type cells, but was strongly diminished in NER deficient XP-C cells.

The fusion to a mCherry tag allowed direct visualization of PLs and showed that both CPD-PL and 6-4PP-PL are expressed mainly in the nucleus (left panels of Figure 1C and D). While the CPD-PL is excluded from the nucleoli, the 6-4PP-PL was enriched in the nucleoli (bottom panels of Figure 1C and 1D), however, the mechanism behind this different nucleolar localization is unknown. As PLs bind CPDs and 6-4PPs light independently, but need white light to initiate catalysis, we subsequently tested whether the PLs were capable of binding to UV-induced DNA damage, while cells were kept in the dark. Both CPD-PL and 6-4PP-PL accumulated at local UV damage induced through micropore filters [62], as shown by a co-localization with the DNA damage recognizing protein DDB2 (Figure 1C, right panel). Of note, the exogenous expression of the PLs did not block DDB2 recruitment to sites of DNA damage. Furthermore, both CPD-PL and 6-4PP-PL co-localized with the respective lesion-specific antibodies (Supplementary Figure S1C). Importantly, CPD-PL and 6-4PP-PL were efficiently recruited to locally induced DNA damage in living cells (Figure 1D, right panel), demonstrating that PLs can be used to directly detect UV-induced CPD and 6-4PP

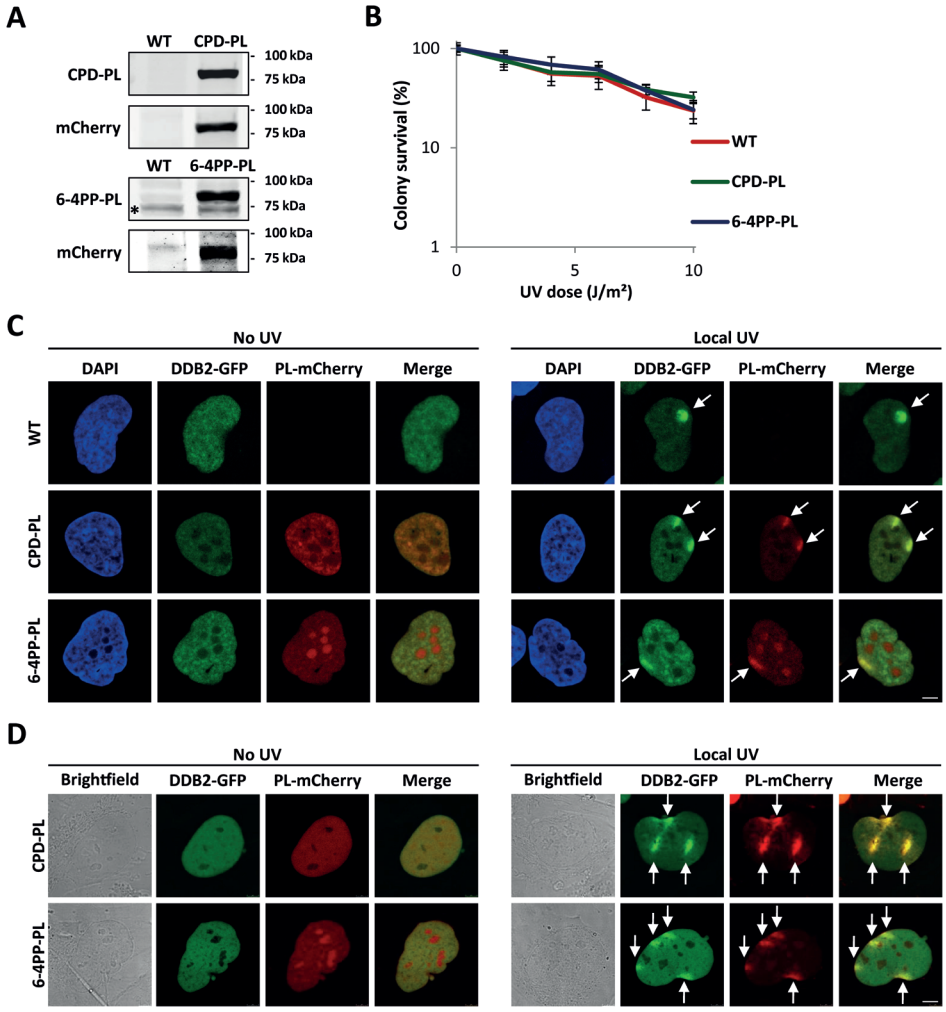

Figure 1. Characterization of mCherry-tagged photolyase-expressing cells. (A) Western blot of lysates of VH10 cells stably expressing GFP-DDB2 (WT), or co-expressing GFP-DDB2 and either CPD-PL-mCherry (CPD-PL, upper panel, expected size 75kDa) or 6-4PP-PL-mCherry (6-4PP-PL, lower panel, expected size 85kDa). Blots were stained with the indicated antibodies. Relevant marker sizes are indicated and * indicates an unspecific band. **(B)** UV-C sensitivity of WT or PL-expressing VH10 cells, determined by colony-forming ability (mean ± SEM). Percentage of surviving cells is plotted against the applied UV-C dose, colony number at 0 J/m^2 is set at 100 %. **(C and D)** Representative images of WT and PL-expressing VH10 cells. Cells were either non-irradiated (no UV, left panel) or locally irradiated with 60 J/m^2 UV-C (Local UV, right panel). Cells were either fixed directly after DNA damage induction **(C)** or monitored directly by live cell imaging **(D)**. Arrows indicate local UV damage. Scale bar: 5 µm.

recognizing protein DDB2 (Figure 1C, right panel). Of note, the exogenous expression lesions in living cells, which is not possible with photo lesion-specific antibodies.

CPD-PL and 6-4PP-PL as quantitative, real-time, damage and repair markers in living cells

Both CPD-PL and 6-4PP-PL were able to precisely detect the UV-induced DNA damage without interfering with NER activity (Figure 1B-D, Supplementary Figures S1A and B). Binding of repair proteins to DNA damage generally immobilizes them on chromatin, which can be quantified by fluorescence recovery after photo-bleaching (FRAP) [43, 66]. Therefore, we performed FRAP experiments to quantitatively assess differences in the chromatin-bound fraction of PLs in response to different UV doses. FRAP of PLs showed that both CPD-PL and 6-4PP-PL are highly mobile in unperturbed cells (no UV) (Figure 2A and B), indicating that PLs are not stably bound to chromatin in the absence of DNA damage. Interestingly, both CPD-PL and 6-4PP-PL were immobilized in a dose-dependent manner after UV irradiation (Figure 2A and B). From these FRAP curves, we determined the immobile fractions of the PLs (Supplementary Figure S2A and B), which revealed a linear increase for both CPD-PL and 6-4PP-PL with increasing UV doses up to 10 J/m^2. To assess whether the PL immobilization correlates with the actual quantity of CPDs and 6-4PPs, we quantified the relative amount of CPDs and 6-4PPs induced at these UV doses by immunofluorescence using photo lesion-specific antibodies [32] (Supplementary Figure S2C-E). Importantly, this revealed that the PL immobilization determined by PL FRAP (Figure 2C and D, primary Y-axis) at the indicated UV doses correlates very well with antibody-detected CPD and 6-4PP damage loads (Figure 2C and D, secondary Y-axis). This shows that FRAP of PLs allows a direct, relative quantification of UV-induced DNA damage in living cells. Interestingly, above 10 J/m^2, hardly any increase in PL immobilization was observed. This is most likely caused by limiting amounts of non-bound PLs at higher UV doses, in line with the almost complete immobilization of PLs at 10J/m^2 (Figure 2A and B). This may indicate that PL expression levels influence UV-induced PL immobilization. To test this, we compared the UV-induced PL immobilization in cells with low and high PL expression levels. This revealed that PL expression levels determine the dynamic range of PL mobility (Supplementary Figure S2F and G). Cells with low PL expression levels showed an increased immobilization at lower UV doses (e.g. 1 and 3 J/m^2). However, this dose-dependent increase in immobilization levelled off around 5J/m$^{2.}$ (Supplementary Figure S2F and G, left panels). In contrast, cells with high PL expression showed a reduced

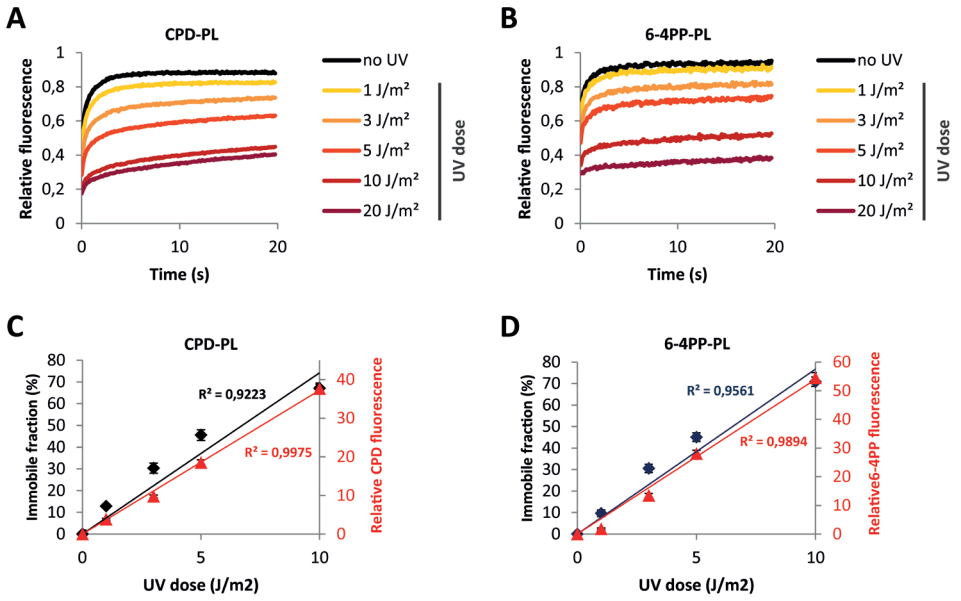

Figure 2. mCherry-tagged PLs as quantitative and real-time damage markers in living cells. (A and B) UV dose-dependent immobilization of CPD-PL **(A)** and 6-4PP-PL **(B)**. PL-expressing VH10 cells were non-irradiated or global UV-irradiated with the indicated UV doses and were directly analyzed by FRAP. The plotted values were normalized over the average pre-bleach signal (n=20 cells from 2 independent experiments). **(C and D)** Immobile fractions of CPD-PL **(C)** and 6-4PP-PL **(D)** at the indicated UV-C doses were plotted together with the relative quantity of CPD and 6-4PP lesions at the same UV-C doses as determined by the mean fluorescence intensities in immunofluorescence assays using lesion-specific antibodies.

immobilization at low UV doses, but PL immobilization continued to increase at high damage loads (e.g. 10-20 J/m^2) (Supplementary Figure S2F and G, right panels). These experiments demonstrate the importance of using cells with similar PL expression levels to avoid variation due to differences in the dynamic range of PL immobilization.

To test whether FRAP of PLs can also be used to study live-cell repair kinetics of CPDs and 6-4PPs, we UV irradiated cells and determined PL immobilization in time (Figure 3, Supplementary Figure S3A and B). In line with the previous experiments, both CPD-PL and 6-4PP-PL were strongly immobilized immediately upon UV exposure (10 J/m^2). As expected, this immobilization decreased over time, reflecting the repair of CPD and 6-4PP lesions. While 6-4PP-PL was quickly mobilized, with a 50% reduction at

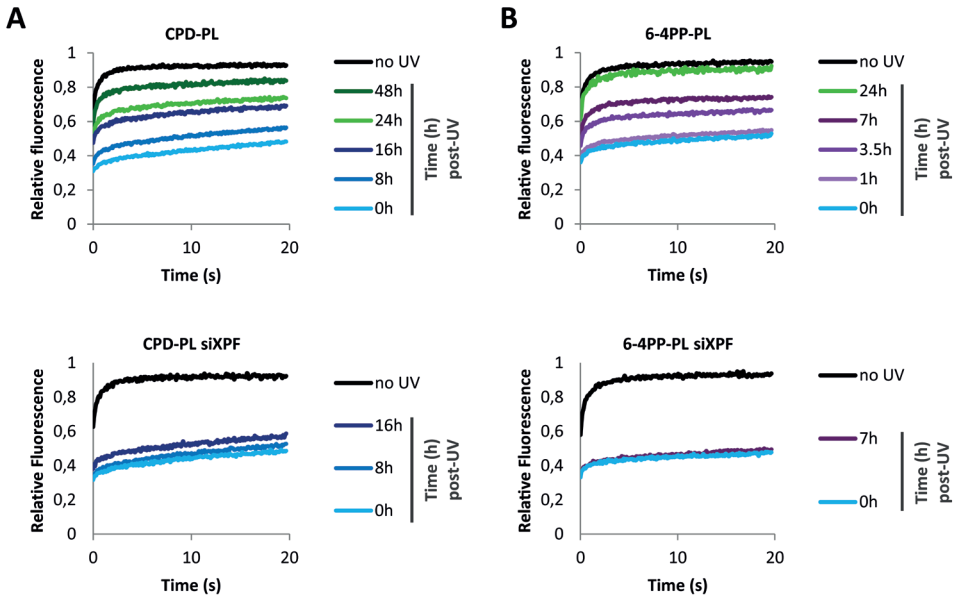

Figure 3. mCherry-tagged PLs to monitor DNA repair in living cells . (A) CPD-PL and **(B)** 6-4PP-PL expressing VH10 cells were transfected with the control (upper panel) or XPF siRNAs (siXPF) (lower panel). The plotted PL mobilities in non-irradiated or globally UV-C irradiated (10 J/m^2) cells were determined by FRAP at the indicated time points post UV irradiation. (n ≥ 25 cells from 2 independent experiments for control siRNA experiment, n ≥ 15 for siXPF).

7h post UV and an almost complete mobilization at 24h post UV, the reduction in binding to damaged DNA by CPD-PL was much slower, in line with previously shown differences in repair rates of CPD and 6-4PP lesions [42, 44, 67]. The mobilization of PLs over time was almost completely blocked by siRNA-mediated depletion of the NER factor XPF (Figure 3 lower panel, Supplementary Figure S3A and B, lower panel and Supplementary Figure S3C), indicating that the mobilization of PLs in time represented repair of CPD and 6-4PP by NER. These results demonstrate that FRAP of PLs enables the real-time monitoring of DNA damage load in living cells and thus provides a sensitive method to detect perturbations of the NER reaction in living cells.

Lesion-specific repair of UV-induced DNA damage in living cells

In addition to their use as quantitative live-cell damage markers, PLs can be used to specifically remove either CPD or 6-4PP lesions by direct reversal of the DNA damage using energy from near UV light (300–500 nm) [68, 69]. First, we determined optimal

PR times for the repair of CPD and 6-4PP lesions (Figure 4A and B). PL-expressing cells were UV-irradiated and DNA damage was photo-reactivated with white light for the indicated times. While 5 min of PR was not enough for complete removal of DNA damages, 10 min PR resulted in a PL mobility similar to that of non-irradiated cells, indicative of an almost complete removal of DNA lesions (Figure 4A and B, Supplementary Figure S4A and B). Of note, the PL mobility was not affected in cells that were shielded from the white light during PR (UV + 10min mock).

Having determined the optimal PR conditions, we assessed the previously described PR specificity of each PL. For this purpose, UV-induced DNA damage was photo-reactivated and the CPD or 6-4PP lesions were detected using immunofluorescence with specific antibodies. As expected, we observed an almost complete loss of CPDs following PR in CPD-PL-expressing cells, while the quantity of 6-4PP lesions was not affected (Supplementary Figure S4C). In 6-4PP-PL-expressing cells, removal of only 6-4PP lesions, but not of CPD, was observed upon PR (Supplementary Figure S4C).

After confirming that PL-expressing cells can specifically repair CPD or 6-4PP lesions, we made use of this feature to study live-cell DNA binding kinetics of XPC, the main damage sensor in GG-NER [4]. For this purpose, we co-expressed GFP-XPC and CPD-PL or 6-4PP-PL in HCT116 cells (Supplementary Figure S4D, left panel), and performed FRAP experiments to simultaneously asses the mobility of mCherry-tagged PLs and GFP-tagged XPC (Figure 4C and D). As shown in the FRAP curves (Figure 4C and D) and the respective immobile fractions (Supplementary Figure S4E and F), UV irradiation led to the binding of GFP-XPC to damaged DNA resulting in its immobilization. Upon PR of each type of photo lesion, GFP-XPC immobilization was reduced, however not to the same extent as in non-irradiated cells. This is most likely due to the fact that XPC has affinity for both CPD and 6-4PP lesions [4, 70, 71]. PR of 6-4PPs and CPDs was successful as shown by the mobilization of both PLs upon PR (Supplementary Figure S4G and H). We observed more increase in the GFP-XPC mobilization upon PR of 6-4PPs compared to CPDs. Although XPC is able to directly recognize 6-4PP lesions, DDB2 facilitates this recognition and is crucial for XPC to detect CPD lesions [5, 6, 72]. This suggests that the residual damage binding of XPC, following 6-4PP removal, represents DDB2-mediated binding to CPDs. To test this, we performed the same FRAP experiments in DDB2-deficient cells (Supplementary Figure S4D, right panel). In line with a stimulatory effect of DDB2 on XPC damage

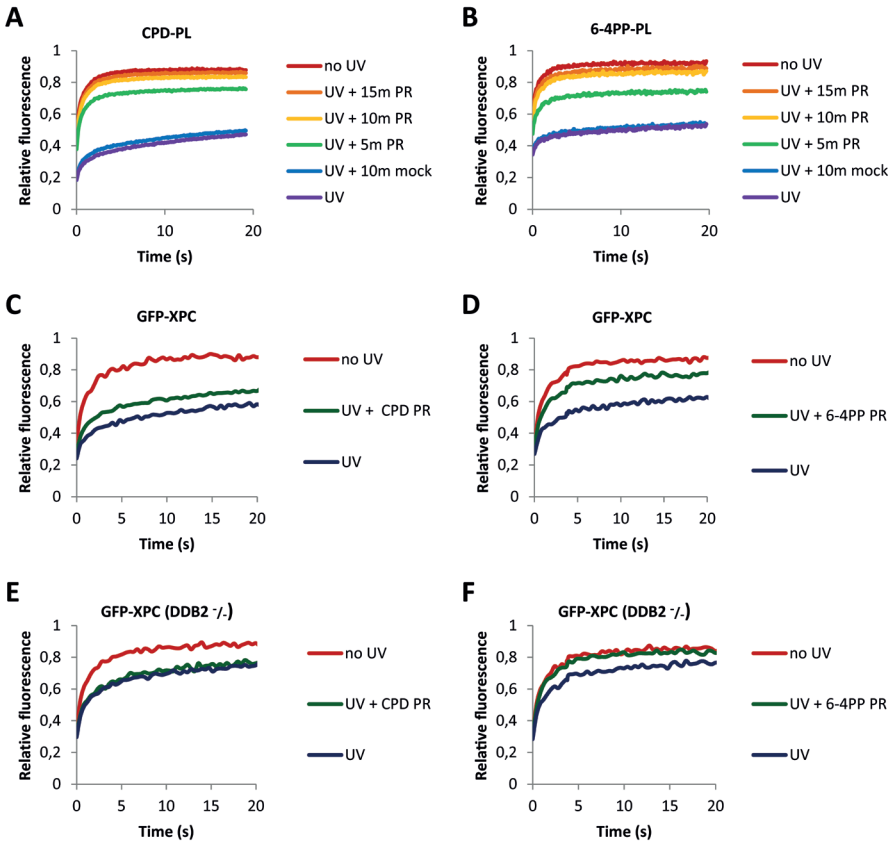

Figure 4. Lesion-specific repair of UV-induced DNA damage in living cells. (A and B) Mobility of **(A)** CPD-PL and **(B)** 6-4PP-PL as determined by FRAP analysis. Cells were non-irradiated (no UV), globally UV-C irradiated with 10 J/m^2 (UV), or globally UV-irradiated with 10 J/m^2 and photo-reactivated (UV + PR) for the indicated times by exposure to white light at 37°C. Cells were directly analyzed by FRAP after each treatment. ''UV + 10min mock" cells were UV-irradiated and mock photo-reactivated by shielding from white light during PR. (n ≥ 20 cells from 2 independent experiments) **(C and D)** GFP-XPC mobility was determined by FRAP in non-irradiated, globally UV-C irradiated (10 J/m^2), or globally UV-C irradiated (10 J/m^2) and photo-reactivated (10 min PR) in CPD-PL **(C)** or 6-4PP-PL **(D)** expressing cells. **(E and F)** Similarly, GFP-XPC mobility analysis was performed in DDB2 deficient cells (GFP-XPC DDB2$^-$/-) (n ≥ 20 cells from 2 independent experiments).

recognition, the UV-induced XPC immobilization was reduced by approximately 50% in DDB2 deficient cells (Figure 4E and F, Supplementary Figure S4E and F). Furthermore, in the absence of DDB2, GFP-XPC immobilization fully recovered after PR of 6-4PPs (Figure 4F and Supplementary Figure S4J), indicating that the UV-induced

immobilization of XPC in DDB2-deficient cells is caused solely by 6-4PPs. In contrast, PR of CPDs (Supplementary Figure S4I) did not affect the XPC immobilization (Figure 4E), which confirms that XPC does not bind CPDs in DDB2-deficient cells. These experiments illustrate firstly, that the PL-mediated removal of specific UV-induced lesions can provide important quantitative insights into the behavior of NER factors on specific types of DNA lesions. Secondly, the direct comparison of PL and XPC mobility by FRAP in the same cell following the same UV exposure illustrated that fluorescently-labelled PLs can quantify DNA damage with a bigger dynamic range than XPC, as shown by the bigger immobile fraction of PLs (Supplementary Figure S4K). Thirdly, the mobility of PLs was not affected by the presence or absence of DDB2, which like PLs directly binds to DNA lesions [3] (compare Supplementary Figure S4G and I, and Supplementary Figure S4H and J). This shows that the dynamic range of PLs as live cell damage markers is not influenced by competitive substrate binding of PLs and DDB2.

Local repair of UV-induced DNA damage in living cells

A limitation of the PR-based DNA damage removal described above is that full PR takes ~10 minutes and needs to be performed before live-cell imaging. This interferes with the real-time measurement of the effects of DNA damage removal on proteins of interest in the cells. To improve our system, we set out to perform PR during live-cell imaging. As *Potorous tridactylis* CPD-PL and *Arabidopsis thaliana* 6-4PP-PL have absorption spectra that peak between 360 nm and 450 nm [65, 73], we tested whether it was possible to remove UV-induced damage by activating the PLs using a 405 nm laser during live cell imaging. CPD-PL-expressing cells were locally UV-irradiated resulting in accumulation of CPD-PL at sites of DNA damage (Figure 5A, upper panel). These locally accumulated CPD-PLs were subsequently exposed to different intensities of the 405 nm laser, which almost instantaneously released the damage-accumulated PLs already at 0.5 % 405 nm laser power (Figure 5A and B), reaching complete PR at 1 % laser power. To exclude that the loss of fluorescence at the damage site was caused by photo bleaching of mCherry, the 405 nm laser was also activated at a region outside the damage within the nucleus, which did not result in any reduction in signal intensity (Supplementary Figure S5A). To further confirm that PL exposure to the 405 nm laser induced CPD removal by PR, we first photo-reactivated damaged DNA in a specific region (marked with the cross) in the nucleus and then stained the cells with a CPD specific antibody (Figure 5C). CPD lesions within the marked area were completely removed. In line with this, the mCherry signal of CPD-PL was reduced in the 405 nm laser-exposed region. This can

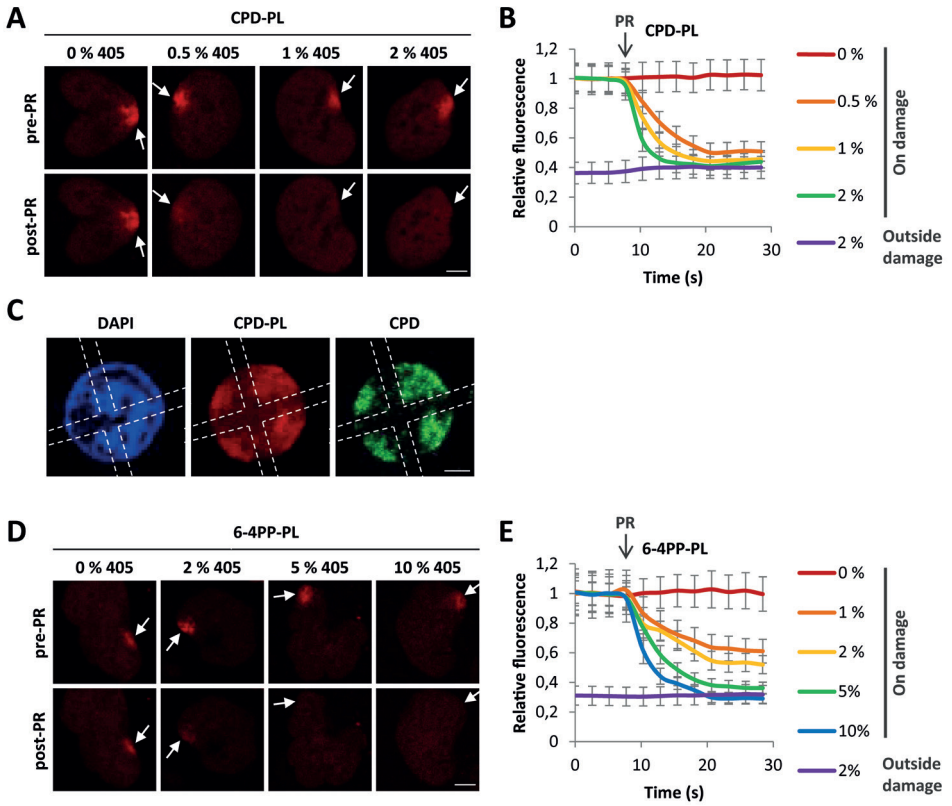

Figure 5. Local repair of UV-induced DNA damage in living cells. (A) Representative images of CPD-PL-expressing VH10 cells before and 13 s after PR (pre-PR and post-PR, respectively) using 405 nm laser at the indicated intensities. Arrows indicate local UV damage. Cells were locally UV-irradiated (60 J/m^2), the local DNA damage spot and a region of the exact same size outside the damage within the nucleus were exposed after 7.8 s (indicated by arrow and PR) to the indicated intensities of 405 nm laser for 13 s. Scale bar: 5 µm. **(B)** Relative mCherry fluorescence signal of CPD-PL was quantified inside and outside the DNA damage within the nucleus and normalized to pre-PR intensities at the local damage. (n = 8 cells, mean ± SEM) **(C)** Representative immunofluorescence images of CPD-PL-expressing VH10 cells after PR. Global UV-irradiation (10 J/m^2) of the cells was followed by photo-reactivation of the damaged DNA by 5% 405 nm laser for 13 s in a specific region (region marked with dotted line) in the nucleus and the cells were subsequently fixed and stained with CPD antibody using immunofluorescence. **(D)** Representative images of locally UV-irradiated (60 J/m^2) 6-4PP-PL-expressing VH10 cells before and 13 s after PR (pre-PR and post-PR, respectively) using 405 nm laser at the indicated intensities as described above in Figure 4A. Arrows are indicating the local UV-C damage spots. Scale bar: 5 µm. **(E)** Relative mCherry fluorescence signal of 6-4PP-PL was quantified inside and outside the DNA damage within the nucleus and normalized to pre-PR intensities at the local damage. (n = 8 cells, mean ± SEM)

be explained by its release and its subsequent binding to the areas in the nucleus where the damage is not removed. Additionally, 6-4PP lesions could also be removed upon PR by 6-4PP-PL, however, this required slightly higher 405 nm laser intensities (>5%) (Figure 5D and 4E, and Supplementary Figure S5B).

Importantly, this live-cell PR is compatible with GFP imaging, as the PR-based repair is hardly triggered by the 488 nm laser at intensities that are commonly used for imaging GFP-tagged factors (Supplementary Figure S5C-H). Altogether, these results show that PLs can be used to photo reactivate UV-induced DNA damage in real-time in living cells, using the 405 nm laser. In conclusion, while the induction of DNA damage in living cells has been an available tool for many years [74] and resulted in many important mechanistic insights in the repair reaction, in this study, we introduce the repair of specific UV-induced DNA damage in living as a unique tool to study the dissociation of DNA repair factors and behavior of other cellular processes upon damage removal.

DISCUSSION

The currently available assays to investigate UV-induced DNA damage and repair have proven to be invaluable tools to study NER factors in both fundamental and clinical research. However, these assays cannot be performed in living cells, and are therefore confined to endpoint measurements instead of monitoring the DNA damage quantities in real time. Therefore, in this study, we developed a novel method using fluorescently-tagged PLs to directly recognize and quantify UV-induced DNA damage in a highly sensitive manner in living cells.

For this purpose, we made use of the high affinity of PLs for UV-induced DNA damage, which was confirmed by their accumulation at locally induced UV damage (Figure 1C and D), and their immobilization on damaged DNA during FRAP. Both CPD-PL and 6-4PP-PL showed a strong and reproducible UV dose-dependent immobilization. This approach allowed to quantitatively monitor the relative DNA damage loads (Figure 2A-D) and NER-mediated repair kinetics in a highly sensitive manner (Figure 3). FRAP of PLs proved to be highly sensitive and enabled the detection of physiological relevant damage loads as low as 1 J/m^2, which are difficult to quantify with other techniques. Furthermore, we observed a linear and relatively large dynamic range of PL immobilization between 0-10 J/m^2 UV, enabling precise quantification of the DNA damage loads. Of note, at higher UV doses (20 J/m^2) the dose-dependent immobilization was not linear

anymore, which might be caused by limiting amounts of non-chromatin bound PLs, in line with the almost complete immobilization of PLs at 10 J/m^2 (Figure 2A and B).

In line with this, in cells with higher PL expression levels this levelling off of PL immobilization at higher UV doses was reduced, indicating that cells with higher PL levels are more suitable to quantify high damage loads (>5J/m^2) (Supplementary Figure S2F and G, right graphs). On the other hand, our experiments show that cells with low PL expression levels allow a more sensitive detection of low damage loads (<5J/m^2) (Supplementary Figure S2F and G, left graphs). Together these data show that the dynamic range of FRAP-based UV damage detection using fluorescently-tagged PLs can be adjusted to experimental needs by choosing cells with distinct PL expression levels. PL expression levels can easily be fine-tuned in the used lentiviral transduction system by the choice of promoter [64]. These data furthermore show the importance of using cells with similar PL expression levels when studying PL kinetics in different conditions. To achieve a very homogenous expression of fluorescently-tagged PLs, thereby potentially even increasing the precision of PL-mediated damage quantification, CRISPR/Cas9-mediated genomic targeting of PL expression cassettes to safe harbor loci like ROSA26 or AAVS1 [75] could be used.

Furthermore, mutated PLs that are still capable of binding the UV-induced DNA damage, but are incapable of PR, might be developed, as these catalytically dead PLs will be insensitive to unintentional day light exposure during experimental handling. Of note, the FRAP-based PL assay is already very sensitive, as shown by the direct comparison of the PL immobilization to that of XPC (Supplementary Figure S4K), the main damage sensor of GG-NER [4]. XPC is one of NER factors that shows the highest immobilization on UV-damaged DNA [42, 76, 77], however our FRAP data show that the fluorescently labeled PLs detect damage with even higher sensitivity than XPC.

The precise correlation between PL immobilization and DNA damage load is most likely explained by the fact that exogenously expressed PLs, which function as single proteins, are most likely not regulated by the activity of other proteins, post-translational modifications or other forms of regulation in mammalian cells. Especially, these types of regulation have been shown to influence the direct correlation of the NER factor immobilization with the DNA damage quantity [17-19, 45, 47-49, 78]. The direct recognition of DNA damage with high affinity makes PLs ideally suited to visualize

DNA damage in both living and fixed cells. Fluorescently-tagged PLs can therefore be used as sensitive, lesion-specific quantitative damage markers while studying the accumulation of other proteins at sites of local UV-induced damage [62, 74].

Of note, although the PLs have high affinity for DNA damage and are highly immobilized on damaged DNA, they did not interfere with NER. No differences were observed in the UV survival of parental and PL-expressing cells (Figure 1B). In line with this, PL expression did not block the accumulation of DDB2 on local UV damages (Figure 1C) or inhibit the NER-mediated repair, as shown by PL immobilization in time (Figure 3). The absence of interference with the NER reaction might be explained by a transient binding of the PLs to DNA damage, thereby allowing NER factors to access DNA lesions. In line with this, even though a large fraction of the PLs were immobilized following UV exposure, these PLs were not long-term immobilized on chromatin but were rather continuously released and rebound as evidenced by the continuous increase in the FRAP curves over time (Figure 2A and B). Overall, our data showed that the use of fluorescently-labeled PLs is a robust and sensitive new method for the direct detection and quantification of UV-induced DNA damage in living cells.

In addition to their use as sensitive DNA damage markers, the fluorescently-tagged PLs can also be used to revert the UV-induced damage by PR. In this case, the fluorescent tag could be used to monitor directly the DNA damage reversion by assessing PL immobilization. This feature allowed us to determine the minimally required PR times for CPD-PL and 6-4PP-PL (Figure 4A and B). Our results showed that 10-15 minutes of PR by exposure to white light was enough for both PLs to repair almost all of the lesions (Figure 4A and B). This minimal PR duration is much shorter than the PR times of 1-4 h used in most previous studies performed in mammalian cells [6, 79-83]. The lesion-specific repair by CPD-PL and 6-4PP-PLs can be used to investigate the lesion-specific behavior of NER factors [6, 84]. These fluorescently-tagged PLs can be also used in combination with NER factors with different fluorescent tags, to simultaneously study the dynamic behavior of NER factor of interest while confirming the successful PR of CPD or 6-4PP lesions by PLs in the same FRAP experiment. As a proof of principle, we compared the GFP-XPC kinetics before and after PR, by simultaneously monitoring PR-mediated repair by PL mobility (Figure 4E and F). This approach could be applied to investigate the behavior of any fluorescently-tagged repair factor while monitoring the progress of either PR-based or endogenous repair over time in living cells.

Despite the short required PR times, white light mediated-PR is technically incompatible with live cell imaging. To study cellular processes directly upon, or even during PR we developed PR using a 405 nm laser as a new method to repair DNA lesions during live-cell imaging. As the CPD-PL and 6-4PP-PL absorption spectra peak between 360 nm and 450 nm, we photo-reactivates PLs using the 405 nm laser, which is commonly available in live cell imaging setups. Using laser pulses as short as 12.5 s, with relatively low laser power, allowed us to efficiently photo-reactivate DNA damage in live cell imaging experiments (Figure 5). Of note, while the 405 nm laser light can also be used to generate DNA damage, [85, 86], the laser intensity used for efficient PR is more than 10-fold lower than the intensities required to induce DNA damage [74]. Our results indicated that PR is rather specific for 405 nm laser, as PLs were not efficiently activated by the 488 nm laser at settings normally used for imaging GFP-tagged factors (Supplementary Figure S5C-H).

Thus far, mainly association kinetics (K_{on}) of NER factors were studied using local DNA damage infliction during live cell imaging [74]. This has been a powerful tool to study the accumulation kinetics and recruitment order of fluorescently-tagged NER factors and has revealed crucial information about molecular mechanism and interdependencies of NER factors [41, 87]. Thus far the dissociation kinetics (K_{off}) of NER factors following DNA repair were more difficult to address, as the endogenous NER-mediated repair is expected to happen in a stochastic manner over time. Interestingly, our 405 nm laser-assisted live-cell repair method enables to almost instantaneously remove DNA damage. This approach can be used to gain important insights into the release of NER factors, repair times and stability of NER intermediates. In addition, as the PLs are lesion-specific, these parameters could be specifically attributed to CPD or 6-4PP lesions. PR activity of the CPD and 6-4PP-PLs can also be used simultaneously to repair the vast majority of UV-induced lesions directly. This allows testing whether specific cellular effects are caused by the DNA damage itself, or by other types of damages generated by UV exposure, such as membrane, protein, or RNA damage [88-90]. Additionally, 405 nm laser-mediated PR can be used to instantly repair sub-nuclear regions, which could be used to determine the contribution of DNA damage (*in cis)* or signaling pathways (*in trans)* to transcription inhibition, replication stress, or other cellular effects following UV damage [91-93].

In conclusion, here we describe how fluorescently-labeled PLs can be used as highly

sensitive UV-induced DNA damage markers to quantitatively determine damage load and repair in real-time, in living cells. Moreover, the instant repair of DNA damage by activating PLs during live cell imaging opens new possibilities to assess the cellular effects following damage removal. In addition, lentiviral expression is highly efficient to stably express PLs in a broad range of cell lines. Overall, the methods described here are a valuable extension of the current toolbox to study factors involved in the UV-induced DNA damage response, and will contribute to a better understanding of the molecular mechanism of NER in living cells.

ACKNOWLEDGEMENTS

We thank the Optical Imaging Centre (OIC) at the Erasmus MC for their support with microscopes and image analysis and Dr. A. Theil for FACS sorting. Dr. H. Lans generously provided us with the lentiviral CPD-PL-mcherry construct. We thank Prof. B. van der Horst and Dr. I. Chaves for 6-4PP Photolyase cDNA and antibodies against 6-4PP and CPD PLs.

FUNDING

This work is part of the Oncode Institute which is partly financed by the Dutch Cancer Society. This work was supported by the Dutch Organization for Scientific Research ZonMW TOP Grant [912.12.132]; TOP ALW grant [854.11.002]; Horizon Zenith [935.11.042]; VIDI ALW [864.13.004]; NWO Graduate Programme Erasmus MC - Medical Genetics Grant [022.004.002]; and Erasmus MC fellowship. Funding for open access charge: Dutch Science Organization (NWO).

CONFLICT OF INTEREST

The authors declare they have no conflict of interest.

REFERENCES

1. Hoeijmakers, J.H., *Genome maintenance mechanisms for preventing cancer.* Nature, 2001. **411**(6835): p. 366-74.
2. Jackson, S.P. and J. Bartek, *The DNA-damage response in human biology and disease.* Nature, 2009. **461**(7267): p. 1071-8.
3. Marteijn, J.A., et al., *Understanding nucleotide excision repair and its roles in cancer and ageing.* Nat Rev Mol Cell Biol, 2014. **15**(7): p. 465-81.
4. Sugasawa, K., et al., *Xeroderma pigmentosum group C protein complex is the initiator of global genome nucleotide excision repair.* Mol Cell, 1998. **2**(2): p. 223-32.
5. Wakasugi, M., et al., *DDB accumulates at DNA damage sites immediately after UV irradiation and directly stimulates nucleotide excision repair.* J Biol Chem, 2002. **277**(3): p. 1637-40.
6. Fitch, M.E., et al., *In vivo recruitment of XPC to UV-induced cyclobutane pyrimidine dimers by the DDB2 gene product.* J Biol Chem, 2003. **278**(47): p. 46906-10.
7. Vermeulen, W. and M. Fousteri, *Mammalian transcription-coupled excision repair.* Cold Spring Harb Perspect Biol, 2013. **5**(8): p. a012625.
8. Hanawalt, P.C. and G. Spivak, *Transcription-coupled DNA repair: two decades of progress and surprises.* Nat Rev Mol Cell Biol, 2008. **9**(12): p. 958-70.
9. Yokoi, M., et al., *The xeroderma pigmentosum group C protein complex XPC-HR23B plays an important role in the recruitment of transcription factor IIH to damaged DNA.* J Biol Chem, 2000. **275**(13): p. 9870-5.
10. Volker, M., et al., *Sequential assembly of the nucleotide excision repair factors in vivo.* Mol Cell, 2001. **8**(1): p. 213-24.
11. Compe, E. and J.M. Egly, *TFIIH: when transcription met DNA repair.* Nat Rev Mol Cell Biol, 2012. **13**(6): p. 343-54.
12. Sugasawa, K., et al., *Two-step recognition of DNA damage for mammalian nucleotide excision repair: Directional binding of the XPC complex and DNA strand scanning.* Mol Cell, 2009. **36**(4): p. 642-53.
13. Camenisch, U., et al., *Recognition of helical kinks by xeroderma pigmentosum group A protein triggers DNA excision repair.* Nat Struct Mol Biol, 2006. **13**(3): p. 278-84.
14. Staresincic, L., et al., *Coordination of dual incision and repair synthesis in human nucleotide excision repair.* EMBO J, 2009. **28**(8): p. 1111-20.
15. Ogi, T., et al., *Three DNA polymerases, recruited by different mechanisms, carry out NER repair synthesis in human cells.* Mol Cell, 2010. **37**(5): p. 714-27.

16. Moser, J., et al., *Sealing of chromosomal DNA nicks during nucleotide excision repair requires XRCC1 and DNA ligase III alpha in a cell-cycle-specific manner.* Mol Cell, 2007. **27**(2): p. 311-23.
17. van Cuijk, L., W. Vermeulen, and J.A. Marteijn, *Ubiquitin at work: the ubiquitous regulation of the damage recognition step of NER.* Exp Cell Res, 2014. **329**(1): p. 101-9.
18. Dijk, M., et al., *Insight in the multilevel regulation of NER.* Exp Cell Res, 2014. **329**(1): p. 116-23.
19. Dantuma, N.P. and H. van Attikum, *Spatiotemporal regulation of posttranslational modifications in the DNA damage response.* EMBO J, 2016. **35**(1): p. 6-23.
20. Lans, H., J.A. Marteijn, and W. Vermeulen, *ATP-dependent chromatin remodeling in the DNA-damage response.* Epigenetics Chromatin, 2012. **5**: p. 4.
21. Mandemaker, I.K., W. Vermeulen, and J.A. Marteijn, *Gearing up chromatin: A role for chromatin remodeling during the transcriptional restart upon DNA damage.* Nucleus, 2014. **5**(3): p. 203-10.
22. Steurer, B. and J.A. Marteijn, *Traveling Rocky Roads: The Consequences of Transcription-Blocking DNA Lesions on RNA Polymerase II.* J Mol Biol, 2017. **429**(21): p. 3146-3155.
23. Novarina, D., et al., *Mind the gap: keeping UV lesions in check.* DNA Repair (Amst), 2011. **10**(7): p. 751-9.
24. de Boer, J. and J.H. Hoeijmakers, *Nucleotide excision repair and human syndromes.* Carcinogenesis, 2000. **21**(3): p. 453-60.
25. Lehmann, A.R., *DNA repair-deficient diseases, xeroderma pigmentosum, Cockayne syndrome and trichothiodystrophy.* Biochimie, 2003. **85**(11): p. 1101-11.
26. DiGiovanna, J.J. and K.H. Kraemer, *Shining a light on xeroderma pigmentosum.* J Invest Dermatol, 2012. **132**(3 Pt 2): p. 785-96.
27. Decordier, I., K.V. Loock, and M. Kirsch-Volders, *Phenotyping for DNA repair capacity.* Mutat Res, 2010. **705**(2): p. 107-29.
28. Latimer, J.J. and C.M. Kelly, *Unscheduled DNA synthesis: the clinical and functional assay for global genomic DNA nucleotide excision repair.* Methods Mol Biol, 2014. **1105**: p. 511-32.
29. Cleaver, J.E., *Defective repair replication of DNA in xeroderma pigmentosum.* Nature, 1968. **218**(5142): p. 652-6.
30. Friedberg, E.C., *The discovery that xeroderma pigmentosum (XP) results from defective nucleotide excision repair.* DNA Repair (Amst), 2004. **3**(2): p. 183, 195.

31. Mellon, I., et al., *Preferential DNA repair of an active gene in human cells.* Proc Natl Acad Sci U S A, 1986. **83**(23): p. 8878-82.
32. Kobayashi, N., et al., *Quantitation and visualization of ultraviolet-induced DNA damage using specific antibodies: application to pigment cell biology.* Pigment Cell Res, 2001. **14**(2): p. 94-102.
33. Langie, S.A., et al., *Development and validation of a modified comet assay to phenotypically assess nucleotide excision repair.* Mutagenesis, 2006. **21**(2): p. 153-8.
34. Hu, J., et al., *Genome-wide analysis of human global and transcription-coupled excision repair of UV damage at single-nucleotide resolution.* Genes Dev, 2015. **29**(9): p. 948-60.
35. Mayne, L.V. and A.R. Lehmann, *Failure of RNA synthesis to recover after UV irradiation: an early defect in cells from individuals with Cockayne's syndrome and xeroderma pigmentosum.* Cancer Res, 1982. **42**(4): p. 1473-8.
36. Nakazawa, Y., et al., *A semi-automated non-radioactive system for measuring recovery of RNA synthesis and unscheduled DNA synthesis using ethynyluracil derivatives.* DNA Repair (Amst), 2010. **9**(5): p. 506-16.
37. Johnson, J.M. and J.J. Latimer, *Analysis of DNA repair using transfection-based host cell reactivation.* Methods Mol Biol, 2005. **291**: p. 321-35.
38. Bohr, V.A., et al., *DNA repair in an active gene: removal of pyrimidine dimers from the DHFR gene of CHO cells is much more efficient than in the genome overall.* Cell, 1985. **40**(2): p. 359-69.
39. Guo, J., P.C. Hanawalt, and G. Spivak, *Comet-FISH with strand-specific probes reveals transcription-coupled repair of 8-oxoGuanine in human cells.* Nucleic Acids Res, 2013. **41**(16): p. 7700-12.
40. Wienholz, F., W. Vermeulen, and J.A. Marteijn, *Amplification of unscheduled DNA synthesis signal enables fluorescence-based single cell quantification of transcription-coupled nucleotide excision repair.* Nucleic Acids Res, 2017. **45**(9): p. e68.
41. Marteijn, J.A., et al., *Nucleotide excision repair-induced H2A ubiquitination is dependent on MDC1 and RNF8 and reveals a universal DNA damage response.* J Cell Biol, 2009. **186**(6): p. 835-47.
42. van Cuijk, L., et al., *SUMO and ubiquitin-dependent XPC exchange drives nucleotide excision repair.* Nat Commun, 2015. **6**: p. 7499.
43. Vermeulen, W., *Dynamics of mammalian NER proteins.* DNA Repair (Amst), 2011. **10**(7): p. 760-71.
44. Pines, A., et al., *PARP1 promotes nucleotide excision repair through DDB2*

stabilization and recruitment of ALC1. J Cell Biol, 2012. **199**(2): p. 235-49.

45. Robu, M., et al., *Poly(ADP-ribose) polymerase 1 escorts XPC to UV-induced DNA lesions during nucleotide excision repair.* Proc Natl Acad Sci U S A, 2017. **114**(33): p. E6847-E6856.
46. Niida, H., et al., *Phosphorylated HBO1 at UV irradiated sites is essential for nucleotide excision repair.* Nat Commun, 2017. **8**: p. 16102.
47. Zhang, L., et al., *The chromatin remodeling factor BRG1 stimulates nucleotide excision repair by facilitating recruitment of XPC to sites of DNA damage.* Cell Cycle, 2009. **8**(23): p. 3953-9.
48. Aydin, O.Z., et al., *Human ISWI complexes are targeted by SMARCA5 ATPase and SLIDE domains to help resolve lesion-stalled transcription.* Nucleic Acids Res, 2014. **42**(13): p. 8473-85.
49. Jiang, Y., et al., *INO80 chromatin remodeling complex promotes the removal of UV lesions by the nucleotide excision repair pathway.* Proc Natl Acad Sci U S A, 2010. **107**(40): p. 17274-9.
50. Dulbecco, R., *Reactivation of ultra-violet-inactivated bacteriophage by visible light.* Nature, 1949. **163**(4155): p. 949.
51. Thompson, C.L. and A. Sancar, *Photolyase/cryptochrome blue-light photoreceptors use photon energy to repair DNA and reset the circadian clock.* Oncogene, 2002. **21**(58): p. 9043-56.
52. Husain, I., et al., *Mechanism of damage recognition by Escherichia coli DNA photolyase.* J Biol Chem, 1987. **262**(27): p. 13188-97.
53. Sancar, A., *Structure and function of photolyase and in vivo enzymology: 50th anniversary.* J Biol Chem, 2008. **283**(47): p. 32153-7.
54. Huang, Y., et al., *Crystal structure of cryptochrome 3 from Arabidopsis thaliana and its implications for photolyase activity.* Proc Natl Acad Sci U S A, 2006. **103**(47): p. 17701-6.
55. Wang, H., et al., *Femtosecond dynamics of flavin cofactor in DNA photolyase: radical reduction, local solvation, and charge recombination.* J Phys Chem B, 2005. **109**(4): p. 1329-33.
56. Sancar, G.B., *Enzymatic photoreactivation: 50 years and counting.* Mutat Res, 2000. **451**(1-2): p. 25-37.
57. Eker, A.P., et al., *DNA repair in mammalian cells: Direct DNA damage reversal: elegant solutions for nasty problems.* Cell Mol Life Sci, 2009. **66**(6): p. 968-80.
58. Schul, W., et al., *Enhanced repair of cyclobutane pyrimidine dimers and improved*

UV resistance in photolyase transgenic mice. EMBO J, 2002. **21**(17): p. 4719-29.

59. Jans, J., et al., *Powerful skin cancer protection by a CPD-photolyase transgene.* Curr Biol, 2005. **15**(2): p. 105-15.
60. Jans, J., et al., *Differential role of basal keratinocytes in UV-induced immunosuppression and skin cancer.* Mol Cell Biol, 2006. **26**(22): p. 8515-26.
61. Dull, T., et al., *A third-generation lentivirus vector with a conditional packaging system.* J Virol, 1998. **72**(11): p. 8463-71.
62. Mone, M.J., et al., *Local UV-induced DNA damage in cell nuclei results in local transcription inhibition.* EMBO Rep, 2001. **2**(11): p. 1013-7.
63. Schindelin, J., et al., *Fiji: an open-source platform for biological-image analysis.* Nat Methods, 2012. **9**(7): p. 676-82.
64. Campeau, E., et al., *A versatile viral system for expression and depletion of proteins in mammalian cells.* PLoS One, 2009. **4**(8): p. e6529.
65. Nakajima, S., et al., *Cloning and characterization of a gene (UVR3) required for photorepair of 6-4 photoproducts in Arabidopsis thaliana.* Nucleic Acids Res, 1998. **26**(2): p. 638-44.
66. Houtsmuller, A.B. and W. Vermeulen, *Macromolecular dynamics in living cell nuclei revealed by fluorescence redistribution after photobleaching.* Histochem Cell Biol, 2001. **115**(1): p. 13-21.
67. Mitchell, D.L., *The relative cytotoxicity of (6-4) photoproducts and cyclobutane dimers in mammalian cells.* Photochem Photobiol, 1988. **48**(1): p. 51-7.
68. Sancar, G.B., *DNA photolyases: physical properties, action mechanism, and roles in dark repair.* Mutat Res, 1990. **236**(2-3): p. 147-60.
69. Zhao, X., et al., *Reaction mechanism of (6-4) photolyase.* J Biol Chem, 1997. **272**(51): p. 32580-90.
70. Batty, D., et al., *Stable binding of human XPC complex to irradiated DNA confers strong discrimination for damaged sites.* J Mol Biol, 2000. **300**(2): p. 275-90.
71. Hey, T., et al., *The XPC-HR23B complex displays high affinity and specificity for damaged DNA in a true-equilibrium fluorescence assay.* Biochemistry, 2002. **41**(21): p. 6583-7.
72. Moser, J., et al., *The UV-damaged DNA binding protein mediates efficient targeting of the nucleotide excision repair complex to UV-induced photo lesions.* DNA Repair (Amst), 2005. **4**(5): p. 571-82.
73. Yasui, A., et al., *A new class of DNA photolyases present in various organisms including aplacental mammals.* EMBO J, 1994. **13**(24): p. 6143-51.

74. Dinant, C., et al., *Activation of multiple DNA repair pathways by sub-nuclear damage induction methods.* J Cell Sci, 2007. **120**(Pt 15): p. 2731-40.
75. Sadelain, M., E.P. Papapetrou, and F.D. Bushman, *Safe harbours for the integration of new DNA in the human genome.* Nat Rev Cancer, 2011. **12**(1): p. 51-8.
76. Nishi, R., et al., *UV-DDB-dependent regulation of nucleotide excision repair kinetics in living cells.* DNA Repair (Amst), 2009. **8**(6): p. 767-76.
77. Hoogstraten, D., et al., *Versatile DNA damage detection by the global genome nucleotide excision repair protein XPC.* J Cell Sci, 2008. **121**(Pt 17): p. 2850-9.
78. Puumalainen, M.R., et al., *Chromatin retention of DNA damage sensors DDB2 and XPC through loss of p97 segregase causes genotoxicity.* Nat Commun, 2014. **5**: p. 3695.
79. Chigancas, V., A. Sarasin, and C.F. Menck, *CPD-photolyase adenovirus-mediated gene transfer in normal and DNA-repair-deficient human cells.* J Cell Sci, 2004. **117**(Pt 16): p. 3579-92.
80. Asahina, H., et al., *Expression of a mammalian DNA photolyase confers light-dependent repair activity and reduces mutations of UV-irradiated shuttle vectors in xeroderma pigmentosum cells.* Mutat Res, 1999. **435**(3): p. 255-62.
81. de Lima-Bessa, K.M., et al., *CPDs and 6-4PPs play different roles in UV-induced cell death in normal and NER-deficient human cells.* DNA Repair (Amst), 2008. **7**(2): p. 303-12.
82. You, Y.H., et al., *Cyclobutane pyrimidine dimers are responsible for the vast majority of mutations induced by UVB irradiation in mammalian cells.* J Biol Chem, 2001. **276**(48): p. 44688-94.
83. Chigancas, V., et al., *Photorepair prevents ultraviolet-induced apoptosis in human cells expressing the marsupial photolyase gene.* Cancer Res, 2000. **60**(9): p. 2458-63.
84. Chigancas, V., et al., *Defective transcription/repair factor IIH recruitment to specific UV lesions in trichothiodystrophy syndrome.* Cancer Res, 2008. **68**(15): p. 6074-83.
85. Martin, R.F., et al., *Comparative studies of UV-induced DNA cleavage by analogues of iodoHoechst 33258.* Int J Radiat Biol, 1994. **66**(5): p. 517-21.
86. Martin, R.F., et al., *Radiation sensitization by an iodine-labelled DNA ligand.* Int J Radiat Biol, 1990. **57**(5): p. 939-46.
87. Luijsterburg, M.S., et al., *Heterochromatin protein 1 is recruited to various types of DNA damage.* J Cell Biol, 2009. **185**(4): p. 577-86.
88. Schwarz, T., *UV light affects cell membrane and cytoplasmic targets.* J Photochem

Photobiol B, 1998. **44**(2): p. 91-6.

89. Pattison, D.I. and M.J. Davies, *Actions of ultraviolet light on cellular structures.* EXS, 2006(96): p. 131-57.
90. Wurtmann, E.J. and S.L. Wolin, *RNA under attack: cellular handling of RNA damage.* Crit Rev Biochem Mol Biol, 2009. **44**(1): p. 34-49.
91. Ciccia, A. and S.J. Elledge, *The DNA damage response: making it safe to play with knives.* Mol Cell, 2010. **40**(2): p. 179-204.
92. Sirbu, B.M. and D. Cortez, *DNA damage response: three levels of DNA repair regulation.* Cold Spring Harb Perspect Biol, 2013. **5**(8): p. a012724.
93. Tresini, M., J.A. Marteijn, and W. Vermeulen, *Bidirectional coupling of splicing and ATM signaling in response to transcription-blocking DNA damage.* RNA Biol, 2016. **13**(3): p. 272-8.

SUPPLEMENTARY FIGURES

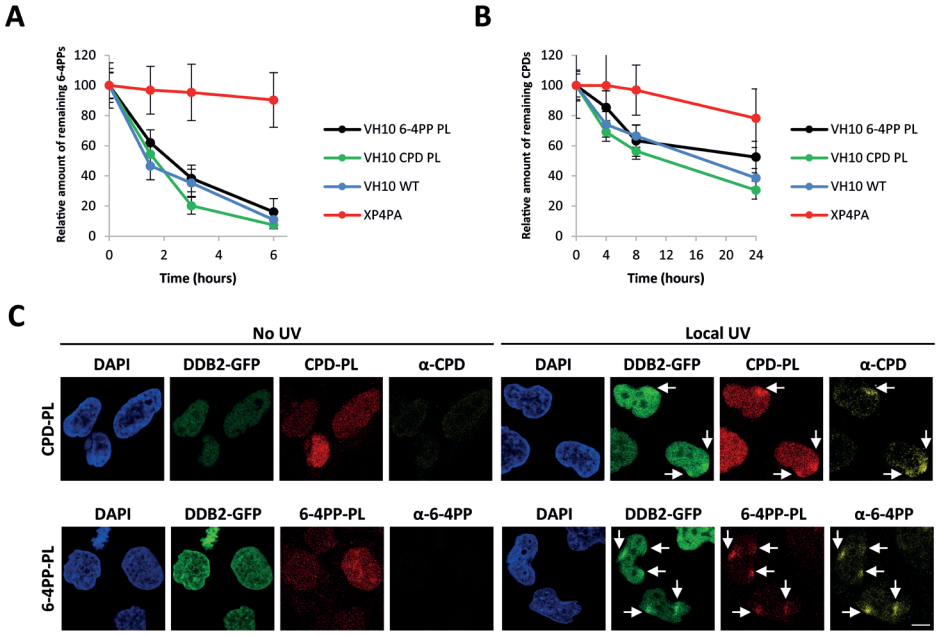

Supplementary Figure 1.

(A and B) The kinetics of endogenous DNA damage removal by NER was determined by quantifying the levels of 6-4PPs in time after 16 J/m^2 **(A)** and CPDs in time after 10 J/m^2 **(B)** by immunofluorescence using 6-4PP and CPD specific antibodies. VH10 wild type cells (WT), VH10 cells expressing CPD-PL or 6-4PP-PL, and NER-compromised (XP-C) XP4PA cells were UV-irradiated and allowed to repair for the indicated time points. Relative fluorescence directly after UV exposure was set at 100% and average fluorescence intensities were plotted in time (n>150 cells of 2 independent experiments +/- SEM). **(C)** Representative immunofluorescence images of GFP-DDB2 expressing VH10 cells that were transduced with either CPD-PL (upper panel) or 6-4PP-PL (lower panel). Cells were non-irradiated or locally UV-C irradiated (60 J/m^2), directly fixed and stained with CPD or 6-4PP antibodies as indicated. Arrows indicate local UV damages. Scale bar: 7.5 µm.

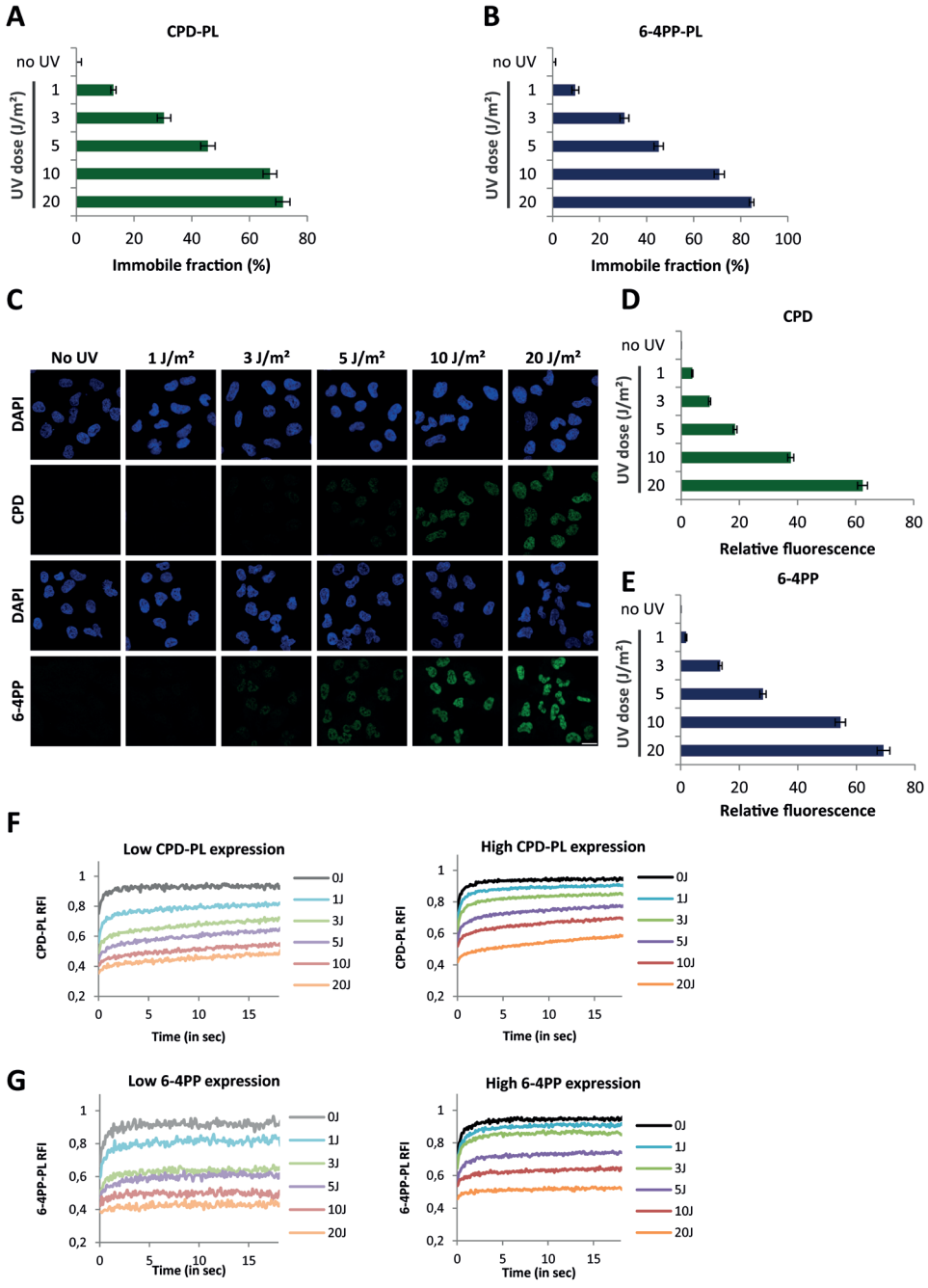
A
CPD-PL
no UV
UV dose (J/m²)
1
3
5
10
20
0
20
40
60
80
Immobile fraction (%)
B
6-4PP-PL
no UV
UV dose (J/m²)
1
3
5
10
20
0
20
40
60
80
100
Immobile fraction (%)
C
No UV
1 J/m²
3 J/m²
5 J/m²
10 J/m²
20 J/m²
DAPI
CPD
DAPI
6-4PP
D
CPD
no UV
UV dose (J/m²)
1
3
5
10
20
0
20
40
60
80
Relative fluorescence
E
6-4PP
no UV
UV dose (J/m²)
1
3
5
10
20
0
20
40
60
80
Relative fluorescence
F
Low CPD-PL expression
CPD-PL RFI
1
0,8
0,6
0,4
0,2
0
5
10
15
Time (in sec)
0J
1J
3J
5J
10J
20J
High CPD-PL expression
CPD-PL RFI
1
0,8
0,6
0,4
0,2
0
5
10
15
Time (in sec)
0J
1J
3J
5J
10J
20J
G
Low 6-4PP expression
6-4PP-PL RFI
1
0,8
0,6
0,4
0,2
0
5
10
15
Time (in sec)
0J
1J
3J
5J
10J
20J
High 6-4PP expression
6-4PP-PL RFI
1
0,8
0,6
0,4
0,2
0
5
10
15
Time (in sec)
0J
1J
3J
5J
10J
20J

Supplementary Figure 2.

(A and B) Immobile fractions of CPD-PL **(A)** and 6-4PP-PL **(B)** expressing VH10 cells in non-irradiated or globally UV-C irradiated at the indicated UV doses as determined by FRAP analyses shown in Figure 2A and 2B. Immobile fractions are calculated using the following formula: Immobile fraction (%) = 1 – ((average fluorescence intensity of UV-irradiated cells – the first post-bleach data point) / (average fluorescence intensity of non-irradiated cells–the first post-bleach data point)). The average fluorescence intensities are calculated over the measurements of the last 10 s. (n = 20 cells from 2 independent experiments, mean ± SEM). **(C)** Representative immunofluorescence images of non-irradiated (no UV) or globally UV-irradiated VH10 cells with the indicated UV doses, directly fixed and stained with CPD or 6-4PP antibodies as indicated. Scale bar: 25 μm. **(D)** CPD or **(E)** 6-4PP lesions (Supplementary Figure S3C) were quantified by determining the mean relative fluorescence intensities in immunofluorescence assays using lesion-specific antibodies. (n ≥ 50 cells, mean ± SEM). UV-treated conditions were background corrected by subtracting the mean fluorescence intensity of the non-irradiated condition. **(F and G)** UV dose-dependent immobilization of CPD-PL **(F)** and 6-4PP-PL **(G)** expressing VH10 cells with low (left panel) or high (right panel) PL expression levels. Non-irradiated or globally UV-irradiated cells were analyzed directly after irradiation with the indicated UV doses. Relative fluorescence intensity (RFI) values were normalized to the average pre-bleach signal (n=20 cells from 2 independent experiments).

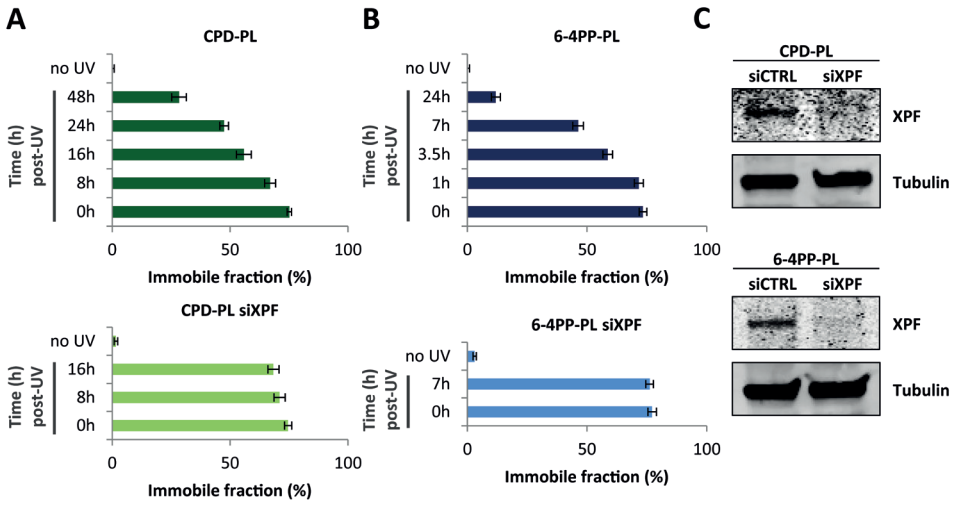

Supplementary Figure 3.

(A and B) Immobile fractions of CPD-PL **(A)** and 6-4PP-PL **(B)** in VH10 cells, which were transfected with control (upper panel) or XPF (lower panel) siRNAs, were determined by FRAP analyses shown in Figure 3E and 3F. (n ≥ 15 cells from 2 independent experiments, mean ± SEM). **(C)** siRNA-mediated XPF knockdown was assessed by immunoblotting VH10 lysates with XPF antibody, tubulin staining was used as loading control.

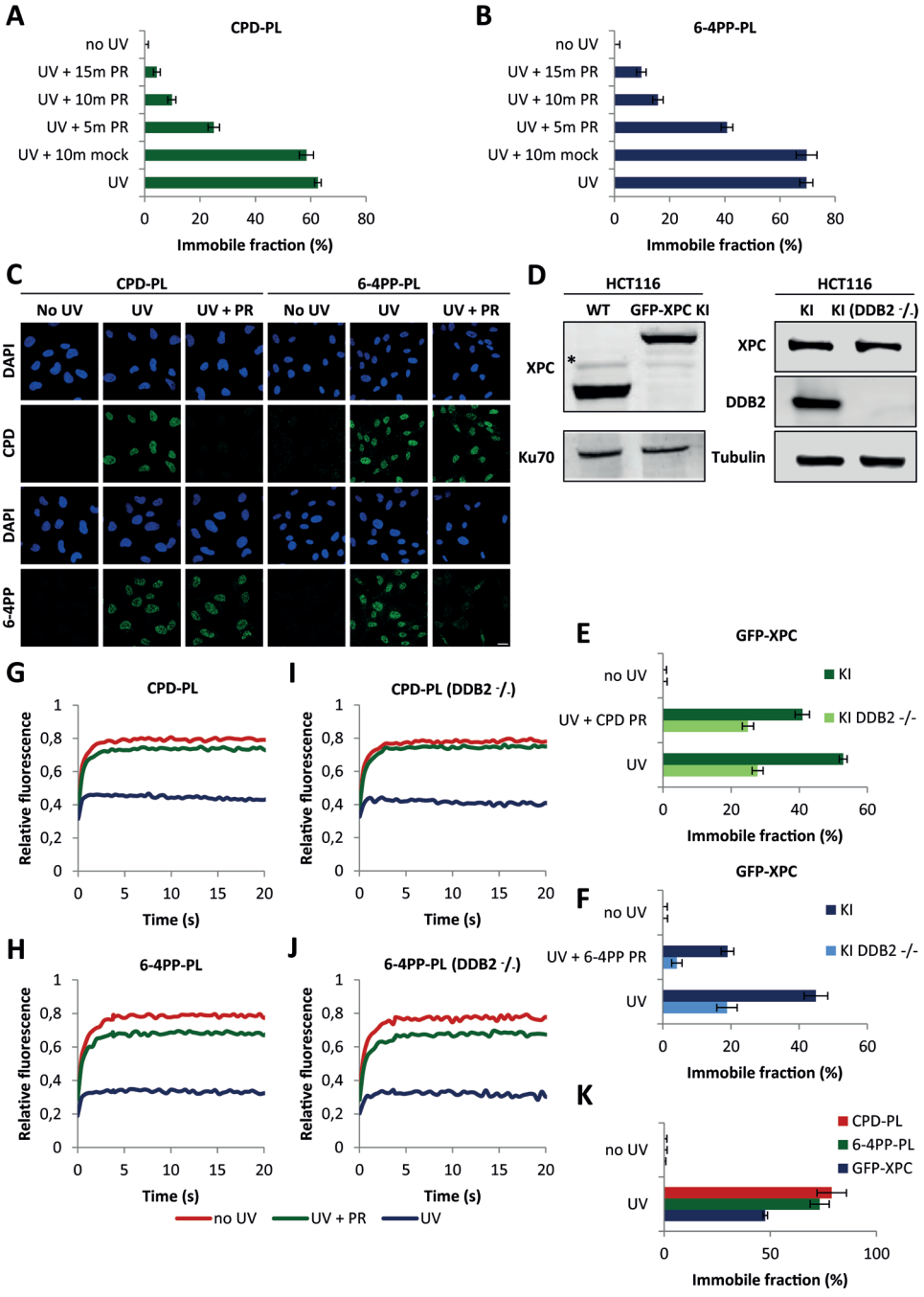
A
CPD-PL
no UV
UV + 15m PR
UV + 10m PR
UV + 5m PR
UV + 10m mock
UV
0 20 40 60 80
Immobile fraction (%)
B
6-4PP-PL
no UV
UV + 15m PR
UV + 10m PR
UV + 5m PR
UV + 10m mock
UV
0 20 40 60 80
Immobile fraction (%)
C
CPD-PL
6-4PP-PL
No UV
UV
UV + PR
No UV
UV
UV + PR
DAPI
CPD
DAPI
6-4PP
D
HCT116
WT
GFP-XPC KI
XPC
*
Ku70
HCT116
KI
KI (DDB2 -/-)
XPC
DDB2
Tubulin
E
GFP-XPC
no UV
UV + CPD PR
UV
KI
KI DDB2 -/-
0 20 40 60
Immobile fraction (%)
F
GFP-XPC
no UV
UV + 6-4PP PR
UV
KI
KI DDB2 -/-
0 20 40 60
Immobile fraction (%)
G
CPD-PL
Relative fluorescence
1
0,8
0,6
0,4
0,2
0
0 5 10 15 20
Time (s)
I
CPD-PL (DDB2 -/-)
Relative fluorescence
1
0,8
0,6
0,4
0,2
0
0 5 10 15 20
Time (s)
H
6-4PP-PL
Relative fluorescence
1
0,8
0,6
0,4
0,2
0
0 5 10 15 20
Time (s)
J
6-4PP-PL (DDB2 -/-)
Relative fluorescence
1
0,8
0,6
0,4
0,2
0
0 5 10 15 20
Time (s)
no UV
UV + PR
UV
K
no UV
UV
CPD-PL
6-4PP-PL
GFP-XPC
0 50 100
Immobile fraction (%)

Supplementary Figure 4.

(A and B) Immobile fractions of non-irradiated, globally UV-irradiated (10 J/m^2), or globally UV-irradiated (10 J/m^2) and photo-reactivated CPD-PL **(A)** and 6-4PP-PL **(B)** as determined by the FRAP analyses depicted in Figure 3A and 3B. **(C)** Representative immunofluorescence images of CPD-PL or 6-4PP-PL-expressing VH10 cells using 6-4PP or CPD lesion specific antibodies as indicated. Cells were non-irradiated, globally UV-irradiated (10 J/m^2), or globally UV-irradiated (10 J/m^2) and photo-reactivated (10 min PR), directly fixed and stained using immunofluorescence. Scale bar: 25 µm. **(D)** Upper panel; Expression of the full-length GFP-XPC protein and the concomitant loss of wild type (WT) XPC expression was confirmed by western blotting the lysates from WT and GFP-XPC knock-in HCT116 cell lines with an XPC antibody. Ku70 staining was used as loading control. * indicates an unspecific band. Lower Panel; CRISPR/Cas9-mediated DDB2 knock-out in GFP-XPC HCT116 cells was confirmed by western blotting with a DDB2 antibody. **(E and F)** Immobile fractions of non-irradiated, globally UV-irradiated (10 J/m^2), or globally UV irradiated (10 J/m^2) and photo-reactivated (10 min) CPD-PL **(E)** and 6-4PP-PL **(F)** expressing GFP-XPC or GFP-XPC DDB2$^-$/- (DDB2$^-$/-) HCT116 cells determined in the FRAP analyses depicted in Figure 3C-F. **(G and H)** FRAP analyses of PL-mCherry in non-irradiated, globally UV-irradiated (10 J/m^2), or globally UV-irradiated (10 J/m^2) and photo-reactivated (10 min) CPD-PL **(G)** and 6-4PP-PL **(H)** expressing GFP-XPC HCT116 cells. **(I and J)** FRAP analyses of PL-mCherry in non-irradiated, globally UV-irradiated (10 J/m^2), or globally UV-irradiated (10 J/m^2) and photo-reactivated (10 min) CPD-PL **(I)** and 6-4PP-PL **(J)** expressing GFP-XPC DDB2$^-$/- HCT116 cells (n ≥ 20 cells from 2 independent experiments, mean ± SEM). **(K)** Direct comparison of immobile fractions of CPD-PL, 6- 4PP-PL and GFP-XPC in non-irradiated or globally UV-irradiated (XX J/m^2) cells (n ≥ 20 cells from 2 independent experiments, mean ± SEM).

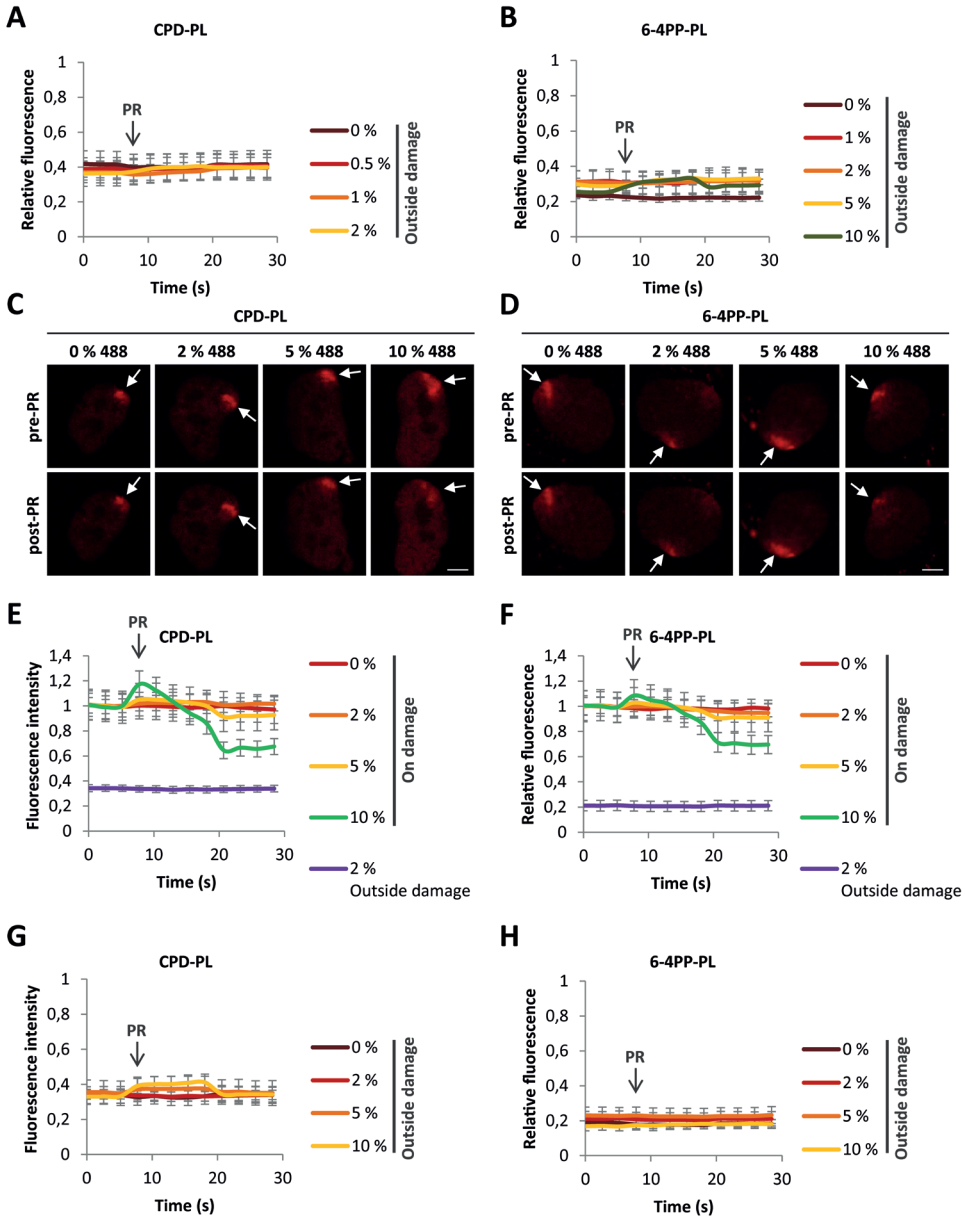
A
CPD-PL
Relative fluorescence
PR
Time (s)
0 %
0.5 %
1 %
2 %
Outside damage
B
6-4PP-PL
Relative fluorescence
PR
Time (s)
0 %
1 %
2 %
5 %
10 %
Outside damage
C
CPD-PL
0 % 488
2 % 488
5 % 488
10 % 488
pre-PR
post-PR
D
6-4PP-PL
0 % 488
2 % 488
5 % 488
10 % 488
pre-PR
post-PR
E
PR
CPD-PL
Fluorescence intensity
Time (s)
0 %
2 %
5 %
10 %
On damage
2 %
Outside damage
F
PR
6-4PP-PL
Relative fluorescence
Time (s)
0 %
2 %
5 %
10 %
On damage
2 %
Outside damage
G
CPD-PL
Fluorescence intensity
PR
Time (s)
0 %
2 %
5 %
10 %
Outside damage
H
6-4PP-PL
Relative fluorescence
PR
Time (s)
0 %
2 %
5 %
10 %
Outside damage

Supplementary Figure 5.

(A and B) Relative mCherry fluorescence signal of CPD-PL **(A)** and 6-4PPPL **(B)** in a non-damaged nuclear region following PR normalized to pre-PR intensities at the local damage (n = 8 cells, mean ± SEM). Cells were locally UV-irradiated (60 J/m^2), then a non-damaged nuclear region was exposed after 7.5 sec (indicated by arrow and PR) to the indicated intensities of 405 nm laser for 13 s. (n = 8 cells, mean ± SEM). **(C and D)** Representative images of CPD-PL **(C)** and 6-4PP-PL **(D)** expressing VH10 cells before and 13 s after PR using 488 nm laser at the indicated intensity. Arrows indicate local UV damages. Scale bar: 5 μm. **(E, F, G and H)** Cells were locally UV irradiated (60 J/m^2), the local DNA damage spot and a region of the exact same size outside the damage within the nucleus were exposed after 7.5 s (indicated by arrow and PR) to the indicated intensities of 488 nm laser for 13 s. Relative fluorescence signal normalized to pre-PR intensities at the local damage of the mCherry-tagged PLs was quantified inside **(E and F)** and outside **(G and H)** the DNA damage within the nucleus. (n = 8 cells, mean ± SEM).

Appendix

THESIS SUMMARY

All the information required to generate and sustain an organism is stored in the genome. However, this precious source of genetic information is not damage resistant as its integrity is continuously challenged by endogenous and exogenous factors which can cause a range of structurally different DNA lesions. The three main culprits responsible for inducing DNA damage are cellular metabolism byproducts, spontaneous DNA alterations, and environmental agents. In this thesis, we focus on DNA damage induced by one of the most abundant environmental DNA damaging agents, ultraviolet (UV) light found in sunlight. Only a few hours of skin exposure to sunlight could lead to > 100,000 lesions of cyclobutane pyrimidine dimers (CPDs) and 6-4 photoproducts (6-4PPs), the two most abundant UV-induced DNA lesions, in each skin cell. These lesions can impede essential cellular mechanisms such as DNA replication and RNA transcription, initially leading to mutations, cellular malfunction, or even cell death, which could eventually result in the onset of cancer or accelerated aging. Fortunately, these adverse consequences could be averted by highly efficient DNA repair pathways. UV-light induced DNA damage is efficiently removed by nucleotide excision repair (NER) which eradicates a broad array of DNA helix-destabilizing lesions. If left unrepaired due to inactivating mutations in NER genes, these lesions could lead to severe human disorders, like the cancer-prone disease xeroderma pigmentosum (XP) or the premature aging disorder Cockayne's syndrome (CS), reflecting the significance of NER.

NER is a complex repair pathway entailing at least 30 proteins in successive reaction stages of damage recognition, verification, excision, and gap-filling repair synthesis, as described in detail in **Chapter 1**. For such a complex, multi-protein reaction to function efficiently, both the sequential NER factor recruitment and their timely release to allow the loading of the consecutive NER factors are essential. For this, it is necessary that tightly regulated lesion handover mechanisms exist between NER proteins at each consequent repair step. Moreover, since NER functions in a dynamic chromatin environment, NER is also influenced by other activities such as DNA replication, RNA transcription, or chromatin remodeling, which collectively escalate the complexity of NER pathway regulation. Although our understanding of the NER mechanism has greatly expanded since its discovery more than fifty years ago, our current knowledge is still limited about its dynamic regulation in time and space, specifically that of lesion handover between successive steps.

In **Chapter 2**, we set out to identify novel NER regulators to obtain a better understanding of NER regulation. For this, we focused on the interactors of general transcription factor II H (TFIIH), as TFIIH is a central NER player with various roles in multiple reaction steps—i.e., unwinding DNA around the lesion, verifying the lesion, helping the building of the incision complex and being released together with the incised lesion-containing oligonucleotide. TFIIH contains ten subunits, which form the core TFIIH complex and the CAK sub-complex, and was originally identified as an essential transcription initiation factor. We studied endogenous TFIIH complexes using cells derived from a knock-in mouse model that expresses YFP-tagged XPB, a core TFIIH subunit, from its endogenous gene locus. Utilizing SILAC-based quantitative mass spectrometry (MS) in combination with two immunoprecipitation (IP) approaches, native and cross-linking IP, we successfully purified TFIIH protein complexes and investigated UV damage-induced changes in the TFIIH interaction network in detail. We validated our approach by confirming by MS the presence of known UV-induced TFIIH interactors; ERCC1, XPF, XPG, and XPA. Most interestingly, we identified a new UV-induced interaction partner of TFIIH, the helicase-like transcription factor (HLTF).

HLTF is the closest human orthologue of the yeast Rad5 protein that functions in the post-replication repair pathways (PRR) template switching (TS) and translesion synthesis (TLS). Yet, HLTF has never been described to function in NER before. This is why, in **Chapter 3**, we investigated the functional relevance of the uncovered TFIIH-HLTF interaction for the NER reaction. Our results show that HLTF is recruited to the TFIIH-containing NER-intermediate after double incision and before repair synthesis. The use of non-replicating cells or depletion of Rad18, which is required for HLTF's full activity during PRR, confirmed that our observations are independent of the role of HLTF in PRR. Our results acquired using an *in vivo* excision assay and staining for γH2AX-mediated signaling suggest that HLTF is responsible for the release of the excised DNA damage containing oligonucleotide. HLTF possesses multiple domains—i.e., a ubiquitin ligase RING domain, a dsDNA translocase SWI/SNF helicase domain, and a 3'-OH ssDNA end binding HIRAN domain. By using specific HLTF mutants that inactivate either of these domains, we uncovered that the RING domain is not required for NER, suggesting that the role of HLTF in PRR to ubiquitylate PCNA is not relevant for NER. Interestingly, our data indicate that the HIRAN domain is required to recruit HLTF to NER complexes by enabling HLTF to interact with 3'-OH at the dsDNA/ssDNA junction generated by XPF-ERCC1, in line with its 3'-OH ssDNA end binding

ability. The SWI/SNF helicase domain appeared to be important for the eviction of the excised damage-containing short stretch of DNA, together with associated incision complex members. A similar mechanism is already described in bacterial NER in which the helicase UvrD releases the endonuclease UvrC and incised DNA fragment, and in this way enabling repair synthesis by DNA polymerase I. In line with this, we observed severely impaired unscheduled DNA synthesis, which measures repair synthesis, upon HLTF depletion. Overall, similar to UvrD in bacterial NER, our study presents HLTF as a novel NER factor which removes the incised lesion-containing DNA fragment likely together with associated incision complex members to enable repair synthesis.

In NER, DNA lesions located throughout the whole genome are recognized by the global genome NER (GG-NER) specific damage recognition factors. Transcription-coupled NER (TC-NER) is triggered by transcription-blocking DNA lesions (TBLs) in actively transcribed genes, in which the TC-NER factors CSA, CSB, and UVSSA are recruited to lesion-stalled RNA Pol II to allow further processing by core-NER factors. Currently, it is not completely known how these TC-NER factors are recruited to TBLs and build up the TC-NER machinery. To gain more insight into this mechanism, in **Chapter 4**, we studied the accumulation kinetics of TC-NER factors in living cells. We demonstrated that the recruitment of UVSSA to TBLs is independent of CSA and CSB and we made use of specific UVSSA domain mutants to further dissect the role of this protein in TC-NER. Our results show that both the C-terminal DUF2043 domain and the N-terminal VHS domain are necessary for TC-NER, with the former being required for UVSSA recruitment to TBLs and the latter being required for UVSSA interaction with CSA. Utilizing these UVSSA mutants in combination with quantitative interaction proteomics, we observed that UVSSA interacts with both subunits of the H2A/H2B chaperone FACT complex, Spt16 and SSRP1, through its DUF2043 domain. Interestingly, although SSRP1 depletion had no effect, Spt16 depletion reduced UVSSA accumulation but had no effect on CSB accumulation. These observations suggest that Spt16 specifically facilitates UVSSA recruitment to TBLs. Moreover, Spt16 depletion resulted in a significant reduction of the TC-NER-mediated UDS, suggesting that by mediating UVSSA recruitment, Spt16 enhances TC-NER repair. Overall, we reveal Spt16 as a TC-NER regulator and provide important insights into the TC-NER factor recruitment to TBLs.

Although NER is the sole pathway to eradicate UV-induced DNA damage in placental mammals, another repair mechanism, namely photo-reactivation (PR), has been evolutionarily conserved in all branches of life, from bacteria to non-placental mammals. Whereas NER is a complex repair pathway involving at least 30 proteins, PR requires only one damage-specific protein for each of the CPD and 6-4PP lesions, namely CPD and 6-4PP photolyases (PLs), which catalytically reverse the damaged DNA to the original DNA within ~1 ns utilizing the energy absorbed from visible light. This swift damage removal and lesion specificity of the PLs make them attractive tools to investigate UV-induced damage and repair. In **Chapter 5**, we made use of these characteristics of PLs to quantify UV-induced DNA damage and repair, by tagging the CPD and 6-4PP PLs with mCherry fluorescent protein. Using these PLs in fluorescence recovery after photo-bleaching (FRAP) assays, we established a new method that enables quantifying UV-induced DNA damage and repair kinetics in a highly sensitive and dose-dependent manner, in real-time, in living cells. Additionally, we established a new method that enables immediate reversal of UV-induced DNA damage in a lesion-specific manner in living cells in a subnuclear region, utilizing 405 nm laser-mediated photo-reactivation of the PLs. This method could be used to examine lesion-specific NER dynamics and cellular responses upon damage removal. Altogether, our results show that fluorescently-tagged PLs can be utilized as a powerful tool to detect, quantify and repair UV-induced DNA damage, in order to investigate NER kinetics and UV-induced DNA damage response in living cells.

In **Chapter 6**, we discuss our main findings, focus on remaining issues, and provide an outlook over the possible future directions in the field of UV-induced DNA damage and repair within the context of the research questions addressed in this thesis.

SAMENVATTING

Alle informatie die nodig is om een organisme te vormen en onderhouden is opgeslagen in het genoom. Deze waardevolle bron van genetische informatie is echter niet resistent tegen schade, omdat deze continu blootgesteld wordt aan zowel endogene en exogene factoren, welke een legio aan structureel verschillende DNA-schades kunnen veroorzaken. De drie voornaamste bronnen van DNA-schade zijn bijproducten van het cellulaire metabolisme, spontane DNA-veranderingen en invloeden van uit het milieu. In dit proefschrift ligt de focus op DNA-schade geïnduceerd door ultraviolette (UV) straling vanuit zonlicht, één van de meest voorkomende DNA-schades. Slechts een paar uur blootstelling van de huid aan zonlicht kan al leiden tot meer dan 100.000 laesies per huidcel. De twee meest voorkomende UV-geïnduceerde DNA laesies zijn cyclobutaan pyrimidine dimeren (CPDs) en 6-4 photoproducten (6-4PPs). Deze DNA-beschadigingen kunnen essentiële cellulaire mechanismen, zoals DNA-replicatie en RNA-transcriptie verstoren, welke kunnen leiden tot mutaties, cellulaire disfunctie of zelfs celdood. Dit kan uiteindelijk resulteren in kanker of versnelde veroudering. Deze nadelige gevolgen worden gelukkig tegengegaan door zeer efficiënte DNA-reparatie mechanismen. Zo wordt DNA-schade geïnduceerd door UV-licht bijvoorbeeld efficiënt verwijderd door nucleotide excisie reparatie (NER). Dit DNA-reparatie proces kan een breed spectrum van DNA helix-destabiliserende laesies repareren. Wanneer deze laesies niet gerepareerd worden, bijvoorbeeld door inactiverende mutaties in één van de NER-genen, dan kan dit leiden tot ernstige erfelijke aandoeningen, zoals de kankergevoelige ziekte xeroderma pigmentosum (XP) of Cockayne's syndrome (CS) waarvan de patiënten gekarakteriseerd worden door vroegtijdige veroudering. De ernstige symptomen van deze DNA-reparatie syndromen illustreren het belang van een goed functionerend NER.

NER is een complexe reparatieroute waarbij minstens 30 verschillende eiwitten betrokken zijn, die in verschillende opeenvolgende reactiestappen functioneren, namelijk schadeherkenning, verificatie, excisie en DNA-reparatie synthese. Deze stappen worden in detail in **Hoofdstuk 1** beschreven. Om een dergelijke reparatieroute efficiënt te laten functioneren is het essentieel dat zowel de rekrutering van NER factoren als het op tijd loslaten hiervan goed gecoördineerd verloopt. Daarom is het van belang dat er een gecontroleerd mechanisme bestaat die de verschillende NER-eiwitten bij de opeenvolgende reparatie stappen aan de laesie laat binden. Omdat NER in een dynamische chromatine-omgeving functioneert, wordt NER ook beïnvloedt door andere processen die in chromatine plaatsvinden, zoals DNA-replicatie, RNA-transcriptie en

remodeleren van chromatine. Hoewel onze kennis over het NER-mechanisme flink is toegenomen sinds de ontdekking hiervan, meer dan vijftig jaar geleden, is onze kennis over de dynamische regulatie in tijd en ruimte, specifiek die van de laesie doorgave tussen opeenvolgende reactiestappen nog steeds beperkt.

In **Hoofdstuk 2** zijn we opzoek gegaan naar nieuwe NER regulerende eiwitten om zo het NER-mechanisme beter te begrijpen. Hiervoor hebben we ons geconcentreerd op eiwitten die binden aan het basale transcriptie factor II H (TFIIH) complex, omdat TFIIH een multifunctionele rol speelt binnen verschillende NER stappen. TFIIH is belangrijk voor het ontwinden van DNA rondom de laesie, speelt een belangrijke rol bij de opbouw van het incisie-complex en wordt tenslotte samen met de laesie-bevattende oligonucleotide verwijdert na de dubbele incisie. TFIIH, origineel geïdentificeerd als essentiële transcriptie initiatie factor, bevat tien eiwitten welke de kern van het TFIIH-complex en het CAK sub-complex vormen. Wij hebben endogene TFIIH-complexen bestudeerd, waarbij we cellen hebben gebruikt die afkomstig zijn uit een knock-in muizenmodel, welke een YFP-gemarkeerde versie van XPB, een TFIIH eiwit, tot expressie brengt van zijn endogene genomische locus. Door gebruik te maken van kwantitatieve massaspectrometrie (MS) in combinatie met zowel een native en een cross-linking immunoprecipitatie (IP) methode hebben we succesvol TFIIH eiwit complexen gezuiverd en vervolgens de UV schade-geïnduceerde veranderingen in het TFIIH interactienetwerk in detail onderzocht. De aanwezigheid van bekende UV-geïnduceerde TFIIH interactie-eiwitten zoals ERCC1, XPF, XPG en XPA laat zien dat onze methodes succesvol zijn. De meest interessante vinding echter, was de identificatie van een nieuwe UV-geïnduceerde interactie partner van TFIIH, de helicase-like transcriptiefactor (HLTF).

HLTF is de humane ortholoog van het gist eiwit Rad5 dat een rol speelt in de post-replicatie processen (PRR): template switching (TS) en translaesie synthese (TLS). Van HLTF is echter nooit eerder een rol in NER beschreven. In **Hoofdstuk 3** hebben we om deze reden de rol van de TFIIH-HLTF interactie tijdens de NER reactie onderzocht. Onze resultaten laten zien dat HLTF gerekruteerd wordt door het TFIIH-bevattende NER-intermediair na dubbele incisie, maar vóór de reparatiesynthese. Het gebruik van niet-replicerende cellen of depletie van Rad18, welke nodig is voor HLTF's rol in PRR, bevestigde dat onze observatie losstaat van de rol van HLTF in PRR. Onze resultaten laten zien dat HLTF verantwoordelijk is voor het actief verwijderen van de uitgeknipte

DNA-schade-bevattende oligonucleotiden. HLTF bevat meerdere domeinen; een ubiquitine ligase (RING) domein, een dsDNA translocase (SWI/SNF-helicase) domein en een 3'-OH ssDNA einde bindend HIRAN domein. Door specifieke HLTF-mutanten te gebruiken hebben we ontdekt dat het RING domein niet nodig is voor NER, wat suggereert dat de HLTF-gemedieerde PCNA ubiquitylatie niet relevant is voor het NER proces. Onze data geeft, interessant genoeg, aan dat het HIRAN domein nodig is om HLTF te rekruteren naar NER complexen, waarschijnlijk doordat HLTF bindt aan de 3'-OH groep van ssDNA na incisie door XPF-ERCC1. Na zijn rekrutering naar het NER complex, is het SWI/SNF-helicase domein van HLTF essentieel voor de verwijdering van het schade bevattende stukje DNA na dubbele incisie. Een soortgelijk mechanisme is eerder beschreven in bacterieel NER, waarin de helicase UvrD het door UvrC ingeknipte DNA fragment verwijdert, waardoor DNA reparatie synthese door DNA polymerase I kan plaatsvinden. Samengevat hebben we HLTF geïdentificeerd als nieuwe NER factor, die actief het stuk DNA met schade na dubbele incisie verwijdert samen met eiwitten van het gebonden incisie complex zodat de laatste NER-stap, de DNA-synthese, kan plaatsvinden.

In globaal genoom NER (GG-NER) worden DNA laesies in het gehele genoom herkent door specifieke schade herkenningsfactoren. Transcriptie-gekoppeld NER (TC-NER) vindt alleen plaats in de getranscribeerde DNA streng van actieve genen. TC-NER wordt geïnduceerd door de TC-NER factoren CSA, CSB en UVSSA die gerekruteerd worden naar RNA Polymerase II dat is vast gelopen op de DNA-schade. Na de schade herkenning is het verdere verloop van GG-NER en TC-NER hetzelfde. Er is nog veel onbekend hoe deze TC-NER factoren gerekruteerd worden naar DNA-schade en hoe ze vervolgens het TC-NER complex opbouwen. Om meer inzichten in dit mechanisme te verkrijgen hebben we in **Hoofdstuk 4** de schade rekruterings-kinetiek van TC-NER factoren in levende cellen bestudeerd. We hebben aangetoond dat de schade rekrutering van UVSSA onafhankelijk is van CSA en CSB. Vervolgens hebben we gebruik gemaakt van specifieke UVSSA-mutanten om de rol van dit eiwit in TC-NER verder te onderzoeken. Onze resultaten laten zien dat zowel het C-terminale DUF2043 domein, als het N-terminale VHS domein nodig zijn voor TC-NER, waarbij de eerstgenoemde nodig is voor UVSSA rekrutering naar schade, terwijl het VHS domein nodig is voor de UVSSA interactie met CSA. Door gebruik te maken van deze UVSSA-mutanten in combinatie met kwantitatieve interactie proteomics, hebben we laten zien dat UVSSA bindt aan de Spt16 en SSRP1 eiwitten van het H2A/H2B-chaperone FACT complex,

via het DUF2043 domein. Na depletie van Spt16 vonden we dat de UVSSA binding aan DNA schade sterk gereduceerd wordt, maar dat dit geen effect had op CSB ophoping. Verrassend was de vinding dat SSRP1 depletie geen effect had op de UVSSA-rekrutering naar DNA-schade. Deze observaties suggereren dat Spt16 specifiek UVSSA-rekrutering naar DNA-schade faciliteert. In overeenstemming met deze observatie, vonden we dat Spt16 depletie leidt tot een significante reductie van TC-NER-gemedieerde DNA-synthese. Dit suggereert dat Spt16 TC-NER stimuleert door UVSSA naar RNA polymerases te rekruteren die vast gelopen zijn op een DNA schade.

NER is het enige reparatie proces dat UV-geïnduceerde DNA schade kan verwijderen in zoogdiercellen. Echter in alle andere takken van het leven, van bacteriën tot zoogdieren zonder placenta, is er een evolutionair geconserveerd ander reparatiemechanisme, namelijk photo-reactivatie (PR). Terwijl NER een complexe reparatieroute is waar tenminste 30 eiwitten bij betrokken zijn, bestaat PR slechts uit één schade-specifiek eiwit, de zogenaamde photolyases, om of CPDs, of 6-4PPs te repareren. Deze CPD en 6-4PP photolyases (PLs) katalyseren het terugbrengen van de photo-dimeren naar de originele losse nucleotiden van het DNA, in slechts ~1 ns. Bij dit proces wordt de energie van geabsorbeerd licht gebruikt. Deze snelle schade verwijdering en laesiespecificiteit van de PLs maken deze eiwitten aantrekkelijke gereedschappen om UV-geïnduceerde schade en reparatie te onderzoeken. In **Hoofdstuk 5** hebben we van deze eigenschappen gebruik gemaakt om UV-geïnduceerde DNA-schade en reparatie te kwantificeren. Hiervoor hebben we de CPD en 6-4PP PLs gemarkeerd met het mCherry fluorescente eiwit. Door deze fluorescente PLs te gebruiken in de zogenaamde fluorescence recovery after photo-bleaching (FRAP) meetmethode, hebben we een nieuwe methode opgezet om met een hoge gevoeligheid de kinetiek van UV-geïnduceerde DNA-schade en reparatie te kwantificeren, in levende cellen. Verder hebben we een nieuwe methode ontwikkeld om direct UV-geïnduceerde schade te repareren in een klein gedeelte van de celkern in levende cellen door gebruik te maken van een 405 nm laser om zo de PLs te (photo)activeren. Deze methode zou gebruikt kunnen worden om de laesie-specifieke NER-dynamiek te onderzoeken en om cellulaire reacties na verwijdering van schade te bestuderen. Onze resultaten laten zien dat fluorescent-gelabelde PLs gebruikt kunnen worden als krachtige methode om UV-geïnduceerde DNA-schade te detecteren, te kwantificeren en te repareren, zodat zowel de NER-kinetiek als de respons van levende cellen op UV-geïnduceerde DNA-schade onderzocht kan worden.

In **Hoofdstuk 6** bediscussiëren we onze belangrijkste bevindingen, met nadruk op de belangrijkste openstaande vragen binnen het NER-veld en blikken we vooruit op de mogelijke toekomstige richtingen in het veld van UV-geïnduceerde DNA-schade en reparatie binnen het kader van de onderzoeksvragen die in dit proefschrift geadresseerd zijn.

CURRICULUM VITAE

UNIVERSITY EDUCATION

Master of Science	2009-2011
Molecular Mechanisms of Disease, Radboud University Nijmegen	
Bachelor of Science	2004-2009
Biology, Middle East Technical University, Ankara	

WORK EXPERIENCE

Data Steward	2018-Present
Faculty of Mechanical, Maritime and Materials Engineering, Delft University of Technology	
PhD candidate	2013-2017
Department of Molecular Genetics, Erasmus MC, Rotterdam	

AWARDS

RDA 12th Plenary European Early Career grant winner	2018
NWO grant based on own PhD proposal from Erasmus MC Medical Genetics Graduate School	2013
Study Fund UMC St Radboud	2009-2011
Radboud Scholarship Programme	2009-2011
Graduated as an honor student from Middle East Technical University	2009

LIST OF PUBLICATIONS

van Cuijk, L. [#], van Belle G.J. [#], **Turkyilmaz Y.**, et al. SUMO and ubiquitin-dependent XPC exchange drives nucleotide excision repair. Nat. Commun. 6:7499 DOI: 10.1038/ncomms8499 (2015)

Steurer B., **Turkyilmaz Y.**[#], et al., Fluorescently-labelled CPD and 6-4PP photolyases: new tools for live-cell DNA damage quantification and laser-assisted repair. Nucleic Acids Research, DOI: 10.1093/nar/gkz035 (2019)

Wienholz F., Zhou D.[#], **Turkyilmaz Y.**[#], et al., FACT subunit Spt16 controls UVSSA recruitment to lesion-stalled RNA Pol II and stimulates TC-NER. Nucleic Acids Research, DOI: 10.1093/nar/gkz055 (2019)

van Toorn M.[#], **Turkyilmaz Y.**[#], et al., From incision to excision: active damage eviction by HLTF stimulates repair. Submitted.

Cruz, M., Kurapati, S. and **Turkyilmaz Y.** The Role of Data Stewardship in Software Sustainability and Reproducibility. IEEE DOI: 10.1109/eScience.2018.00009 (2018)

Andrews Mancilla, H., Teperek, M., van Dijck, J., den Heijer, K., Eggermont, R., Plomp, E., **Turkyilmaz-van der Velden, Y.** and Kurapati, S. On a Quest for Cultural Change - Surveying Research Data Management Practices at Delft University of Technology. LIBER Quarterly, DOI: 10.18352/lq.10287 (2019)

Cruz, M., Dintzner, N., Dunning, A., van der Kuil, A., Plomp, E., Teperek, M., **Turkyilmaz-van der Velden, Y.** and Versteeg, A. Policy Needs to Go Hand in Hand with Practice: The Learning and Listening Approach to Data Management. Data Science Journal, DOI: 10.5334/dsj-2019-045 (2019)

# These authors contributed equally.

PhD PORTFOLIO

Name: Yasemin Türkyilmaz
PhD period: April 2013 – October 2017

Erasmus MC Department: Molecular Genetics
Research School: Biomedical Sciences, MGC

Promoter: Prof. dr. Wim Vermeulen
Co-promoter: Dr. Jurgen Marteijn

General courses

Biomedical English Writing and Communication	2017
Research Integrity	2015
Biostatistical Methods I: Basic Principles Part A	2015
Cell and Developmental Biology	2014
Genetics	2013
Biochemistry and Biophysics	2013
Safely Working in the Laboratory	2013
ML-I (work permit for GMOs)	2013
ML-II (work permit for Adenovirus and Lentivirus)	2013

Specialized courses

Workshop on Microsoft Excel 2010: Basic	2014
Genome Maintenance and Cancer	2014
MGC Technology Facilities: Proteomics	2014
Microscopic Image Analysis: From Theory to Practice	2014
Functional Imaging and Super Resolution	2013
Leica Confocal Introduction Course	2013

Teaching Assistance and Project Supervision

MSc student internship supervisor	2017
BSc student internship supervisor	2015
Practical BSc Nanobiology, Erasmus MC and TU Delft	2013-2016

Seminars, workshops and (inter)national conferences

Oral presentations:

Koç University, Molecular Biology and Genetics Department, Istanbul, Turkey (invited talk)	2017
Nucleotide excision repair and crosslink repair, FEBS Workshop, Slovakia (selected talk based on abstract)	2017
MGC DNA Repair Meeting, Leiden, the Netherlands	2017
22nd MGC PhD Workshop, Maastricht, the Netherlands	2015

Poster presentations:

Nucleotide excision repair and crosslink repair, FEBS Workshop, Slovakia	2017
Responses to DNA damage: from molecule to disease, Egmond aan Zee, the Netherlands	2016
PTMs in Cell Signaling, Copenhagen, Denmark	2014
21st MGC PhD Workshop, Munster, Germany	2014
20th MGC PhD Workshop, Luxembourg City, Luxembourg	2013

Attendance only:

Genomic Instability in Cancer, CGC.nl annual meeting, Amsterdam, the Netherlands	2016
25th MGC Symposium, Leiden, the Netherlands	2015
CGC.nl Annual Scientific Meeting, Utrecht, the Netherlands	2014
23rd MGC Symposium, Rotterdam, the Netherlands	2013

ACKNOWLEDGEMENTS

This is the most important part of my thesis, thanking all who accompanied me during my PhD journey. I will try my best to thank all who crossed paths with me during this journey and contributed to it one way or another. Apologies in advance if there are any I forget to mention, 7 years is a long time after all.

Jurgen, when I first came to the lab for the rotation process of the grant I applied for, I thought that it was just going to be a chat. Instead, there was a whole experiment arranged for me. I was quite impressed with the professionalism and being quite interested in the research topic, I wanted to pursue my PhD in your group. Thank you for agreeing, for all your scientific input with many nice ideas and interesting discussions, and for your support and encouragement. I learned a lot from you during this journey. I also appreciate that you take the effort in celebrating the successes of the team together with your team members.

Wim, thank you for your open door policy, and being so supportive and encouraging from the very beginning till the very end of this journey. Your calm and positive attitude has helped me a lot, especially during the harder parts. Thank you for all the lab day outs, gezellige BBQ's in your garden, and nice chats about your travels in Turkey and other countries.

Franzi, Cristina & Jana, it was such a pleasure to have you as colleagues and more importantly as friends. I don't know how I would have made it through my PhD without all the nice moments and laughter we shared together, as well as all your support during the hard parts. We have shared many nice memories including three weddings, five children, Turkish breakfasts, fancy dinners, picnics, and many more. I am so glad to have you as my friends! **Franzi,** you are the most efficient and productive person I have ever seen, I believe that it is the German genes ;P. I was so lucky to have you as a colleague that I can always rely on and ask for help with experiments, protocols, data analysis, and so on. I think that I got almost all my protocols and excel sheets with formulas for data analysis from you. Thanks for the UDS experiments as well. Also thanks for organizing a surprise bachelor party for me and all your nice ideas for our wedding ;) **Cristina,** starting our PhD journeys with only two months apart, we shared a lot together. It was especially very nice to go through the last bit together. Thank you for answering all my questions, all your support and encouragement. Also thanks for the

RRS experiments, all your help with the microscope, and other things in the lab. You are a critical and objective thinker and that is why I regularly ask for your advice. Thank you so much for all your valuable advice about not only scientific matters but also real-life matters, much appreciated! **Jana**, your time with us was short and sweet. You are missed a lot. I hope to meet again soon because there is a lot to catch up ;)

Many thanks to current and ex-lab members for all the nice chats and moments we shared. I am afraid that I will epically fail at acknowledging everything but here are some highlights. **Hannes**, thanks for all the nice discussions, especially those about music. Sorry that you missed the performance of Thijs van Leer, it was awesome :) **Karen,** thanks for all the emotional support and taking time to listen, much appreciated! **Alex**, thanks for all the protocols, papers, and ideas you shared with me, and no thanks for crawling on the lab floor and trying to scare me :) **Roel,** thanks for complaining together about NS trains not arriving on time ;) **Maria**, thanks for being kind and encouraging. **Arjan**, thanks for providing me cell lines and FACS sorting them, and no thanks for the smelly slagroom taart :) **Anja,** thanks for the UDS experiments.

Mariangela, thank you for always being so kind and positive, much needed in a PhD journey. **Imke,** thank you for all your help, especially at the beginning of my PhD and all the fun parts. **Barbara,** thank you for the nice conversations. **Marit** and **Angela**, thanks for being such nice office mates. **Marvin**, thanks for all your hard work on the XPC, Photolyase and HLTF projects. Thanks to you, the HLTF story is finally complete and it is very impressive work ;) **Masaki**, thanks for all the CPD and 6-4PP assays, the delicious Japanese food, and the nice photos from your journeys. **Loes**, thank you for showing me many lab protocols at the beginning of my PhD.

Maikel, **Petra, Bert-Jaap, Serena, Aida, Marjolein, Akos, Kishan,** the internship students, and others that I am possibly forgetting, thanks for all the nice moments. All the new recruits, unfortunately we did not have much time together. I wish you all lots of success in your journeys.

The Turkish gang at Erasmus MC, **Özge, Nesrin, Nilhan, Merih** and our French side-kick **Fanny**, thank you for all the laughter, drinks, Turkish breakfasts, dinners, belly dancing, singing and all other nice moments we shared together. **Özge**, ilk baştan itibaren hem labtaki bütün yardımların, hem de gösterdiğin sıcak dostluk icin ne kadar

teşekkür etsem az. Az derdimi sıkıntımı dinlemedin ama çok da gülüp eğlendik de :) Hollanda'dan iki kere Türkiye'ye dönüşün sebebiyle iki kere hüzünlü şekilde vedalaşmak durumunda olmasaydık keşke. Sen döndükten sonra yerin dolmadı hiç, eğer bir gün geri dönme kararı alırsan çok mutlu edeceğin dostların var burda ;) **Nesrin,** özellikle doktoranın başında beni sayısız kere evinde ağırladığın için gerçekten çok teşekkür ederim, hakkını ödeyemem. Walenburgerweg'teki evinizde ne güzel anılarımız oldu, bütün cana yakınlığın için teşekkürler. **Nilhan**, bir türlü çalışmak ya da bitmek bilmeyen deneyler arasında kahve molaları ve yemek araları derken günün modunu değiştiren keyifli sohbetler için teşekkürler. **Merih,** bir kaç yıl aradan sonra birgün Hollanda'nın küçük kasabası Berkel'de Albert Heijn'da tesadüfen karşılaşıp tekrar buluşmak varmış. Ne de güzel bir tesadüf oldu gerçekten :) Annemle ortak arkadaşım sevgili **Nur**, herşey için çok teşekkür ederim. En kısa zamanda hepinizle tekrardan görüşmek dileğiyle.

This section would be incomplete without thanking my current colleagues for all the nice moments as well as all their support. **André**, many thanks for being ever so supporting and encouraging, for not only my current role but also my PhD. Also many thanks for always giving me room to explore and grow. **Marja**, thank you as well. **Roy**, thanks for regularly asking about the progress of my thesis and making sure that I was on track, and thanks to both you and **Mascha** for all your support. **Marta**, I cannot thank you enough. You have always been so supportive, encouraging, and inspiring, and I have learned so much from you. I am so glad to have you as a colleague and most importantly as a friend. Members of the Data Steward and Research Data Support teams and other colleagues, **Heather, Kees, Nicolas, Yan, Santosh, Jeff, Esther, Ellen, Paula, Madeleine, Deirdre, Alastair, Anke, Just, Frederique, Esther M., Meta and Susan,** I am so glad to get to know you, it is such a joy not only to work with you but also to have chats and (nowadays zoom) drinks outside work. Ex-colleagues, you are of course not forgotten. **Shalini** and **Maria,** the amazing ladies, we seem to find new ways to work together and catch-up, and I am really glad about that ;) **Jasper,** I am always looking forward to our catch-ups with you and **Sara**. **Connie,** I cannot express how much I am looking forward to your return so we can meet again not only as colleagues but also as friends ;)

Açık Bilim Türkiye öncü ekibi **Gültekin, İlkay ve Orçun**, sizlerle yalnızca kısa bir süredir tanışıyor olmamıza rağmen, bu kısa zamanda seminerler, çalıştaylar, kongreler ve webinarlar derken pek çok güzel iş çıkardık, eminim devamı da gelecek. Daha da önemlisi

sizin gibi dostlar edindiğim için ne mutlu bana. Köpüklü kahvelerimizi yudumladığımız daha nice "Olabildiğince Açık, Gerektiğince Kapalı" günlerimiz olsun :D

Esther, Astrid & Kari-Pekka, I am really glad to get to know you through Maarten. I am always looking forward to our catch-ups, which are unfortunately on hold now due to the current situation. I hope to see you soon for another game night ;) Speaking of people that I got to know through Maarten, **Sabine & Uwe,** I am really glad to get to know you as well. I always enjoyed our meetings, now we have some distance between us, but I really hope to catch up soon again :)

Temeli yıllara dayanan dostlarıma da hem biriktirdiğimiz onca güzel anı, hem de doktora sürecindeki bütün destekleri için burada ayrıca teşekkür etmesem olmaz. Sevgili kadim dostum **Pınar**, iki doktora, yurtiçi ve yurtdışı pek çok farklı şehirde buluşma, pek çok konser gibi saymakla bitmeyecek pek çok güzel anının yanı sıra, akademik aktivitelerden de ödün vermeyip beraber makale yazıp aynı oturumda sunum yapmaya kadar pek çok güzel paylaşımımız oldu. Özellikle doktoranın engebeli dönemlerindeki içten desteğin için ne kadar teşekkür etsem az. **Sıla**, insanın kuzeniyle önce ilkokulda, sonra üniversitede beraber okuyup, bir de üstüne benzer zamanlarda benzer alanlarda master ve doktora yapması ne büyük bir şans gerçekten. Tabi ki yalnızca akademik değil başka da pek çok güzel paylaşımlarımız oldu, ne de güzel oldu ;) **Ela,** ta ortaokul yıllarında başlayan dostluğumuzda, pek çok güzel anıyı biriktirmenin yanı sıra ikimizin de önce biyolog olup sonra başka alanlara yöneldiği bugünlere gelmek varmış :) Kardeşim **Burak,** Apoplexy, Timesailor, Jesus Christ Superstar derken pek çok güzel paylaşımımız oldu, o günleri özlemiyor değilim. Tabi müzik aktivitelerinin yanı sıra, daha pek çok güzel anıyı da biriktirdik beraber. **Ayşe, Can ve Esin**, ODTÜ yıllarından başlayarak bugünlere gelen dostluğumuzda stadyumdan tenis kortlarına kampüs içi ve dışında pek çok güzel anımız oldu. **Ayşe,** Hollandalı beylerimiz sayesinde, birbirine epey yakın Hollanda şehirlerinde oturup tekrardan buluşmak ne büyük bir şans gerçekten :) **Can**, bugünlerde biraz sekteye uğramış olsa da, neyse ki Türkiye - Hollanda arası gidip gelip arayı kapatıyoruz bir şekilde. **Esin,** kısa da olsa bir süre Hollanda'da da beraber olduk, ne de güzel oldu. **Şahika** ile beraber ikiniz de gri Hollanda-MMD günlerine renk kattınız ;) MMD'den bahsetmisken, **Seçil** sen de iyi ki geldin ve buraya gelip geri dönen arkadaşlara kıyasla (;P) iyi ki burada kaldın ki, birbirimize destek olabildik ;) Hepiniz iyi ki varsınız!

Charlotte & Joop, jullie hebben me heel erg gesteund gedurende niet alleen deze reis, maar mijn gehele reis in Nederland. Ik kan jullie niet genoeg bedanken voor alles wat jullie voor me hebben gedaan, voor de hulp bij mijn verblijfsvergunning, de meerdere verhuizingen en zelfs het verbeteren van jullie Engels om met me te kunnen praten. Erg bedankt voor jullie liefde en alle emotionele steun in moeilijke tijden. Ik wil de rest van de **familie** bedanken voor alle mooie momenten, gezelligheid en het verbeteren van mijn Nederlands. Also the **family in Australia**, many thanks for making sure that we had a great time there which really meant a lot.

Annecim ve Babacım, doktora süreci dahil her zaman ve her aldığım kararda yanımda olduğunuz, koşulsuz ve sınırsız sevginiz, güveniniz ve desteğiniz için ne kadar teşekkür etsem az. Çocukluğumdan itiraben piyano derslerinden okul eğitimine kadar her türlü alanda en iyi eğitimi alabilmem için gösterdiğiniz bütün çabalarınız için çok teşekkür ederim. Bugün bu noktaya gelebildiysem bu ancak sizin sınırsız özveriniz, emeğiniz ve sevginiz sayesinde. **Denizim,** bir insanın sahip olabileceği en tatlı abla olarak her zamanki sevgin ve desteğin için ne kadar teşekkür etsem az. Saymakla bitmeyecek pek çok güzel anı paylaşmanın yanı sıra, birimizin uzman doktor, öbürümüzün akademik doktor olduğu bugünlere gelmek varmış. **Özgür**, ailemize katılarak bizi çok mutlu ettin. **Tarçınım** ve **Hattuşum** sizi de unutmadım tabi ki. Daha ailecek beraber dinlenecek çok albüm, izlenecek çok konser ve film, gezilecek çok şehir, yapılacak çok tatil var. Daha pek çok güzel anılarımız olsun ailecek paylaşacak. İyi ki varsınız, hepinizi çok seviyorum, aynı şekilde sizleri de sevgili **teyzelerim, halalarım, yengem, dayılarım, eniştelerim, kuzenlerim** ve maalesef bugün artık aramızda olmayan **anneannem, babaannem ve dedelerim**. Hepinize çok teşekkür ederim bütün desteklerinizi için. Hep beraber nice mutlu anlar paylaşmak ve nice güzel günler görmek dileğiyle.

Wookie & Chewie, you two are the latest and cutest additions of our small family. Thank you for all your binkies and flops, and all the laughter and happiness you cause.

Maarten, I am afraid that there are no words to express how thankful I am for all the support you have provided me, especially during all the dips of this journey. Thank you for always being there for me during not only this journey but also my whole journey in the Netherlands. I am so grateful to have such a nice partner for life with whom I have shared so many invaluable moments. Thank you for your endless support and love. I love you, very much!